

UCLA

UCLA Electronic Theses and Dissertations

Title

Interaction of Relativistic Electrons and Radiation

Permalink

<https://escholarship.org/uc/item/2sc0h2q8>

Authors

Yan, Yi-Ton

also written as Yan, Yiton

Publication Date

1986

Peer reviewed|Thesis/dissertation

UNIVERSITY OF CALIFORNIA

Los Angeles

Interaction of Relativistic Electrons and Radiation

A dissertation submitted in partial satisfaction of the
requirements for the degree Doctor of Philosophy
in Physics

by

Yi-Ton Yan

1986

UNIVERSITY OF CALIFORNIA

Los Angeles

Interaction of Relativistic Electrons and Radiation

A dissertation submitted in partial satisfaction of the
requirements for the degree Doctor of Philosophy
in Physics

by

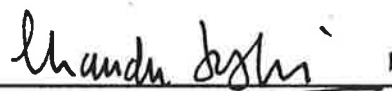
Yi-Ton Yan

1986

The dissertation of Yi-Ton Yan is approved.

A handwritten signature in cursive script, appearing to read "Walter Gekelman", written above a horizontal line.

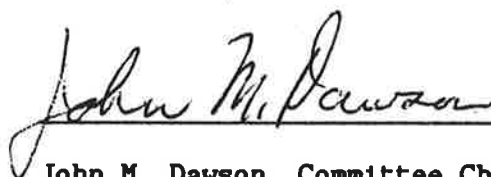
Walter Gekelman

A handwritten signature in cursive script, appearing to read "Chan Joshi", written above a horizontal line.

Chan Joshi

A handwritten signature in cursive script, appearing to read "Anthony T. Lin", written above a horizontal line.

Anthony T. Lin

A handwritten signature in cursive script, appearing to read "John M. Dawson", written above a horizontal line.

John M. Dawson, Committee Chair

University of California, Los Angeles

1986

To my son, Posu
who always wants fancy toys

and

To John Dawson
who inspired the researcher

TABLE OF CONTENTS

	<u>Page</u>
List of Figures.....	vi
List of Tables.....	x
Acknowledgements.....	xi
Vita and Publications.....	xii
Abstract.....	xiv
Chapter 1. Introduction.....	1
§1-1. Motivation for The Dissertation.....	2
§1-2. Organization of The Dissertation.....	5
§1-3. Review of Tunable Coherent Radiation Generation...	7
§1-4. References.....	12
Chapter 2. AC Free Electron Lasers.....	15
§2-1. Introduction.....	15
§2-2. The Dispersion Relation.....	21
§2-3. Nonlinear Saturation and Thermal Effects.....	29
§2-4. Feasibility of AC Free Electron Laser.....	39
§2-5. Summary and Future Work.....	47
§2-6. References.....	49

	<u>Page</u>
Chapter 3. Cherenkov Maser.....	50
§3-1. Introduction.....	51
§3-2. Computer Model.....	55
§3-3. Thermal Effects of Saturated Output Power.....	68
§3-4. Output Power Enhancement.....	77
§3-5. Summary.....	84
§3-6. References.....	85
 Chapter 4. Laser-Plasma Accelerators.....	 87
§4-1. Introduction.....	87
§4-2. Plasma Wave Breaking.....	88
§4-3. Acceleration Mechanisms.....	91
§4-4. Laser-Driven Plasma Waves.....	105
§4-5. Computer Simulations.....	118
§4-6. Discssion and Future Work.....	126
§4-7. References.....	128
 Chapter 5. Conclusions.....	 130

LIST OF FIGURES

<u>FIGURE</u>	<u>Page</u>
<p>2-1 (a) Growth rate vs. wave number and (b) Frequency vs. wave number for the case with $\gamma_o = 3.2$, $\epsilon_o = 0.06$, $\omega_o = 0.5 \omega_p$. The discrete points are from computer simulations. The upper line and lower line in (b) are respectively for $\omega_{EM}(k)/\omega_p$ and $\omega_{ES}(k)/\omega_p$ from theory.....</p>	28
<p>2-2 the unstable electromagnetic and electrostatic power spectrum for the case with $\gamma_o = 3.2$, $\epsilon_o = 0.06$, $\omega_o = 0.5 \omega_p$. The electrostatic power is enlarged by a factor of 20.....</p>	30
<p>2-3 Time evolution of electrostatic, electromagnetic and electron kinetic energy for the case with $\gamma_o=5.0$, $\epsilon_o=0.1$, $\omega_o = 0.5 \omega_p$. The electrostatic energy is enlarged by a factor of 100.....</p>	32
<p>2-4 Time evolution of the averaged electron relativistic factor $\langle \gamma \rangle$ for the case with $\omega_o = 0.5 \omega_p$, $\epsilon_o=0.2$, $\Delta p = 1\%$.....</p>	33
<p>2-5 Theoretical efficiency vs. initial beam energy and the results (discrete points) from simulations.....</p>	35
<p>2-6 Maximum growth rate vs. momentum spread of the electron beam for the case with $\omega_o = 0.5 \omega_p$, $\epsilon_o=0.2$.....</p>	37

2-7 Axial phase space at the time of saturation for the cases all with $\omega_o = 0.5 \omega_p$, $\epsilon_o=0.2$, but different momentum spread: (a) $\Delta p = 1\%$, $\omega_p t = 200.$, (b) $\Delta p = 2\%$, $\omega_p t = 200$, (c) $\Delta p = 3\%$, $\omega_p t = 200.$, (d) $\Delta p = 4\%$, $\omega_p t = 250.$, (e) $\Delta p = 5\%$, $\omega_p t = 350.$, (f) $\Delta p = 6\%$ $\omega_p t = 500$ 38

2-8 Efficiency vs. momentum spread for the case with $\omega_o = 0.5 \omega_p$, $\epsilon_o=0.2$ 40

2-9 A rectangular wave-guide of length L (x-directon), width w (z-direction), and height h (y-direction) upon which an AC electric field is imposed along the y-direction..... 42

3-1 The schematic and characteristic of the dielectric loaded wave-guide. (a) cross-sectional view,(b) the comparison between the theory and simulation of the TM_{01} mode dispersion relation..... 56

3-2 The time evolution of (a) the averaged beam kinetic energy, (b) the wave energy using an electron beam with 1% momentum spread..... 70

3-3 The time history of the axial electron phase space at (a) $\omega_c t = 120$ and (b) $\omega_c t = 160$ 71

3-4 The simulation results using an electron beam with 3.5% momentum spread. (a) the time evolution of the wave energy, (b) the axial electron phase space at $\omega_c t = 160$... 74

FIGURE

Page

3-5 The effects varying the momentum spread and the current on the performance of the Cherenkov maser (a) the nonlinear efficiency versus the momentum spread (b) the saturated power as a function of the electron beam current for cold beam..... 76

3-6 The time history of the axial electron phase space with $E_{dc} = 0.18 E_0$ at (a) $\omega_c t = 192$, (b) $\omega_c t = 384$ 80

3-7 The time evolution of the signal wave energy with different DC electric field strength imposed at $\omega_c t = 140$ 81

3-8 The fraction of electrons that remains trapped and the enhancement rate of the signal wave energy as a function of the DC electric field strength..... 83

4-1 Schematical illustration of the maximum electron density perturbation for a cold plasma with average density n_0 90

4-2 Schematical illustration of the electron acceleration by a electrostatic plasma wave..... 93

4-3 Schematical illustration of the plasma wave excitation by a beat-wave..... 107

4-4 A laser polarized along a preformed plasma density ripple wiggles electrons to produce a relativistic space charge wave..... 112

4-5 Plasma wave electric field, ϵ vs. $\omega_c t$ at fixed X in 1-D simulation..... 120

- 4-6 (a) Profile of ion density $n_1(x)$.
- (b) Plasma wave form $\epsilon(x)$ at $\omega_c t = 360$.
- (c) Electron's longitudinal momentum $\beta_x \gamma$ vs. x at
 $\omega_p t = 360$ 121
- 4-7 (a) Accelerated electron's velocity space β_z vs. β_x at
 $\omega_c t = 480$.
- (b) Accelerated electron's energy γ vs. x at $\omega_p t = 480$ 124

LIST OF TABLES

<u>TABLE</u>	<u>Page</u>
2-1 Design criteria for a rectangular wave guide ACFEL.....	41
2-2 Main advantages of the AC free electron lasers.....	46
4-1 Minimum energies the injected electrons should possess..	97
4-2 Maximum energies for an optimally trapped electron.....	98

ACKNOWLEDGEMENTS

It is my honor to have the opportunity of working with Prof. John Dawson. His resourceful new ideas and great physical intuition have always been very helpful at key points during the course of my three-year study at UCLA. Dr. Anthony Lin introduced me to the field of FEL, and he has always shared his knowledge with me in this field. Advice from Dr. Tom Katsouleas has always been very helpful during the course of my study in the field of plasma accelerators.

The idea of ionizing a solid target to produce density-rippled plasma is basically from Prof. Chan Joshi. He, Prof. Francis Chen and the particle acceleration group have always been very supportive.

Prof. Francis Chen, Prof. Walter Gekelman, Prof. Charles Kennel and Prof. Reiner Stenzel served as my oral committee during their busy hours. Prof. Walter Gekelman once suggested that the thermal effects in AC Free Electron Laser be investigated, which has led to the improvement of this dissertation.

My basic plasma physics knowledge was from the guidance of Prof. David Montgomery and Prof. George Vahala during my three-year stay at The College of William and Mary. The memory of competing for the title of the volleyball league in Williamsburg with my teammates, David Montgomery and John Hunter, et al. will maintain forever.

Miss Aileen Wang helped proof-read this dissertation. Her suggestions and comments were very useful.

Finally, I greatly appreciate my wife, Chiung-Ying, and my parents for their support during the long years of my graduate study.

VITA

- Dec. 20, 1951 — Born in Taiwan, Republic of China
- 1974 to 1975 — Physics Teacher, Chinshui Senior High School,
Chinshui, Taiwan, R.O.C.
- July 1975 — B.S. in Physics, National Taiwan Normal University,
Taipei, Taiwan, R.O.C.
- 1975 to 1977 — Military service of R.O.C.
- 1977 to 1980 — Physics Teacher, Chinshui Senior High School,
Chinshui, Taiwan, R.O.C.
- 1980 to 1982 — Teaching Assistant, College of William and Mary,
Williamsburg, Virginia
- December 1981 — M.S. in Physics, College of William and Mary
THE DELOS PRIZE, College of William and Mary
- 1982 to 1983 — Research Assistant, College of William and Mary
- 1983 to 1986 — Research Assistant, University of California,
Los Angeles

PUBLICATIONS AND PRESENTATIONS

- Y.T. Yan and J.M. Dawson, "AC Free Electron Laser",
Phys. Rev. Lett., 57, 1599 (1986).
- T. Katsouleas, J.M. Dawson, D. Sultana, Y.T. Yan,
"A Side-Injected-Laser Plasma Accelerator",
IEEE Trans. on Nucl. Sci. NS-32, 3554 (1985).

- A.T. Lin, W.W. Chang and Y.T. Yan, "DC Electric-Field Enhancement of Cherenkov-Radiation Output Power", IEEE Transactions on plasma science, vol. PS-13, no. 6, 531, (1985).
- Y.T. Yan, D. Sultana, T. Katsouleas, J.M. Dawson, "Acceleration of Electrons by the Interaction of a Side-Injected-Laser with an Acoustic Wave in a Plasma", UCLA Report PPG-870, (1985).
- Y.T. Yan and J.M. Dawson, "AC Free Electron Laser", UCLA REPORT PPG-888 (1985).
- Y.T. Yan, T. Katsouleas and J.M. Dawson,
"Two Dimensional Particle Simulation of the Side-Injected-Laser Plasma Accelerator", Bull. Am. Phys. Soc. 30, 1613 (1985)
- Y. T. Yan, W. W. cheng, A. T. Lin,
"DC Field Enhancement of the Cherenkov Radiator Output Power"
Bull. Am. Phys. Soc. 29, 1284 (1984).
- G. Vahala, D. J. Sigmar, Y. T. Yan
"Spectral Properties of the Kinetic Alfven Wave in Cylindrical Tokamak Geometry", Proc. of Sherwood Theory Conference,
Arlington, Virginia, March 1983.
- Y. T. Yan, G. Vahala, A. Punjabi
"Effects of Compressibility on the Evolution of Most Probable Equilibrium for REP", Bull. Am. Phys. Soc. 27, 1033 (1982).

ABSTRACT OF THE DISSERTATION

Interaction of Relativistic Electrons and Radiation

by

Yi-Ton Yan

Doctor of Philosophy in Physics

University of California, Los Angeles, 1986

Professor John M. Dawson, Chair

The interaction of relativistic electrons and radiation is studied theoretically and with computer simulations for the amplification of radiation or for the acceleration of electrons. For radiation amplification, we investigate the following two mechanisms: 1.) AC Free Electron Laser (ACFEL) in which a relativistic electron beam (with relativistic factor γ_0) is wiggled by an AC (temporally oscillating but spatially uniform) transverse electric or magnetic structure. Radiation is produced at frequency $f \sim 2\gamma_0^2 f_0$ (for $\gamma_0 \gg 1$), where f_0 is the frequency of the AC field. A rectangular wave-guide design is presented to illustrate one realization of the ACFEL and its performance is compared to conventional FEL's; 2.) Cherenkov Maser in which a mildly relativistic electron beam is propagated along the axis of a

dielectric-lined wave-guide so as to produce microwaves. A newly developed particle simulation code is used to model the TM mode coupling in this scheme. Good agreement is obtained between the simulations and a recent laboratory experiment.

In both cases (1 & 2), the nonlinear saturation is found to be caused by the trapping of the electrons in self generated longitudinal waves. Momentum spread in the electron beam (beam temperature) is observed to result in smaller gain per unit length and reduced saturation efficiency. It is also demonstrated by our computer simulations that the output power can be enhanced if an axial dc electric field of appropriate magnitude is imposed immediately before saturation.

For electron acceleration, we consider laser-plasma accelerator schemes. In these schemes, electromagnetic radiation (e.g. a laser) drives a plasma space charge wave which can trap and accelerate relativistic electrons at rate of order 1 GeV/cm (for a plasma of density 10^{18}cm^{-3}). In particular, we propose and investigate a new scheme to generate the plasma waves by a monochromatic laser injected from the side rather than colinearly with the accelerated electrons. This overcomes the pump depletion problem inherent in previous colinear schemes (e.g. Beat-Wave Accelerators).

Chapter 1

Introduction

The interaction between relativistic electrons and radiation (electromagnetic wave) inevitably leads to energy transfer between them. Under some special arrangement, this energy transfer can be particularly useful. It can, on the one hand, lead to generation of coherent radiation, and on the other hand, lead to electron acceleration. As an example, let us consider an electron together with a plane electromagnetic wave traveling through an AC (temporally periodic but spatially uniform) transverse electric field [1]. Through the Coulomb force due to the presence of the AC transverse electric field, the electron acquires a transverse velocity which allows it to either receive or give energy to the transverse electric field of the plane electromagnetic wave. If the longitudinal velocity of the electron is such that in one period of the electron transverse AC motion the electron slips behind the electromagnetic wave by one wavelength, the transverse velocity of the electron remains in-phase with the electric field of the plane electromagnetic wave. Such electrons will continue to have their energy increased or decreased, depending upon their phase relative to the plane electromagnetic wave. If the relative phase is such that the electrons continue to lose energy, then the electromagnetic

wave is amplified. This is called "AC free-electron laser" (ACFEL). On the other hand, if the relative phase is such that the electrons continue to gain energy, then the electromagnetic wave is diminished. This is called "inverse AC free-electron laser" (ACIFEL). There are many other well-known schemes dealing with the interaction of relativistic electrons and radiation, which achieve the same result, i.e. they can lead to either electron acceleration, radiation generation or both. Some of these schemes may also involve the use of a medium such as a dielectric or a plasma. It is the purpose of this dissertation to explore some interesting schemes for generation of coherent radiation and the inverse process, the acceleration of electrons. Most of these are newly proposed, as is the above example "of the AC free electron laser" which will be further discussed in the next chapter.

§1-1. Motivation for The Dissertation

One special feature of radiation generation by relativistic electrons is its tunability. The radiation frequency (or wavelength) generally depends on the electron energy and the geometrical arrangement that leads to the generation of radiation. Using the previous AC-free-electron-laser example, the radiation wavelength (λ_{rad}) is a function of the longitudinal electron velocity (v_{\parallel}) and the AC frequency (f_0), i.e., $\lambda_{\text{rad}} = F(v_{\parallel}, f_0)$. For a constant

longitudinal electron velocity $v_{||}$, the radiation wavelength λ_{rad} decreases with increasing AC frequency f_0 , since for higher AC frequency, the electron has a shorter time, τ_0 ($\tau_0 = 1/f_0$), to fall one radiation wavelength behind the electromagnetic wave. On the other hand, for a constant AC frequency f_0 , the radiation wavelength λ_{rad} decreases as $v_{||}$ is increased; although in this case the electron has the same amount of time to slip a distance λ_{rad} behind the electromagnetic wave, this slip distance is shorter for a larger $v_{||}$ due to the smaller velocity difference $(c - v_{||})$ between the electromagnetic wave and the electron. Indeed, neglecting the modification due to the electron beam collective effects as well as the AC electric field strength, this required lasing (or inverse lasing) condition can be expressed as:

$$\lambda_{\text{rad}} = (c - v_{||}) \tau_0 ,$$

or

$$f = \frac{f_0}{1 - \beta_{||}} ,$$

or

$$f \sim 2 \gamma_{||}^2 f_0 \quad \text{if } \gamma_{||} \gg 1$$

where f is the radiation frequency; $\gamma_{||} = (1 - \beta_{||}^2)^{-1/2}$ and $\beta_{||} = v_{||}/c$. Thus the radiation frequency can be continuously tuned by either changing the AC frequency or the electron energy. Both can be freely adjusted provided within the available technical limitations. This tunability gives the free-electron lasers broad applications to many

areas, particularly for diagnostics in atomic, molecular and solid state physics, and to applications in heating and diagnosing plasmas, and thus this is a topic of broad scientific and practical interest.

As for the acceleration of electrons using radiation (e.g. laser), the most attractive aspect is the extremely large electric fields (up to 10^{11} V/cm at focus) which can be produced by present laser technology. If such fields can be effectively coupled to charged particles over a significant distance, ultra-high energies may be attained in a short distance, thereby miniaturizing the size of a high energy accelerator. There have been many proposals aimed at coupling these extremely large laser fields to charged particles in the past decade. The inverse free electron laser has been proposed for this purpose; the AC IFEL might also be so used. However, we will be particularly interested in using a plasma as a medium to synchronize the electric fields with the particle motion. These are the so-called laser-plasma accelerators which have some advantages over the other laser schemes. Firstly, plasmas act as transformers in the sense that they can transform the extremely large laser electric fields into equally large (sometimes larger, sometimes smaller) plasma electrostatic fields which can be used to accelerate charged particles. Secondly, the acceleration gradient supported by the plasma electrostatic field is longitudinal and thus is invariant under Lorentz transformation, while the transverse

laser field will be Lorentz transformed into a smaller field seen by comoving electrons (by a factor of γ_{\parallel} when viewed in the electron reference frame). This makes a big difference since γ_{\parallel} can be extremely large for a good accelerator. Finally the phase velocity of the plasma wave can be made to be close to but slightly less than that of light so that particle synchronism with the wave can be maintained.

§1-2. Organization of The Dissertation

We begin by investigating a newly proposed scheme for coherent radiation generation in the next chapter. This scheme replaces the wiggler magnetic field in the conventional magnet FEL by a transverse AC (temporally periodic but spatially uniform) electric or magnetic field (ACFEL) as briefly described in the above example. We first derive the linear dispersion relation theoretically using the fluid theory. The theory is then checked by numerical simulation using a one and two halves dimensional fully relativistic, fully electromagnetic particle code. One realization of the ACFEL with a rectangular wave guide design is also presented and its performance is compared to more conventional FEL's.

In Chapter 3, we study another scheme for generation of coherent radiation. This scheme uses a dielectric lined wave-guide in which a

relativistic electron beam propagates. This is the well-known Cherenkov maser and has been studied by many physicists for several decades. Our focus is on the nonlinear aspects which appear to be analytically intractable. We first describe and test the numerical algorithm which is developed to model the TM mode coupling in a dielectric-lined wave-guide. We then use this model to study the electron thermal effects and the nonlinear radiation saturation. Finally, we present one scheme for output power enhancement by properly using an axial DC electric field and test it by numerical simulation.

Chapter 4 is devoted to studying electron acceleration. Although the schemes described in Chapter 2 and Chapter 3 can also be used for the acceleration of electrons, we are particularly interested in exploiting the special feature of a plasma as a medium for this purpose. We first generally discuss the property of the plasma waves that are used for the electron acceleration; the plasma wave breaking amplitude and the potential acceleration gradient are studied. We then describe the acceleration mechanisms and discuss the possible energy gain for the electrons. The excitation of the plasma waves using radiation (e.g. laser) is then presented; the beat-wave excitation scheme is briefly reviewed, followed by a discussion of our newly proposed side-injected-laser scheme. Finally, numerical simulation results are presented to check the theoretical predictions and to identify nonlinear effects

and limitations.

The conclusions are presented chapter 5.

§1-3. Review of Tunable Coherent Radiation Generation

Tunable coherent radiation generation has been seriously investigated for many decades. Many proposals and experimental reports appear in the literature. Before further discussing the contents of the dissertation, It might be helpful to have a brief review of this subject. While it is impossible to accommodate all of the proposals and reports, more references can be found from the references listed.

In 1951, H. Motz [2] proposed a scheme for production of radiation using relativistic electrons. By passing a fast electron beam through a succession of electric or magnetic fields of alternating parity, part of the electron energy can be converted into radiation. Motz emphasized that the efficiency of energy conversion depended entirely on the coherence of the emitted radiation. K. Landecker [3] at about the same time proposed another scheme. He considered amplifying the frequency and the power of an electromagnetic wave by its reflection from an electron cloud moving with relativistic velocity. Due to the discontinuity of the index of

refraction at the front of the electron cloud, the relativistic electron cloud can be viewed as a moving mirror for the reflection of the incoming electromagnetic wave. Through the double Doppler effect, the frequency of the reflected wave will be upshifted by a factor of $4\gamma^2$.

John Madey and co-workers [4,5] in early 1970's, analyzed the stimulated emission of bremsstrahlung by relativistic electrons in a spatially periodic magnetic field. The physics is related to the problem of stimulated Compton scattering analyzed by many authors such as Driecer [6], Pantell, Soncini, and Puthoff [7], and Sukhatme and Wolff [8]. Since then the group at Stanford has built radiation sources of this type. They reported the observation of 10.6 μm radiation in their experiment using a relativistic electron beam of 24 Mev and a helical magnetic wiggler with a 3.2-cm period and a length of 5.2 m in 1976 [9]. A gain of 7% per pass was obtained at an electron current of 70 mA. In their subsequent experiments, a free-electron-laser oscillator was constructed and operated above threshold at a wavelenth of 3.4 μm using the same magnetic wiggler but a relativistic electron beam of energy 43 Mev [10]. In these experiments the mechanism responsible for the generation of radiation is believed to be stimulated Compton scattering of the static wiggler magnetic field (it looks like an electromagnetic wave to the electrons) since the collective electron effects are essentially negligible due to the use of a low electron beam density

but high electron energy (the debye length λ_D is larger than the radiation wavelength λ_{rad}). If the electron beam density is increased but the electron random energy is reduced such that λ_D is much smaller than λ_{rad} , then the collective electron effects are significant and thus the mechanism responsible for the generation of radiation would be collective, i.e., stimulated Raman scattering of the static wiggler magnetic field. Lin, Dawson and Okuda [11], and Kwan, Dawson and Lin [12] at UCLA investigated such a mechanism with computer simulation as well as theoretical analysis. They found that the instability which is responsible for the amplification of the radiation wave was caused by the coupling of negative energy electrostatic beam modes to positive energy electromagnetic waves through the wiggler magnetic field. They also found that the linear gain and nonlinear saturation efficiency in such a mechanism were much higher than that in Compton regime. However, the radiation frequency is somewhat lower due to the fact that the slow plasma wave has phase velocity lower than that of the electrons. There were also some experimental studies for this high gain collective mechanism at Columbia university [13] and MIT [14], which showed qualitative agreements with the theory and simulations.

A general nonlinear theoretical discussion of FEL's with variable parameter magnetic wigglers is given by Kroll, Morton, and Rosenbluth [15] with a view towards the production of high power optical radiation at reasonable efficiency. This theory was

experimentally checked for the Compton regime FEL by Orzechowski, et al. [16]. Recently, it was also experimentally checked for a Raman regime FEL by the group at MIT [17]. They found that the output power agreed well with the predictions of the nonlinear theory.

Although Landecker's idea [3] was further theoretically investigated [18,19], the lack of a coherent tunable intense radiation source for operation of the laser in the attractive subcentimeter regime prevented simple implementation of such an idea. Nonetheless, various solutions to the problem have been suggested in the literature. The two-stage free-electron-laser approach [20] is the furthest developed at present. In this type of laser a conventional wiggler-based free-electron laser, in a first stage, generates an intense electromagnetic wave, which in turn, in a second stage, serves as a pump for either the same electron beam or another fresh electron beam. Carmel, Granatstein, and Gover [21] have recently implemented similar ideas, and demonstrated the first operation of a two-stage backward-wave free electron laser.

Other free-electron amplifiers have also been proposed. Hirshfield, et al. [22,23] proposed and developed the electron cyclotron maser in which a relativistic electron beam with a transverse-velocity component moved through a uniform axial magnetic field. The lasing process is based on an instability due to the phase bunching of electrons caused by the fact that the electrons are

not isochronous when they gyrate in a longitudinal magnetic field [24]. Presently, gyrotron oscillators which operate in a regime of negligible Doppler-shift contribution ($\alpha = v_1/v_{\parallel} \gtrsim 1$) have been successfully developed and employed in the magnetic fusion community to perform electron cyclotron resonance heating. If the beam parameter α is much reduced such that $\alpha \ll 1$, then the Doppler-shift contribution will dominate the lasing process. Lin, et al. have performed extensive computer simulations on this subject [25,26,27]. Recently, it has been shown theoretically [28,29] that a relativistic electron beam with a finite transverse dc momentum passing through a region of combined uniform solenoidal and longitudinal wiggler magnetic fields (LOWBITRON) is capable of generating coherent radiation at frequency $\omega \sim 2\gamma_0^2(k_w v_0 + \Omega_c/\gamma_0)$, where Ω_c and v_0 are respectively the electron cyclotron frequency of the solenoidal field and the electron axial velocity; k_w is the wiggler wave number, and γ_0 is the electron relativistic factor. This frequency is higher than that from either a free-electron laser with the same wiggler wave number or a Doppler-shift dominated cyclotron maser with the same solenoidal field. However, the energy conversion mechanism is thought to be a low efficiency process. Generation of radiation based on the Cherenkov mechanism has also received renewed interest. The group at Dartmouth College has employed a dielectric-lined wave-guide through which a relativistic electron beam propagates and is able to produce microwave radiation of 30 Kw at 50 GHz and 100 Kw at a lower frequency [30].

§1-4. Refereces

- [1] Y. T. Yan and J. M. Dawson, Phys. Rev. Lett., 57, 1599 (1986).
Y. T. Yan and J. M. Dawson, UCLA Report PPG-888 (1985).
- [2] H. Motz, J. Appl. Phys., 22, 527 (1951).
- [3] K. Landecker, Phys. Rev., 86, 852 (1952).
- [4] J. M. J. Madey, J. Appl. Phys. 42, 1906 (1971).
- [5] J. M. J. madey, H. A. Schwettman, and W. M. Fairbank, IEEE Trans. Nucl. Sci. 20, 980 (1973).
- [6] H. Dreicer, Phys. Fluids 7, 735 (1964).
- [7] R. H. Pantell, G. Soncini, and H. E. Puthoff, IEEE J. Quant. Elect. 4, 905 (1968).
- [8] V. P. Sukhatme and P. A. Wolff, J. Appl. Phys. 44, 2331 (1973)
- [9] L. R. Elias, et al., Phys. Rev. Lett., 36, 717 (1976).
- [10] D. A. G. Deacon, et al., Phys. Rev. Lett., 38, 892 (1977).
- [11] A. T. Lin, J. M. Dawson, and H. Okuda, Phys. Fluid, 17, 1995 (1974).
- [12] T. Kwan, J. M. Dawson, and A. T. Lin, Phys. Fluid, 20, 581 (1977).
- [13] T. C. Marshall, S. Talmadge, and P. Efthimion, Appl. Phys. Lett. 31, 320 (1977).
- [14] J. Fajans, G. Bekefi, Y. Z. Yin, and B. Lax, Phys. Rev. Lett., 53, 246 (1984).
- [15] N. M. Kroll, P. L. Morton, and M. N. Rosenbluth, IEEE J. Quant. Elec. QE-17, 1436 (1981).

- [16] T. J. Orzechowski, et al., IEEE J. Quant. Elec. QE-21, 831 (1985).
- [17] F. Fajans, et. al., Phys. Rev. Lett., 57, 579 (1986).
- [18] P. Sprangle, V. L. Granatstein, and L. Backer, Phys. Rev., A12, 1697 (1975).
- [19] A. Golding and L. Friedland, Phys. Rev., A32, 2879 (1985).
- [20] L. R. Elias, Phys. Rev. Lett. 42, 977 (1979).
- [21] Y. Carmel, V. L. Granatstein, and A. Gover, Phys. Rev. Lett. 51, 566 (1983).
- [22] J. L. Hirshfield and J. M. Wachtel, Phys. Rev. Lett., 12, 533 (1964).
- [23] J. L. Hirshfield, I. B. Bernstein, and J. M. Wachtel, IEEE J. Quant. Elec., 1, 237 (1965).
- [24] A. V. Gaponov, M. I. Petelin, and V. K. Yulpatov, The Induced Radiation of Excited Classical Oscillators and Its Use in High-Frequency Electronics, Izv, VUZ, Radiofizika, 10, 1414 (1967).
- [25] A. T. Lin, Int. J. Electronics, 57, 1097 (1984).
- [26] A. T. Lin and C. C. Lin, Int. J. Infrared and Millimeter Waves 5, 41 (1985).
- [27] A. T. Lin and C. C. Lin, to appear in the Proceedings of the 6th International Conference on High-Power Particle Beams, Kobe, Japan, June, 1986.
- [28] W. A. McMullin and G. Bekefi, Phys. Rev. A., 25, 1826 (1982).
- [29] R. C. Davidson and W. A. McMullin, Phys. Fluids, 26, 840

(1983).

- [30] S. Von Laven, J. Branscum, J. Golub, R. Layman, and J. Walsh,
Appl. Phys. Lett. 41, 408 (1982).

Chapter 2

AC Free Electron Lasers

In this chapter, we analyze a possible new source of tunable coherent radiation. By passing a relativistic electron beam (relativistic factor γ_0) through a spatially uniform, transverse AC electric or magnetic field of frequency f_0 , electromagnetic radiation of frequency $f \sim 2\gamma_0^2 f_0$ (for $\gamma_0 \gg 1$) is generated by its coupling the negative energy electrostatic beam modes with the high frequency EM modes. Existing superconductor cavities which can supply AC fields of frequency $f_0 \gtrsim 10$ GHz with amplitude $E_{\max} > 20$ MV/m may be used to lead to a new class of submillimeter or even visible generating devices. This mechanism may also be useful for synchrotron radiation sources. Furthermore, if plasma electrostatic waves are considered as the pumping AC field, extreme-ultraviolet radiation generation may be possible.

§2.1 Introduction

Sources of tunable coherent radiation are highly desirable for application to many areas, such as scientific investigation in

atomic, molecular, and solid state physics, radar, laser-pellet fusion, plasma heating and diagnostics, and isotope separation. For the past few decades there has been extensive effort devoted to finding new mechanisms of generation of coherent radiation by using relativistic electron beams as an energy source. Ever since H. Motz [1] examined the radiation from fast electron beams passing through a succession of electric or magnetic fields of alternating parity and K. Landecker [2] examined the frequency multiplication and wave amplification of an electromagnetic wave by reflection from an electron cloud moving with relativistic velocity in the early 1950's, a lot of schemes using relativistic electrons have been proposed to produce radiation with spectral range from microwave to extreme ultraviolet or even X-rays as has been reviewed in chapter 1. Of these schemes, the static magnetic free electron laser has received the most attention in trying to produce ultrahigh frequency radiation generation. This scheme exploits a relativistic electron beam (with relativistic factor γ_0) propagating along a periodic transverse magnetostatic structure (a spatial wiggler with period λ_w) and produces radiation at frequency $\sim 2\gamma_0^2 c/\lambda_w$ (for $\gamma_0 \gg 1$). Experiments have also demonstrated considerable success. However, due to technical reasons, the magnetostatic wiggler wave length is currently limited to $\lambda_w \gtrsim 2\text{cm}$, thus limiting the frequency of the laser to $f \lesssim 30\gamma_0^2$ (GHz). Therefore, to produce extreme ultraviolet radiation or X-ray requires near 1 GeV electron beams and meters of interaction length. Although accelerating electrons to 1 GeV is

common with present particle accelerators, they are large and expensive and the gain of the laser dramatically decreases with increased γ_0 . A natural alternative way, to think, of further increasing the laser frequency for a given value of γ_0 (or reducing the beam energy for a given laser frequency) would be to exploit a high frequency electromagnetic wave as the pump instead of the magnetostatic wiggler. However, the lack of a coherent tunable intense radiation source for operation of the laser in the attractive subcentimeter or other regimes prevents simple, independent implementation of the electromagnetic pump. One possible solution is the two-stage free-electron laser approach [3,4] with a conventional magnet-wiggler-based free electron laser for the first stage to generate an intense electromagnetic wave, which serves as a pump for a second stage. The second stage may or may not use the same electron beam. This is certainly an exciting possibility. However, the basic technical limitation that the magnet wiggler wave length has an upper limit about 2cm is still there. While we hope, due to technological progress, that this technical limitation ($\lambda_w \gtrsim 2\text{cm}$) will soon be much improved, some other new schemes are still worth investigating.

In this chapter we examine a new form of free electron laser and check the validity of the ideas by computer simulation using a 1-2/2 dimensional, relativistic, electromagnetic particle code [5,6]. A relativistic electron beam with velocity v_0 is propagated

along the axis of a temporally oscillating (frequency f_0) but spatially uniform transverse electric or magnetic structure. Temporal oscillations play the same role here as spatial oscillations in the conventional magnet free electron lasers. Relativistically, there is a correspondence between wave number and frequency and between electric and magnetic fields. In the beam frame, the oscillating field appears to be an incident electromagnetic wave with frequency

$$f' = \gamma_0 f_0$$

and wave number

$$k'_0 = -\beta_0 \gamma_0 \omega_0 / c,$$

where

$$\omega_0 = 2\pi f_0, \quad \beta_0 = v_0/c, \quad \gamma_0 = (1 - \beta_0^2)^{-1/2}.$$

Therefore, as in conventional FEL, the radiation generation can be thought of as stimulated scattering of the incident pump wave seen by the electron beam. The frequency of the radiation generated can be roughly derived in the laboratory frame by recognizing that the instability is due to the coupling between the electromagnetic waves and the negative energy electrostatic beam modes (modes with phase velocity less than the electron beam velocity) through the incident pump. For a cold electron beam, the uncoupled dispersion relations

for electromagnetic waves and the negative energy electrostatic beam modes are respectively

$$\omega_{EM}^2 = k_{EM}^2 + \omega_p^2/\gamma_0, \quad (2-1)$$

$$\omega_{ES} = k_{ES}v_0 - \omega_p/\gamma_0^{3/2}. \quad (2-2)$$

where $\omega_p = (4\pi n_0 e^2/m)^{1/2}$ is the electron plasma frequency, n_0 is average electron beam density, m is the electron rest mass. The coupling caused by the spatially uniform tranverse oscillating field required the following wave number and frequency matching:

$$k_{EM} = k_{ES} ,$$

$$\omega_{EM} = \omega_{ES} + \omega_0 ,$$

and modification of the normal mode relations given by equations (2-1) and (2-2). If the pumping field is weak, the modification to the dispersion relation can be neglected. Then, we can solve equations (2-1) and (2-2) for the coupled electromagnetic and electrostatic frequencies and wave numbers in the following:

$$\omega_{EM} = \omega_{ES} + \omega_0 = \bar{\omega} \quad (2-3)$$

$$k_{EM} = k_{ES} = \bar{k} = (\bar{\omega}^2 - \omega_p^2/\gamma_0)^{1/2}/c \quad (2-4)$$

where

$$\bar{\omega} = \frac{(\omega_0 - \omega_p / \gamma_0^{3/2}) \pm \beta_0 [(\omega_0 - \omega_p / \gamma_0^{3/2})^2 - (1 - \beta_0^2) \omega_p^2 / \gamma_0]^{1/2}}{1 - \beta_0^2}$$

This is the unmodified Raman scattering solution. The plus and minus signs are taken for backward and forward scattered waves respectively [7]. Backward and forward refer to the direction of propagation of the pump as seen by the electron beam. The forward scattered waves will not be considered hereinafter because they are down-shifted in frequency and also have a much smaller growth rate than the backward scattered waves. For $\gamma_0 \gg 1$, with reasonable ω_0 the backward scattered wave would have frequency $\bar{\omega} \sim 2\gamma_0^2 \omega_0$ (or $f \sim 2\gamma_0^2 f_0$). It is tunable by adjusting the beam energy γ_0 and/or the pump frequency f_0 . There are superconductor cavities which can supply AC fields of frequency $f_0 \sim 10\text{GHz}$ with amplitudes $E_{\text{max}} > 20\text{ MV/m}$ [8]. This is equivalent to a wiggler magnetic field of 700 Gauss which is comparable to those in use and thus this method may be used to lead to a new class of submillimeter or even visible generating devices. Furthermore, if we propagate a relativistic electron beam parallel to the wave front of a high gradient plasma electrostatic wave, extreme-ultraviolet radiation generation may be possible.

In the next section, we derive the dispersion relation by using the fluid theory [9]. Growth rates are then obtained from this to compare with computer simulation results. In section 2-3 we examine the nonlinear saturation; the efficiencies and thermal effects are

discussed. In section 2-4, we discuss the feasibility of this new form of free electron laser (ACFEL); a suggested design with design criteria is given and its performance is compared to conventional FEL's. The summary and suggestions for future work are presented in section 2-5.

52.2 The dispersion relation

Consider an unmagnetized, neutral, transversely homogeneous, unbounded electron beam with velocity $v_0 \hat{e}_x$ moving through a spatially uniform, transverse oscillating electric field $E_0 \cos \omega_0 t \hat{e}_y$. One may think that a spatially uniform time oscillating electric field is unphysical since Maxwell equations would require an associated magnetic field. However, there are a number of physical situations where this is a good approximation as for example for a wave guide near cut off or for the field of a long wavelength longitudinal plasma oscillation. From Maxwell equations, the electric and magnetic fields can be written as

$$\vec{E} = -\vec{\nabla}\Phi - (1/c)\partial\vec{A}/\partial t,$$

$$\vec{B} = \vec{\nabla} \times \vec{A},$$

where Φ , \vec{A} are respectively the scalar, vector potential and

$$\underline{\nabla} \equiv \hat{e}_x \partial / \partial x.$$

Using the coulomb gauge, i.e., $\underline{\nabla} \cdot \underline{A} = 0$, we readily get [10]

$$\frac{\partial^2}{\partial x^2} \underline{A}_t - \frac{1}{c^2} \frac{\partial^2}{\partial t^2} \underline{A}_t = - \frac{4\pi}{c} \underline{J}_t, \quad (2-5)$$

where the subscript t denotes the transverse components and $\underline{J} = -en\underline{v}$ is the current, n is the electron density. We remind the reader that $\underline{v} = \underline{P}/m\gamma$, where m is the electron rest mass and

$$\gamma = (1 - v^2/c^2)^{-1/2} = (1 + P^2/m^2c^2)^{1/2}.$$

The equation of motion is given by

$$d\underline{P}/dt = -e(\underline{E} + \underline{v} \times \underline{B}/c) - \underline{\nabla}\mathcal{P}/n,$$

where \mathcal{P} is the pressure. From its transverse component, we get

$$\underline{P}_t = (e/c) \underline{A}_t + \text{const.}$$

This follows from the fact that the transverse canonical momentum of a particle is a constant of the motion since (y, z) coordinates are ignored. We then linearize each quantity by denoting the subscripts 0, 1 for the 0th order and 1st order terms respectively so that

$$P_{\omega_0 t} = (e/c) A_{\omega_0 t} + \text{const.},$$

$$P_{\omega_1 t} = (e/c) A_{\omega_1 t}$$

and thus

$$J_{\omega_1 t} = - \frac{e^2 n_0}{\gamma_0 m c} A_{\omega_1 t} - \frac{e P_{\omega_0 t}}{\gamma_0 m} n_1 + \frac{e n_0 P_{\omega_0 t}}{\gamma_0^2 m^2 c^2} (P_{\omega_0} \cdot P_{\omega_1}). \quad (2-6)$$

From the 0th order of the equation of motion

$$dP/dt = -eE_0 \cos \omega_0 t \hat{e}_y,$$

we get

$$P_{\omega_0} = P_{0x} \hat{e}_x + P_{0y} \hat{e}_y,$$

where

$$P_{0x} = P_{0x}(t=0),$$

$$P_{0y} = - (eE_0/\omega_0) \sin \omega_0 t.$$

Assume

$$|P_{0y}| \ll P_{0x}$$

so that

$$\gamma_0 = (1 + P_0^2/m^2 c^2)^{1/2} \cong (1 + P_{0x}^2/m^2 c^2)^{1/2},$$

$$P_{0x} \cong \gamma_0 m v_0,$$

$$P_{\omega_0} \cdot P_{\omega_1} \cong P_{0x} P_{1x}.$$

Substituting (2-5) into (2-6), we therefore get

$$\begin{aligned} & \left(-\frac{\partial^2}{\partial t^2} + c^2 \frac{\partial^2}{\partial x^2} - \frac{\omega_p^2}{\gamma_o} \right) A_{1y} \\ & = - \left(\frac{c \omega_p^2 E_o \sin \omega_o t}{\gamma_o \omega_o} \right) \frac{n_1}{n_o} + \left(\frac{v_o \omega_p^2 E_o \sin \omega_o t}{\gamma_o^2 \omega_o m c} \right) P_{1x}, \quad (2-7) \end{aligned}$$

Equation (2-7) shows the coupling of the linear transverse term A_{1y} to the longitudinal quantities. In order to have a closed set of equations, we need to include those linearized equations governing the longitudinal motion, namely the x component of the equation of motion, the Poisson's equation and the equation of continuity, which are respectively

$$\left(\frac{\partial}{\partial t} + v_o \frac{\partial}{\partial x} \right) P_{1x} = -e E_{1x} + \left(\frac{e^2 E_o \sin \omega_o t}{\gamma_o m \omega_o c} \right) \frac{\partial A_{1y}}{\partial x} - \left(\frac{3m \omega_p^2 \lambda_D^2}{n_o} \right) \frac{\partial n_1}{\partial x}, \quad (2-8)$$

$$\partial E_{1x} / \partial x = -4\pi e n_1, \quad (2-9)$$

$$\frac{\partial n_1}{\partial t} + v_o \frac{\partial n_1}{\partial x} + \left(\frac{n_o}{\gamma_o^3 m} \right) \frac{\partial P_{1x}}{\partial x} = 0, \quad (2-10)$$

where $\lambda_D = (4\pi n_o e^2 / T)^{-1/2}$ is the Debye length, and the last term in Eq. (2-8) comes from the electron pressure; T is the temperature and adiabatic compression has been assumed. Also, note that the equation $\underline{B} = \underline{v} \times \underline{A}$ has been used in deriving the second term on the right hand side of equation (2-8). The four equations (2-7), (2-8), (2-9), and (2-10) form a complete set of equations with four unknowns A_{1y} , P_{1x} , n_1 , E_{1x} , where all the coefficients are either constant or temporal periodic with frequency ω_o . By Floquet's theorem, we therefore

assume the following type of solutions

$$\Psi_1(x,t) = e^{i(kx - \omega t)} \sum_I \hat{\Psi}_I(k,\omega) e^{-I\omega_0 t}, \quad (2-11)$$

where Ψ_1 stands for A_{1y} , P_{1x} , n_1 , E_{1x} . Substituting equation (2-11) into equations (2-7), (2-8), (2-9), (2-10), retaining only the lowest order mode coupling, keeping in mind that the negative energy (slow wave) rather than the positive energy (fast wave) electrostatic beam modes can extract the beam energy and grow, manipulation of the equations yields the following dispersion relation

$$D_{ES}(k,\omega_{ES})D_{EM}(k,\omega_{EM}) = F, \quad (2-12)$$

where

$$D_{ES} = (\omega_{ES} - kv_0)^2 / \omega_p^2 - (1 + 3k^2 \lambda_D^2) / \gamma^3,$$

$$D_{EM} = (\omega_{EM} / \omega_p)^2 - (kc / \omega_p)^2 - 1 / \gamma_0,$$

$$F = \frac{k^2 c^2 \epsilon_0^2}{4\gamma_0^5 \omega_0^2} \left(1 + \gamma_0^2 \beta_0 \left(\frac{kv_0 - \omega_{ES}}{kc} \right) \right)$$

and

$$\epsilon_0 = eE_0 / mc\omega_p,$$

$$\omega_{EM} = \omega_{ES} + \omega_0,$$

where ω_{EM} , ω_{ES} are respectively the electromagnetic and

electrostatic wave frequencies. For the case that the electron beam is moving through a spatially uniform transverse oscillating magnetic field $-B_0 \cos \omega_0 t \hat{e}_z$, we will get the same dispersion relation as given by equation (2-12) except that $\epsilon_0 = \beta_0 e B_0 / mc \omega_p$. If both a spatially uniform oscillating electric field $E_0 \cos \omega_0 t \hat{e}_y$ and magnetic field $-B_0 \cos \omega_0 t \hat{e}_z$ are allowed, we would have $\epsilon_0 = e(E_0 + \beta_0 B_0) / mc \omega_p$. Indeed, as long as ϵ_0 is kept the same, our computer simulation shows the same results no matter whether we use an AC electric or magnetic field or a combination. Equation (8) is valid as long as $\epsilon_0 \omega_p / \omega_0 \ll \gamma_0 \beta_0$ due to the assumption $|P_{Oy}| \ll P_{Ox}$ which was made before. This is usually the case in practice for presently available fields. Under such a condition, the coupling term F is much smaller than unity and the normal modes (given by $D_{ES} = 0$ and $D_{EM} = 0$) are weakly coupled, so the usual mode matching conditions (i.e. $\omega_{EM} = \omega_{ES} + \omega_0$, $k_{EM} = k_{ES}$ in this case) must be satisfied and the instability spectrum is around the normal mode root (ω_n, k_n) , where, for a cold electron beam, $(\omega_n, k_n)_{EM} = (\bar{\omega}, \bar{k})$ given by equation (2-3) and (2-4). For each k near the normal mode k_n , we can solve equation (2-12) for ω_{EM} in the following:

$$\omega_{EM} = \omega_{R,EM} \pm i \frac{\omega_p}{2} (\bar{F} \gamma_0^{3/2} / H - \mu^2)^{1/2}, \quad (2-13)$$

where

$$\omega_{R,EM} = (H - \mu/2) \omega_p, \quad (2-14)$$

and

$$H = \left((kc/\omega_p)^2 + 1/\gamma_0 \right)^{1/2},$$

$$\mu = H - (\omega_0 + kv_0)/\omega_p + (1 + 3k^2\lambda_D^2)^{1/2} \gamma_0^{-3/2},$$

$$\bar{F} = \frac{k^2 c^2 \epsilon_0^2}{4\gamma_0^5 \omega_0^2} \left(1 + \gamma_0^2 \beta_0 \left(\frac{\omega_0 + kv_0 - \omega_{R,EM}}{kc} \right) \right).$$

Equation (2-13) shows that for each $k \sim k_n$, instability will occur only if the strength of the pumping field is greater than a critical value. The threshold is

$$\epsilon_0^{th} = 2\gamma_0^{7/4} H^{1/2} \mu \left(1 + \gamma_0^2 \beta_0 \left(\frac{\omega_0 + kv_0 - \omega_{R,EM}}{kc} \right) \right) \frac{\omega_0}{kc}$$

and for $\epsilon_0 > \epsilon_0^{th}$, the growth rate is given by

$$\omega_i = \frac{1}{2} \omega_p (\bar{F} \gamma_0^{3/2} / H - \mu^2)^{1/2}. \quad (2-15)$$

The maximum growth rate would be (for $\gamma_0 \gg 1$)

$$\omega_i^{max} \cong (\epsilon_0 / 2\sqrt{Z}) \omega_p \gamma_0^{-3/4} (\omega_p / \omega_0)^{1/2}. \quad (2-16)$$

A numerical study for the instability spectrum and the corresponding growth rate given by equations (2-14) and (2-15), along with computer simulation results are given in Figure 2-1. The excellent agreement between the theory and the simulation ensures the accuracy of the simulation modeling as well as the approximations in the theory. The spectral relation, $\omega_{EM} = \omega_{ES} + \omega_0$, is also found from the computer simulations and further confirms

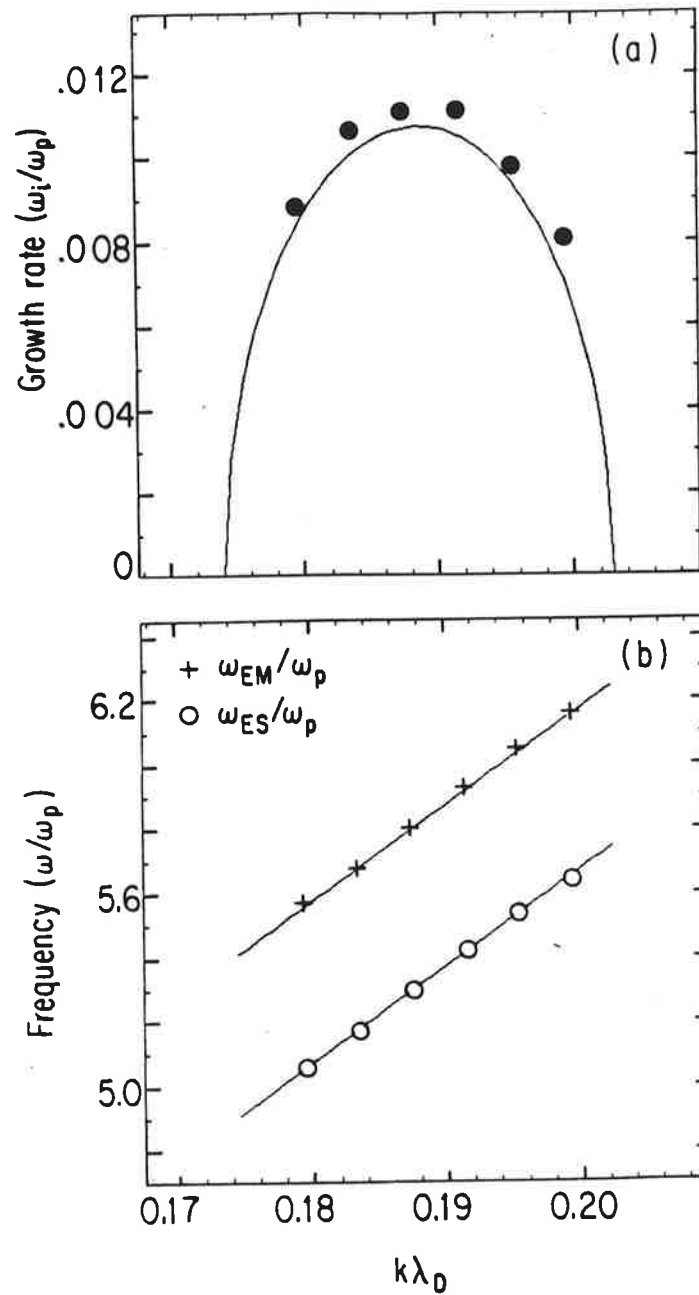


Fig. 2-1 (a) Growth rate vs. wave number and (b) Frequency vs. wave number for the case with $\gamma_o = 3.2$, $\epsilon_o = 0.06$, $\omega_o = 0.5 \omega_p$. The discrete points are from computer simulations. The upper line and lower line in (b) are respectively for $\omega_{EM}(k)/\omega_p$ and $\omega_{ES}(k)/\omega_p$ from theory.

that the instability is due to the coupling between the negative energy electrostatic beam modes and the high frequency EM modes through the pump.

§2-3 Nonlinear Saturation and Thermal Effects

The ac free electron laser, which is being investigated here, makes use of the interaction between a relativistic electron beam and a fast electromagnetic wave (wave with phase velocity faster than the speed of light) which is coupled with a slow electrostatic wave (wave with phase velocity slower than the electron beam velocity) through the ac pump. The lasing amplifying action takes place basically by a continuous interaction of the electrostatic wave and the electron beam. The initial electromagnetic field which is amplified can come from Compton scattering or can be externally injected. The electrons tend to bunch in regions where the electric force ahead is decelerating and the electric force behind is accelerating. Since, initially, electron bunches move slightly faster than the slow electrostatic wave, the waves (both electrostatic wave and electromagnetic wave), on the average, gain energy at the expense of the electron kinetic energy and grow exponentially (for the high gain, collective regime) until the instant when the electrostatic wave reaches an amplitude such that the electron orbits are altered nonlinearly and the orbits change

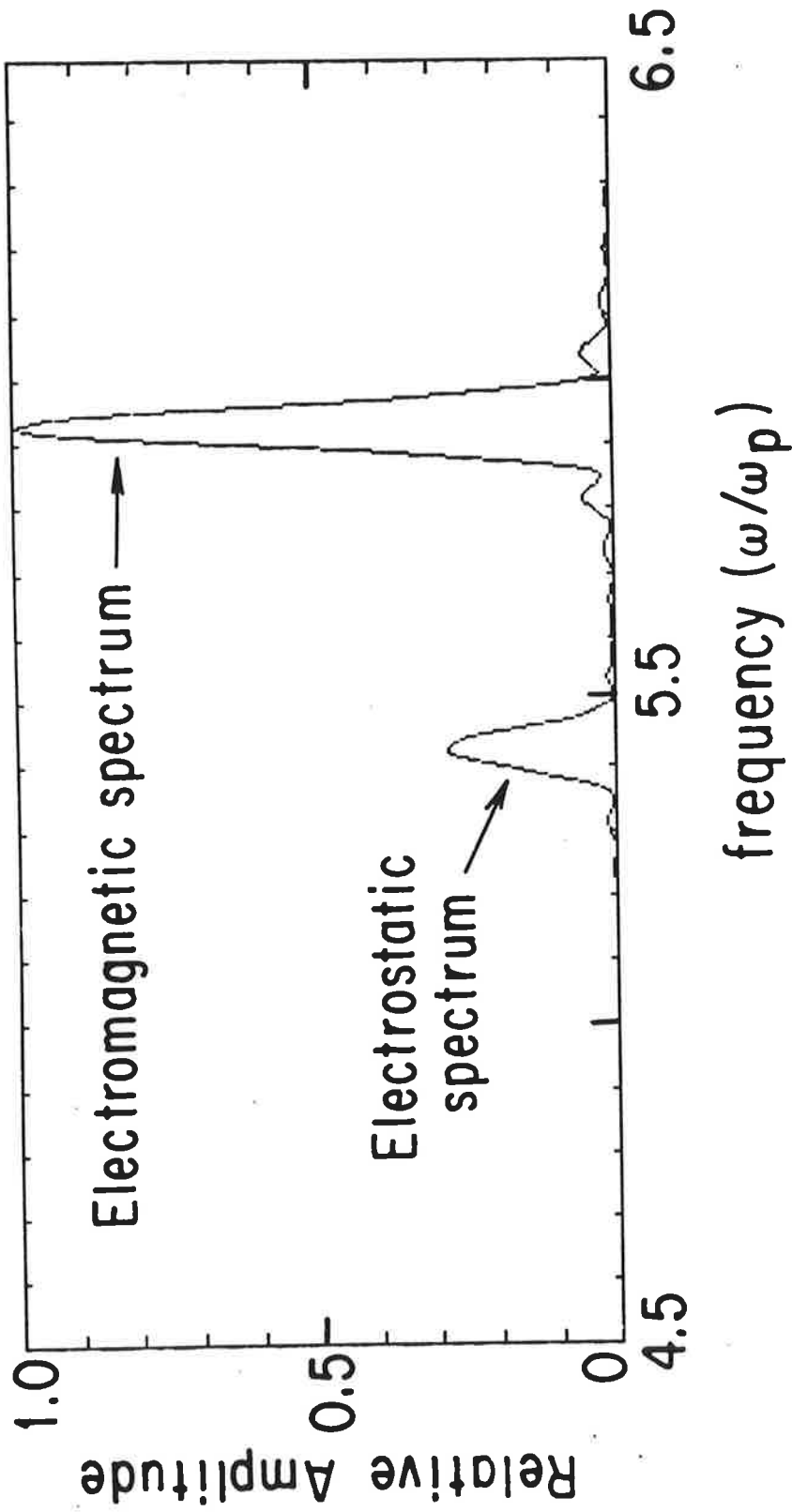


Fig. 2-2 the unstable electromagnetic and electrostatic power spectrum for the case with $\gamma_o = 3.2$, $\epsilon_o = 0.06$, $\omega_o = 0.5 \omega_p$. The electrostatic power is enlarged by a factor of 20.

from freely passing the electrostatic wave into trapped motion. The waves then saturate nonlinearly. The nonlinear saturation level is of considerable importance since it determines the efficiency of the radiation production. One of the common definition for the efficiency is

$$\eta = \frac{\text{saturated electromagnetic energy}}{\text{initial total electron-beam energy}}$$

As shown in Figure 2-2 for the relative power spectrum of the electrostatic wave and electromagnetic wave from simulation. We see that the electromagnetic power is much larger than the electrostatic power. This means that the reduced electron kinetic energy is mainly transferred to electromagnetic energy. This can also be clearly seen in Figure 2-3, where the time evolutions of the electrostatic, electromagnetic, and electron kinetic energy are shown. Thus, neglecting the electrostatic energy, the efficiency can be further defined as

$$\eta = (\gamma_0 - \langle \gamma_s \rangle) / (\gamma_0 - 1),$$

where $\langle \gamma_s \rangle$ is the average electron relativistic factor at the saturation level. From Figure 3 we would get a value $\eta = 10\%$. For some other parameters, efficiencies as high as 25% were obtained in the simulation as shown in Figure 2-4, where the averaged electron relativistic factor $\langle \gamma \rangle$ vs. time is plotted. We see that $\gamma_0 = 5.0$,

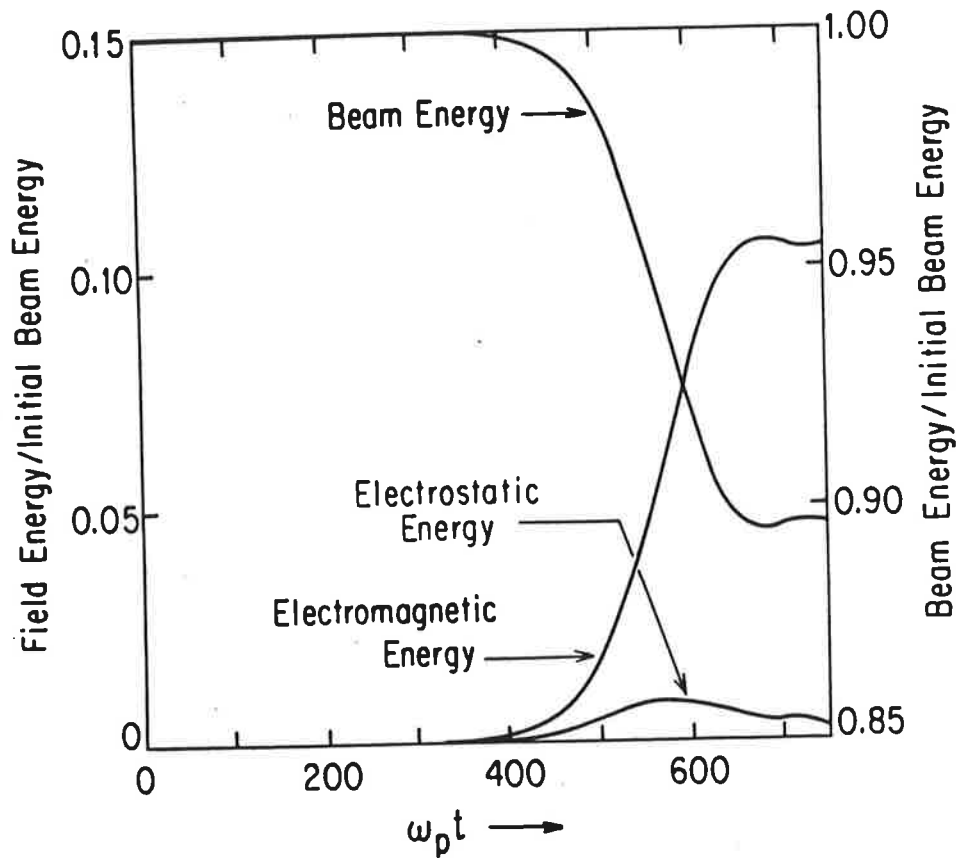


Fig. 2-3 Time evolution of electrostatic, electromagnetic and electron kinetic energy for the case with $\gamma_0=5.0$, $\epsilon_0=0.1$, $\omega_0 = 0.5 \omega_p$. The electrostatic energy is enlarged by a factor of 100.

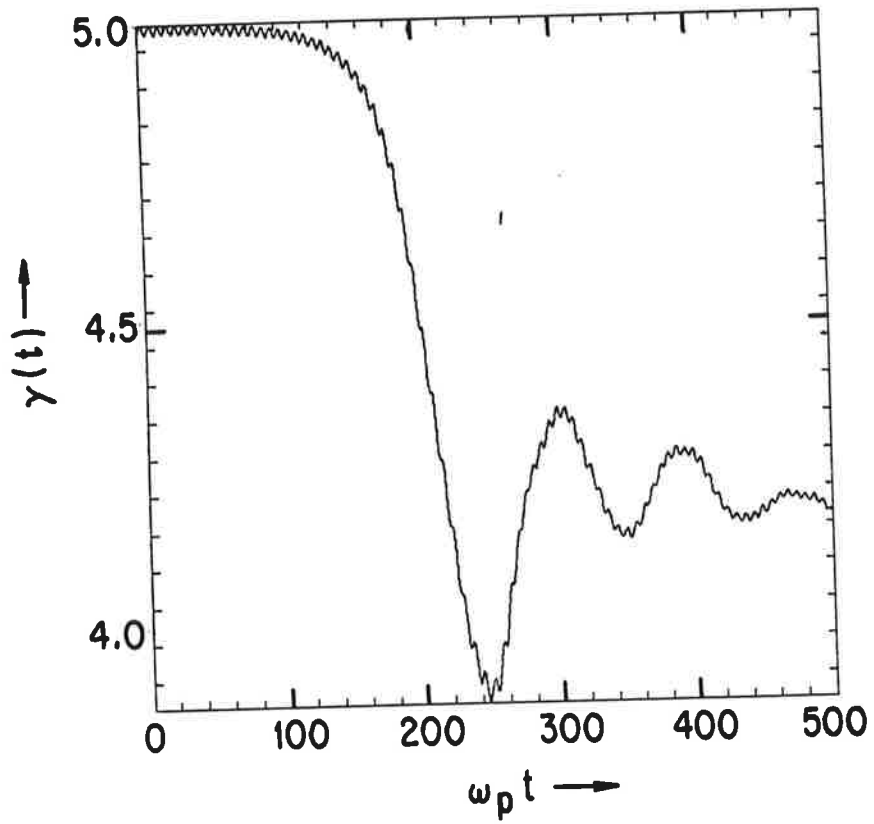


Fig. 2-4 Time evolution of the averaged electron relativistic factor $\langle \gamma \rangle$ for the case with $\omega_o = 0.5 \omega_p$, $\epsilon_o = 0.2$, $\Delta p = 1.7$.

$\langle \gamma_g \rangle \sim 4.0$, thus $\eta \sim 25\%$.

Since the saturation mechanism is due to electron trapping in the electrostatic wave, we can roughly derive a formula to predict the efficiency. From the theory and simulation, the unstable spectrum is quite localized in Fourier space. Furthermore, all the unstable modes have roughly the same phase velocity (ω/k) for the electrostatic wave and electromagnetic wave respectively as shown in Figure 2-1, where we see that the spectral curves are almost straight lines. Therefore, they maintain a coherent wave form and thus we can treat the unstable electrostatic spectrum as a single electrostatic wave. At saturation the electron beam speed is, on the average, slowed down to the phase velocity of the generated electrostatic beam mode

$$v_p \cong v_o - \gamma_o^{-3/2} (1 + 3k_n^2 \lambda_D^2)^{1/2} \omega_p / k_n.$$

Since the electrostatic wave amplitude is much smaller than the electromagnetic wave amplitude, in addition to neglecting the electrostatic wave energy, to a good approximation, we can also neglect the electron trapping oscillation energy in predicting the efficiency. Furthermore, right at the instant when the waves saturate, the electrons are not seriously heated up. Therefore, we predict the efficiency to be

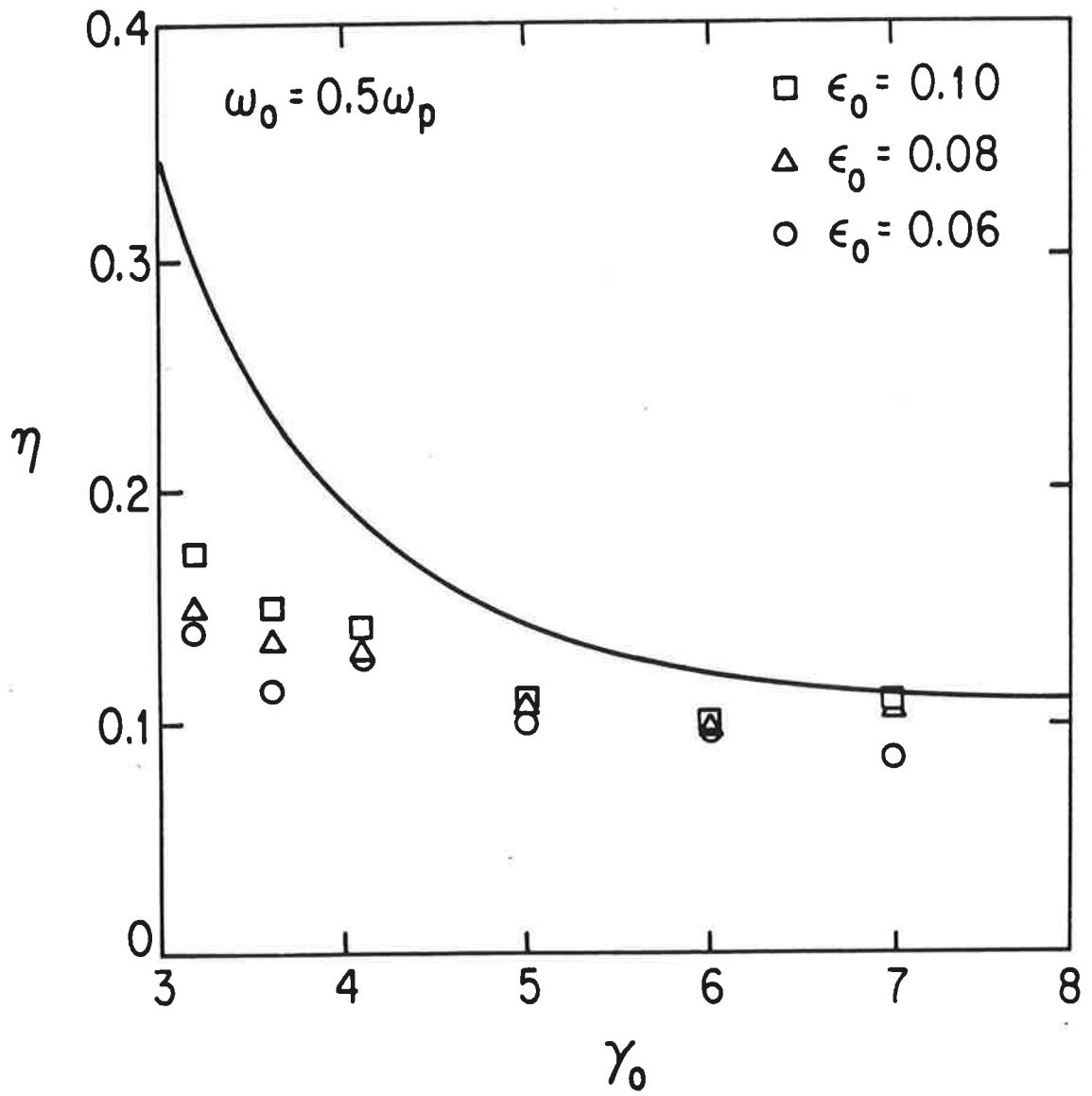


Fig. 2-5 Theoretical efficiency vs. initial beam energy and the results (discrete points) from simulations.

$$\bar{\eta} = (\gamma_0 - \gamma_p) / (\gamma_0 - 1) \quad (2-17)$$

where $\gamma_p = (1 - v_p^2/c^2)^{-1/2}$. A comparison of the computer simulations with the estimated values given by equation (2-17) is shown in Figure 2-5. Both show a similar characteristic dependence on γ and are in good agreement considering the simplicity of the theory.

The above analysis is only valid in the Raman regime, where a high quality (with small velocity spread), mildly relativistic electron beam is provided. If an electron beam with high thermal velocity spread and/or high relativistic factor is used such that the radiation wave number k is larger than λ_D^{-1} , the radiation mechanism is said to be in the Compton regime, i.e. the wave is amplified by only a small region of the velocity distribution which is in resonance. We have also investigated this regime through computer simulation by increasing the electron thermal velocity spread. The instability is weakened, and the growth rate reduced as shown in Figure 2-6, where the maximum growth rate vs. momentum spread of the electron beam is plotted. Figure 2-7 shows axial phase space plots for electron beams all with the same γ_0 and f_0 but with different momentum spread. We see that temperature, T , causes the electron bunches to not be as tight and the electron velocity distribution in the potential well of the longitudinal electrostatic field becomes more spread out with increasing T . This is the reason

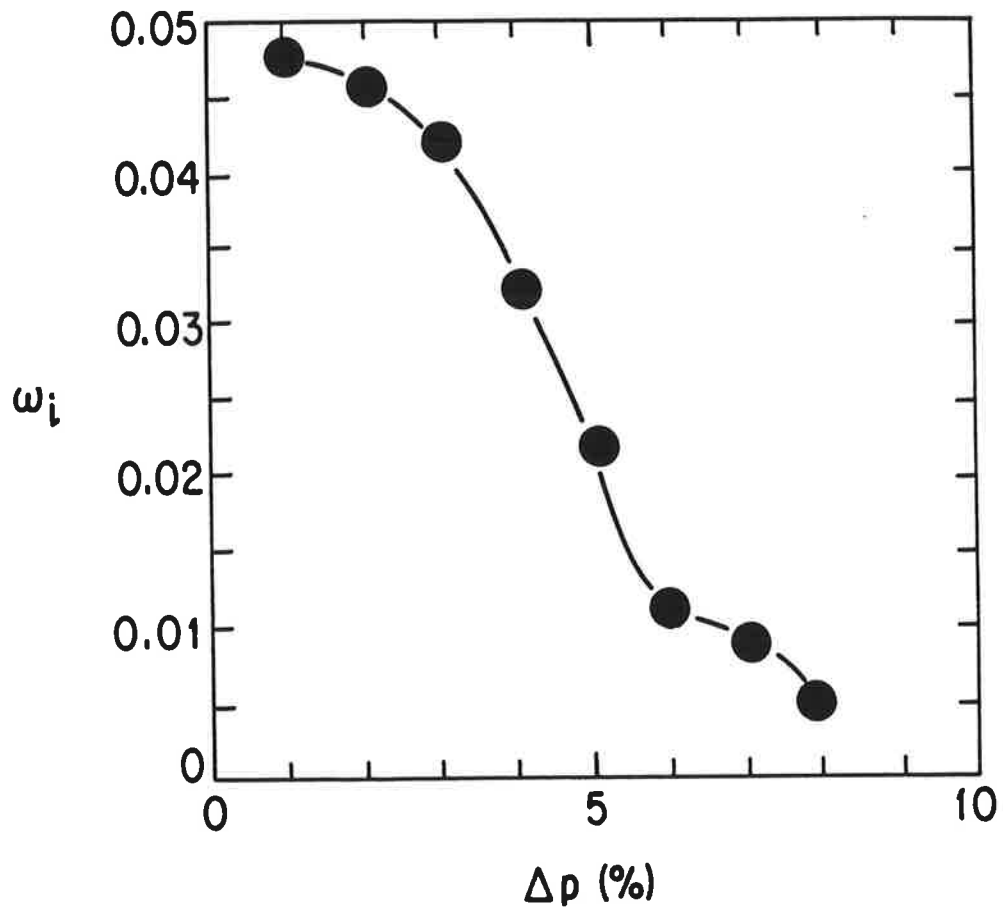


Fig. 2-6 Maxmum growth rate vs. momentum spread of the electron beam for the case with $\omega_o = 0.5 \omega_p$, $\epsilon_o=0.2$.

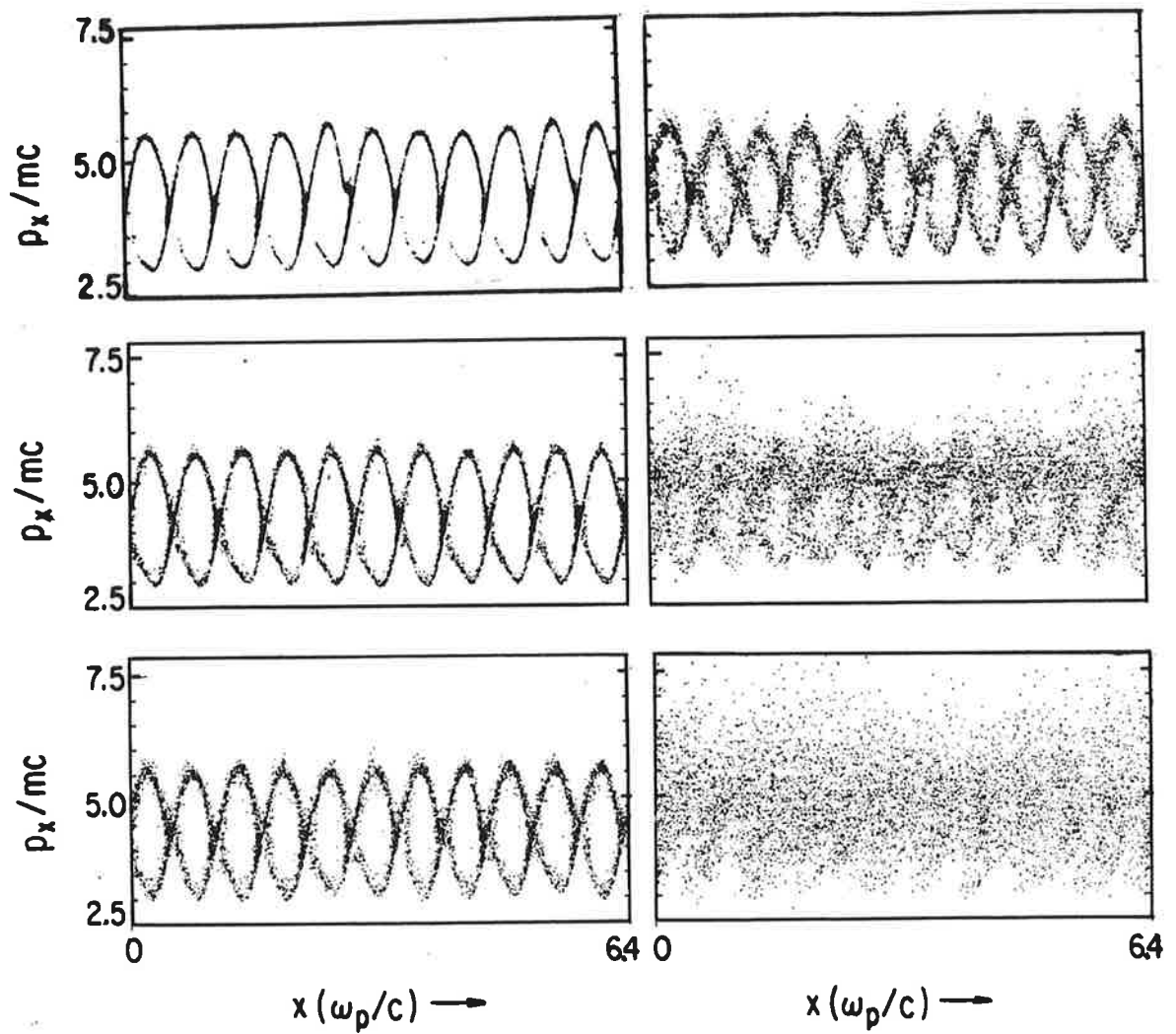


Fig. 2-7 Axial phase space at the time of saturation for the cases all with $\omega_o = 0.5 \omega_p$, $\epsilon_o = 0.2$, but different momentum spread: (a) $\Delta p = 1.7\%$, $\omega_p t = 200.$, (b) $\Delta p = 2.7\%$, $\omega_p t = 200.$, (c) $\Delta p = 3.7\%$, $\omega_p t = 200.$, (d) $\Delta p = 4.7\%$, $\omega_p t = 250.$, (e) $\Delta p = 5.7\%$, $\omega_p t = 350.$, (f) $\Delta p = 6.7\%$, $\omega_p t = 500.$

why the instability is weakened and growth rate reduced. Overall, there are still more electrons losing energy than gaining energy and a finite but reduced amount of electron kinetic energy can still be transferred to the wave. As the momentum spread is further increased, the efficiency eventually approaches zero at around 10 percent momentum spread as shown in Figure 2-8, where the efficiency vs. momentum spread is plotted. There is little efficiency lost for spreads of up to 2% for the parameters run here.

§2-4 Feasibility of the AC Free Electron Laser

From Maxwell's curl equations, as long as a temporally periodic but spatially uniform electric (or magnetic) field exists, there should be an accompanying temporally periodic and spatially dependent magnetic (or electric) field unless there is a canceling current. Both spatially uniform electric (or magnetic) field and spatially dependent magnetic (or electric) field can exert forces on the relativistic electrons. Thus, one may wonder whether such a temporally periodic but spatially uniform electric (or magnetic) field exists or not. Just as in the conventional magnet free electron lasers where the ideal plane wave approximation to magnetic wiggler exists only on the axis due to magnetostatic requirement $\nabla \times \underline{B} = 0$, we can also find a valid AC electric (or magnetic) field with negligible induced spatially dependent magnetic (or electric) field

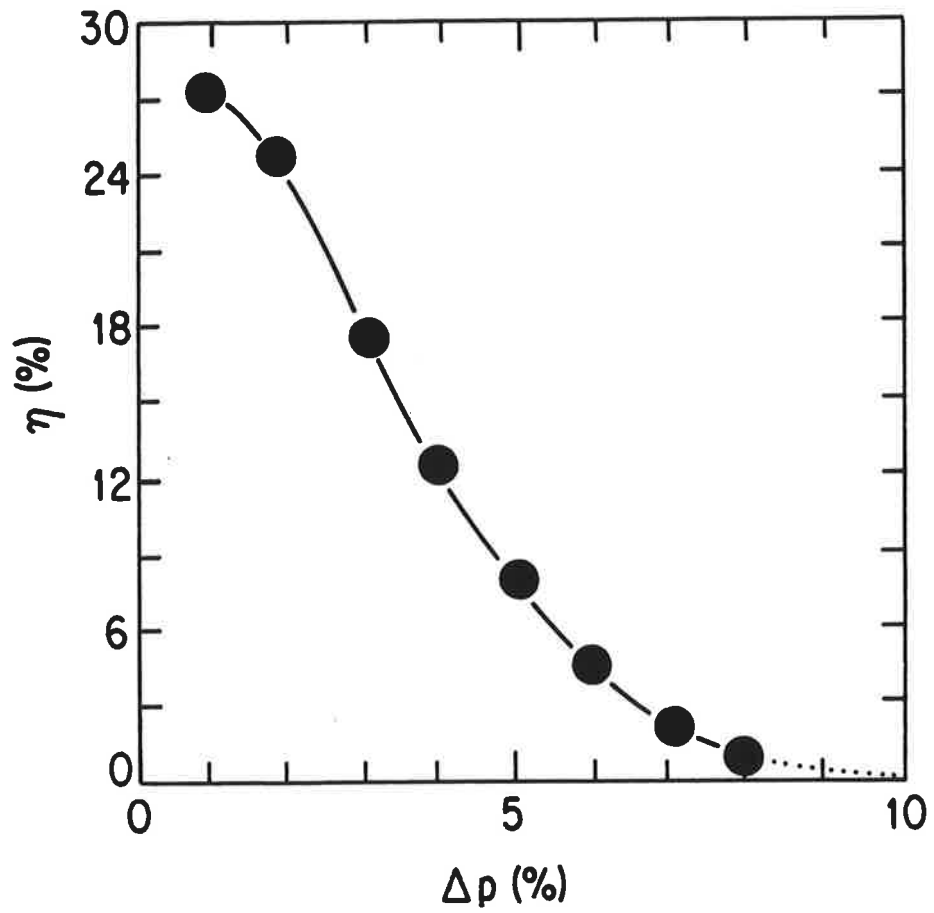


Fig. 2-8 Efficiency vs. momentum spread for the case with $\omega_o = 0.5 \omega_p$, $\epsilon_o=0.2$.

along the interaction region. As an example to show this, let us suggest a specific design. The relativistic electron beam is propagated along the symmetric axis (here labeled the x-direction) of a rectangular wave guide of length L , width w (along the z-direction), and height h (along the y-direction) as shown in Figure 2-9, operating near cut off so that an AC electric field $E_0 \hat{e}_y \cos \omega_0 t$ exists on axis, with the design criteria shown in Table 2-1.

TABLE 2-1

DESIGN CRITERIA FOR A RECTANGULAR WAVE GUIDE ACFEL

- | | |
|-------|---|
| (C-1) | $0.01 < (\epsilon_0/\gamma_0)(\omega_p/\omega_0) < 0.1,$ |
| (C-2) | $\lambda \ll d_y, \text{ and } \lambda \ll d_z,$ |
| (C-3) | $d_y < h - 2\epsilon_0 c \omega_p / \gamma_0 \omega_0^2,$ |
| (C-4) | $d_z \ll w,$ |
| (C-5) | $w \ll L, \text{ and } d_z \ll \gamma_0 c / \omega_0$ |
-
-

where λ ($\lambda \sim \pi c / \gamma_0 \omega_0$) is the radiated wave length, d_y and d_z are respectively the electron beam width along the y-direction and the z-direction, and saying $0.1 \ll 1$ would be endurable.

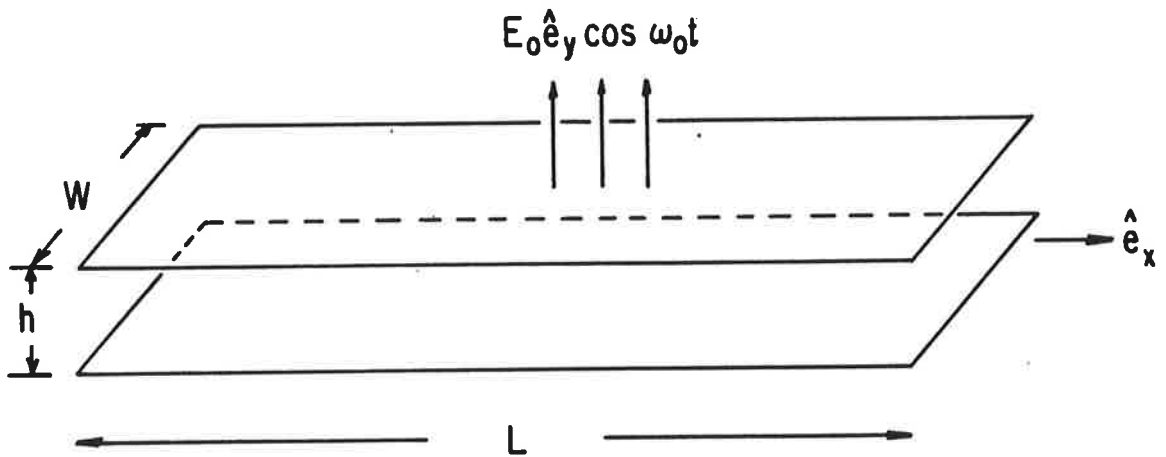


Fig. 2-9 A rectangular wave-guide of length L (x-direction), width w (z-direction), and height h (y-direction) upon which an AC electric field is imposed along the y-direction.

Holding to criterion (C-1) ensures that the imposed AC electric field is strong enough to give meaningful gain in a reasonable distance, but not so strong as to excite higher harmonic modes. Holding to criterion (C-2) ensures the plane wave approximation used in this chapter holds. Both criterion (C-1) and (C-2) are essentially for the ACFEL to work in the high gain, collective regime. Holding to criterion (C-3) prevents the electrons from hitting the walls in the course of their AC motion. Holding to criterion (C-4) implies that the AC wave form approximates very closely a temporally oscillating but spatial uniform electric field in the interaction region. Also, as long as $w \ll L$ is satisfied in criterion (C-5), the induced magnetic field (due to ampere's law) in the interaction region is essentially parallel to the symmetric axis (x-axis) with magnitude $B_{ind}(z,t) \cong (\omega_0 z/c)E_0 \sin \omega_0 t$, where z ($0 \leq z \leq d_z/2$) is the distance away from the symmetric plane $z=0$. The maximum of the amplitude of B_{ind} has a value $(\omega_0 d_z/2c)E_0$ and is invariant under Lorentz transformation to the beam frame. Therefore, holding to $d_z \ll \gamma_0 c/\omega_0$ ensures that this induced field B_{ind} is very small (compared to the AC electric field which, in the beam frame, has electric amplitude $\gamma_0 E_0$ and magnetic amplitude $\gamma_0 \beta_0 E_0$) and is thus negligible. In practice, it is easy to satisfy the above five criteria simultaneously.

Although some what outdated, let us use an astron beam as an example of a feasible electron beam to determine what we might

expect from ACFEL. Typical astron beam parameters are density $n_0 = 3 \times 10^{12} \text{ cm}^{-3}$, energy spread $\Delta\gamma/\gamma_0 \cong 10^{-3}$, and $\gamma_0 = 10$, thus the Debye length $\lambda_D \sim 3 \text{ } \mu\text{m}$ and plasma frequency f_p ($f_p = \omega_p/2\pi$) $\sim 15.6 \text{ GHz}$. Using an AC electric field of frequency $f_0 = 5 \text{ GHz}$ with amplitude $E_0 = 20 \text{ MV/m}$ ($\epsilon_0 \cong 0.12$) would produce radiation at frequency $f \sim 1000 \text{ GHz}$ ($\lambda \cong 300 \mu\text{m}$) so that $k\lambda_D = 2\pi\lambda_D/\lambda \sim 0.07$ and thus equation (12) holds and can be used to predict a growth rate $\omega_i \cong 0.014 \omega_p$. Amplifying the signal by ten e foldings would require an interaction time $\tau = 10/\omega_i \cong 7.5 \times 10^{-9} \text{ sec}$ and thus the interaction length would be $L = c\tau \cong 2.2 \text{ meters}$. To fit the above rectangular wave guide design, choosing beam dimensions, $d_y \sim d_z \sim 2 \text{ mm}$, and wave-guide size, $h \sim 1 \text{ cm}$, $w \sim 3 \text{ cm}$, and $L \sim 4 \text{ m}$ would be appropriate. These parameters are quite comparable to those of the conventional magnet FEL and can be easily realized in the laboratory.

As has been mentioned earlier, due to technical reasons, the wiggler period of the conventional magnet FEL is currently limited to $\lambda_w \gtrsim 2 \text{ cm}$, thus limiting the frequency of the laser to $f \approx 30\gamma_0^2 (\text{GHz})$. On the other hand, using a superconductor cavity, an AC electric field as strong as $E_0 > 20 \text{ MV/m}$ with frequency $f_0 \gtrsim 10 \text{ GHz}$ has been achieved [8]. The technology of such superconducting cavities is developing rapidly; we expect that strong AC field with $f_0 \sim 150 \text{ GHz}$ and good Q should be possible and believe this is a fruitful area for experimental research. This could lead the laser frequency to $f \sim 300\gamma_0^2 (\text{GHz})$. Of course, one can use conventional Cu cavities or

cryogenic Cu cavities if the RF drive power is not critical. The two-stage approach [3,4] which combines the conventional wiggler FEL and EMFEL can also be realized in combining ACFEL and EMFEL. Since the AC field is spatially uniform in the lab frame, technical accuracy is probably easier to achieve than the wiggler magnetostatic field (i.e. precision frequency is probably easier to maintain than precision spatial dependence). In addition, the AC field can be turned on and off when the AC wiggler is desired as for example in a storage ring. Also, if we taper the entrance of the wave guide such that the AC electric field is gradually cut off toward the entrance, an adiabatic transition to the AC wiggling field for the electrons can be achieved. Furthermore, we should also mention that the AC electric field could be produced in a plasma; for example, fields of 10^7 V/cm have been produced by the beat wave mechanism at a frequency of 3×10^{12} cycles/sec [11]. Using a modest energy electron beam (20 Mev) with such waves would produce radiation at frequency $f \sim 6000\gamma^2$ (GHz) = 9.6×10^{15} Hz ($\lambda \approx 312 \text{ \AA}$). To achieve such extreme ultraviolet radiation by conventional magnet FEL would require an electron beam with energy over 300 Mev. We summarize the main advantages of the ACFEL in Table 2-2.

TABLE 2-2

MAIN ADVANTAGES OF THE AC FREE ELECTRON LASERS

- (1) The pumping field is temporally oscillating but spatially uniform, thus technical accuracy is easier to maintain.
 - (2) An adiabatic transition to the AC wiggling field for the beam electrons can be achieved.
 - (3) AC field can be turned on and off at will.
 - (4) The generated laser frequency is $\sim 2\gamma_0^2 f_0$, where f_0 can be $10\text{GHz} \sim 150\text{GHz}$ for superconducting cavities, or $>3000\text{GHz}$ if a plasma electrostatic wave is considered.
-
-

§2-5 Summary and Future Work

In this chapter, a linear fluid theory of the mode coupling between the neagative energy electrostatic beam modes and the positive energy electromagnetic waves through an AC pump has been presented. We have also successfully used a one and two halves dimensional, relativistic, electromagnetic, particle simulation code to model this case. Good agreements between the theory and the simulations have been obtained in the linear regime. The nonlinear saturation was investigated and found to be caused by the trapping of the electrons in the self-generated electrostatic waves. A simple model was then developed to predict the nonlinear efficiency in the high gain collective regime. Thermal effects were also investigated mainly by computer simulations. We found that increasing the momentum spread of the relativistic electron particles reduced the tightness of the electron bunch, thus weakened the instability and reduced the nonlinear efficiency. A rectangular wave guide design was presented to illutrate one realization of the ACFEL. The disign parameters were found to be comparable to the conventional magnet FEL. There are some advantages over the conventional magnet FEL, which make this scheme attractive for the production of electromagnetic radiation.

Further ACFEL research should be done on the use of a plasma wave as the source of the pumping AC field. As we metioned in §2-4,

the high frequency and high amplitude AC electric fields associated with the plasma waves could make it easier to achieve extremely high frequency radiation generation. Part of the necessary research on this topic would involve a study of the complications in the lasing process due to the presence of the plasma. The effects of plasma instabilities such as the two stream instabilities on coherent radiation generation is an open question. Furthermore, the AC lasing process in a plasma may also provide an explanation for radiation observed from laboratory and space plasmas. These include the experiment of Gregory Benford in which a beam-plasma interaction generated radiation at frequencies up to $45 \omega_{pe}$ [12], and the radio bursts associated with solar flares; the origins of which have not been resolved.

§2-6. REFERENCES

- [1] H. Motz, J. Appl. Phys., 22, 527 (1951).
- [2] K. Landecker, Phys. Rev., 86, 852 (1952).
- [3] L. R. Elias, Phys. Rev. Lett. 42, 977 (1979).
- [4] Y. Carmel, V. L. Granatstein, and A. Gover, Phys. Rev. Lett. 51, 566 (1983).
- [5] J. M. Dawson, Rev. Mod. Phys., 55, 403 (1983).
- [6] J. M. Dawson and A. T. Lin, Handbook of Plasma Physics, Vol. II, edited by A. A. Galeev and R. N. Sudan, 555 (1984).
- [7] P. Sprangle, Phys. Quant. Elect. 5, 241 (1978).
- [8] M. Tigner and H. Padamsee, AIP Conference Proc., No. 105, 801 (1983).
- [9] T. Kwan, J. M. Dawson, and A. T. Lin, Phys. Fluid, 20, 581 (1977).
- [10] J. D. Jackson, Classical Electrodynamics, 2nd Ed. (John Wiley & Sons, New York, 1975), p. 222.
- [11] C. E. Clayton, C. Joshi, C. Darrow, and D. Umstadter, Phys. Rev. Lett., 54, 2343 (1985).
- [12] K.G. Kato, G. Benford, and D. Tzach, Phys. Fluids 26, 3636 (1983).

Chapter 3

Cherenkov Maser

In this chapter, we study the Cherenkov emission of the transverse magnetic (TM) mode in a dielectric-lined waveguide by using a relativistic electromagnetic particle simulation model. The parameters used in the simulation are relevant to a recent laboratory experiments [1,2]. Excellent agreement between the simulations and the experiments are obtained. Effects of thermal motions in the electron beam are also studied; increasing electron momentum spread is observed to reduce the tightness of the electron bunches and to increase the energy spread of the electrons trapped in the space potential well, which in turn, results in smaller gain per unit length and reduced saturation efficiency. It is also demonstrated by our computer simulations that the output power can be enhanced by an order of magnitude if an appropriate electric field is applied immediately prior to the electron bunches reaching the bottom of the potential well.

§3-1 Introduction

Cherenkov radiation, i.e. radiation emitted by the motion of a charged particle moving with velocity greater than that of light in a medium, has universally been considered as a potential short wavelength radiation source. The earliest exploration in this field can be traced back to Heaviside's and Sommerfeld's theoretical works. Prior to the development of the special theory of relativity, Heaviside [3], in 1888, analyzed the problem of the radiation produced by a charged particle when it moved with uniform velocity. He assumed that it was possible for a particle to move with a velocity greater than that of light in a vacuum and claimed that radiation could be produced under such a condition. Sommerfeld [4], in 1904, without apparent knowledge of Heaviside's results, performed a similar analysis. There were also some experimental observations that predate the classic experimental work of P.A. Cherenkov [5]. Curie [6], in 1911, observed that radiation produced in the walls of glass containers holding radioactive material was probably due in part to the penetration of the glass by fast charged particles. Mallet's [7] experiments in 1926 were, in part, observations of Cherenkov radiation. However, it is the pioneering experiments performed in 1934 by P.A. Cherenkov [5] (thus the name Cherenkov radiation) that mark the beginning of the recent suggested applications.

Cherenkov's experiments were soon explained theoretically by Frank and Tamm [8] in 1937. A great number of contributions aimed at developing a practical Cherenkov radiation source, both theoretically and experimentally, then appeared. Notable among these contributions were Ginzburg's article [9], in which he considered a number of ways that electrons could be coupled to dielectrics so as to produce radiation in the millimeter or submillimeter regions of the electromagnetic spectrum. Extensive reviews of work prior to about 1960 may be found in Jelley's article [10].

Most of the early work dealt with spontaneous emission by single electrons. This is a rather weak process for radiation production except for extremely high frequency radiation. Since the radiated power is proportional to the square of the number of electrons involved (at least true for radiated wavelength long compared to the length of the electron bunch), it was natural to consider the radiation produced by a bunched electron beam in order to enhance the amount of radiation. Indeed, there were experiments designed to investigate Cherenkov radiation produced by prebunched electron beams moving in close proximity to a dielectric surface [11,12,13]. However, due to the unavailability of high energy, high current beams, in these experiments only single prebunched electron beams were involved in the process of radiation and thus no provision was made for feeding back the emitted radiation to influence subsequent bunches. Therefore, those experimental results could only be

categorized as observations of enhanced spontaneous emission and hence from a practical viewpoint an uninteresting device.

The recent progress on intense relativistic electron beams has changed the outlook for Cherenkov radiation source. The availability of high energy, high current beams has made the Cherenkov mechanism one of the potential competitors for the design of devices to generate high-power, high-quality coherent tunable radiation. Both theoretical and experimental interest has been reawakened. Especially noticable is the strong endeavor undertaken at Dartmouth College to investigate the feasibility of using an intense relativistic electron beam and the Cherenkov mechanism to generate high-power microwave sources [14]. Good results have been reported [1,2]. The emphasis is no longer whether Cherenkov radiation can be a practical radiation source, but is on the art and science of achieving an efficient, economical source.

One practical slow wave structure for a Cherenkov maser can either be a gaseous or liquid dielectric, in which case the relativistic electron beam propagates directly through the medium. A second possibility is to use a dielectric lined waveguide, in which case the relativistic electron beam propagates through a channel and interacts with surface waves on the dielectric. The second scheme can also be thought of in terms of the interaction of the negative energy space charge wave on the beam with a positive energy

electromagnetic surface mode of the dielectric. The first method requires employing a very-high-energy electron beam and is limited by electrical breakdown of the dielectric so that only limited interaction length is allowed. There have been some attempts made to observe stimulated Cherenkov radiation in the visible and UV regions by employing this scheme [15,16], although momentum modulation by an applied electromagnetic field has been observed, there is no clear-cut evidence of true stimulated emission. On the other hand, the group at Dartmouth College has employed the second scheme and is able to produce microwave radiation of 30 KW at 50 GHz and 100 KW at lower frequency [1]. This is certainly an exciting success considering the long time struggle for producing a practical Cherenkov source. However, this device is not yet competitive with gyrotrons which are more efficient and can produce higher output power in this frequency range. Since one of the goals of Cherenkov maser research is to achieve excellent performance in terms of power, efficiency, and frequency, a more detailed knowledge of the interaction process under non-idealized conditions is required than is practical by analytical techniques. It is the main purpose of this chapter to investigate the highly nonlinear process involved in the Dartmouth type Cherenkov maser by applying numerical particle simulation techniques, in particular, those developed by Dawson, Lin, et al. [17,18]. One way to improve the output power has also been suggested; since the saturation mechanism of the Cherenkov maser is due to the trapping of the electrons by the longitudinal

(space charge) component of the wave field, a longitudinal dc electric field can be imposed at the time of saturation to increase its output power. Computer simulations demonstrate that a factor of 10 enhancement in output power is achievable. Furthermore, if the detrapped electrons can be taken out of the system, the efficiency of the device can be substantially improved.

In the next section, we describe the numerical model. The simulation results of effects of momentum spread on nonlinear efficiency and output power scaling with the beam current are presented in section 3. We then discuss the output power enhancement in section 4.

§2 Computer Model

Consider the type of waveguide that is depicted in Fig. 3-1a, which consists of a circular metallic wall with radius r_w and dielectric layer with thickness $(r_w - r_d)$ and dielectric constant ϵ (the permeability $\mu = 1$). It is not possible, in general, to separate the modes in a dielectric waveguide into transverse electric modes (TE) and transverse magnetic modes (TM). In the special case of azimuthal symmetry, the TE and TM modes can be decoupled. The electrons in a Cherenkov maser usually do not have transverse momentum so they can only excite TM modes.

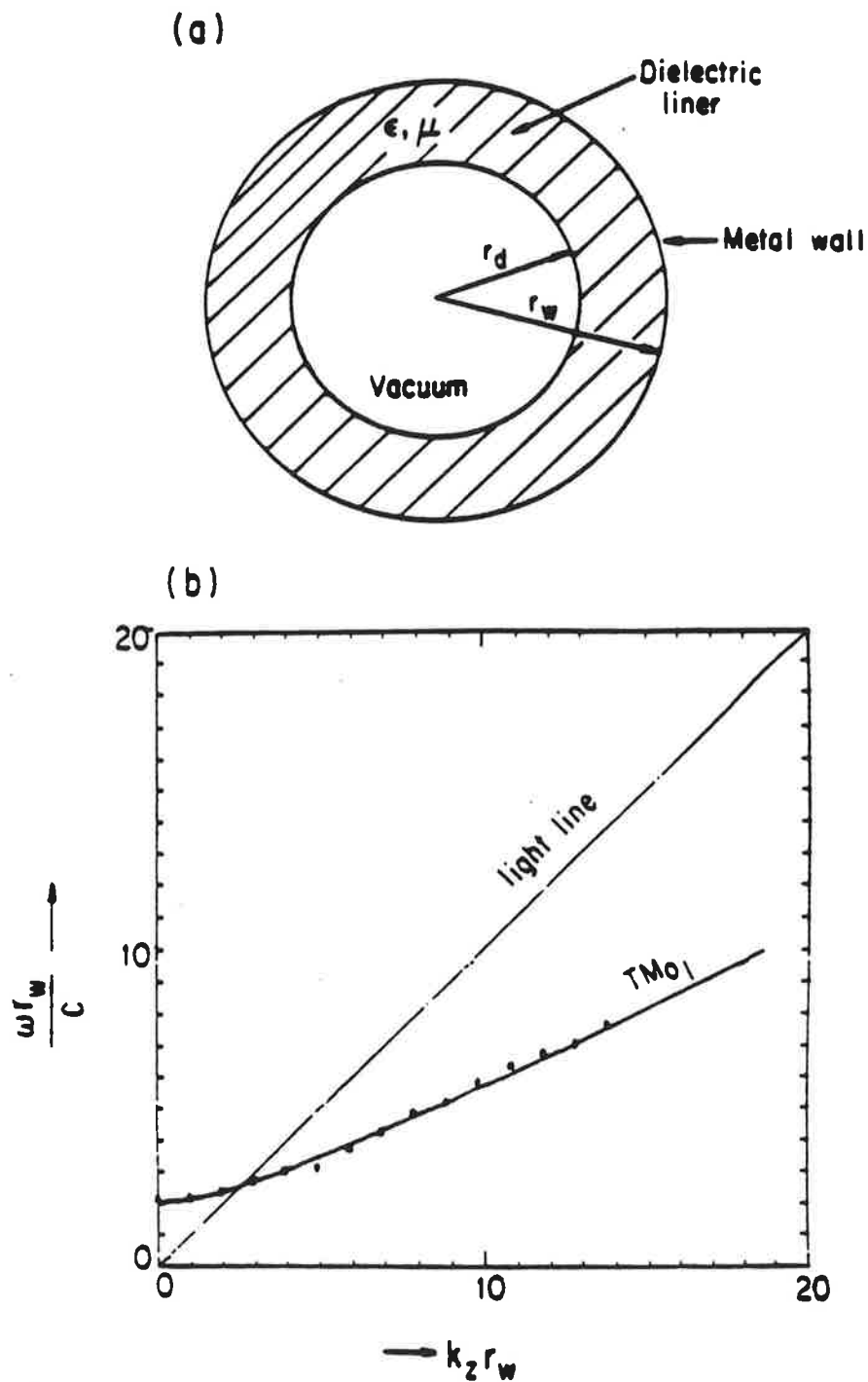


Fig. 3-1 The schematic and characteristic of the dielectric loaded wave-guide. (a) cross-sectional view, (b) the comparison between the theory and simulation of the TM_{01} mode dispersion relation.

Wave Equation

Let us choose cylindrical coordinate with r , θ , z , respectively the radial, azimuthal, axial components and assume all field components vary as $f(r)\exp(-i\omega t + ik_z z)$, then from the following Maxwell Equations for an empty dielectric coated waveguide

$$\nabla \cdot \underline{\underline{D}} = 0,$$

$$\nabla \cdot \underline{\underline{B}} = 0,$$

$$\nabla \times \underline{\underline{E}} = - \frac{1}{c} \frac{\partial \underline{\underline{B}}}{\partial t},$$

$$\nabla \times \underline{\underline{H}} = \frac{1}{c} \frac{\partial \underline{\underline{D}}}{\partial t},$$

$$\underline{\underline{D}} = \epsilon(r)\underline{\underline{E}}, \quad \text{where } \epsilon(r) = \begin{cases} 1, & 0 \leq r \leq r_d \\ \epsilon = \text{const}, & r_d < r \leq r_a \end{cases}$$

$$\underline{\underline{B}} = \mu \underline{\underline{H}} = \underline{\underline{H}}, \quad \text{since } \mu = 1 \text{ is assumed,}$$

we get

$$\nabla \times \underline{\underline{E}} = -i \frac{\omega}{c} \underline{\underline{H}} \quad (3-1)$$

$$\nabla \times \underline{\underline{H}} = -i \frac{\omega}{c} \epsilon(r) \underline{\underline{E}} \quad (3-2)$$

$$\nabla \cdot \underline{\underline{H}} = 0 \quad (3-3)$$

$$\nabla \cdot (\epsilon(r)\underline{\underline{E}}) = 0 \quad (3-4)$$

By Eq. (3-2), we can assume

$$\underline{\underline{H}} = -i \frac{\omega}{c} \nabla \times \underline{\underline{\xi}}, \quad (3-5)$$

where $\underline{\underline{\xi}}$ is the electric type of Hertzian potential. Then, from Eq. (3-1), we get

$$\nabla \times \underline{\underline{E}} = -\frac{\omega^2}{c^2} \nabla \times \underline{\underline{\xi}}$$

or

$$\underline{\underline{E}} = -\frac{\omega^2}{c^2} \underline{\underline{\xi}} + \nabla\phi \quad (3-6)$$

where ϕ is an arbitrary scalar potential. From Eq. (3-2), we get

$$\epsilon(r)\underline{\underline{E}} = \nabla \times \nabla \times \underline{\underline{\xi}}. \quad (3-7)$$

Combining Eqs. (3-6) and (3-7), we get

$$\nabla \times \nabla \times \underline{\underline{\xi}} = \epsilon(r)\frac{\omega^2}{c^2} \underline{\underline{\xi}} + \epsilon(r)\nabla\phi$$

or

$$\nabla (\nabla \cdot \underline{\underline{\xi}}) - \nabla^2 \underline{\underline{\xi}} = \epsilon(r)\frac{\omega^2}{c^2} \underline{\underline{\xi}} + \nabla(\epsilon(r)\phi) - \phi\epsilon(r) \quad (3-8)$$

since ϕ is arbitray, we can choose

$$\Phi = \frac{1}{\epsilon(r)} \nabla \cdot \underline{\xi} \quad (3-9)$$

and Eq. (3-8) can be simplified as

$$\nabla^2 \underline{\xi} - \frac{\nabla \epsilon(r)}{\epsilon(r)} \nabla \cdot \underline{\xi} + \epsilon(r) \frac{\omega^2}{c^2} \underline{\xi} = 0 \quad (3-10)$$

This is the wave equation for a cylindrical waveguide with a radial dependent dielectric constant. Since only TM Modes concern us (a very strong axial DC magnetic field is imposed to prevent electron from doing significant transverse motion), or more specifically, only TM_{0n} Modes will be considered here due to azimuthal symmetry, we can simply assume

$$\underline{\xi} = \hat{e}_z \Psi(r) e^{ik_z z}$$

without losing generality. Then, by using Eq. (3-9), from Eqs. (3-5) and (3-7), we get

$$\underline{B} = \underline{H} = \hat{e}_z \frac{\omega k_z}{c} \Psi(r) e^{ik_z z} = \hat{e}_z B_z(r) e^{ik_z z} \quad (3-11)$$

$$\begin{aligned} \underline{E} &= \frac{1}{\epsilon(r)} \nabla \times \nabla \times \underline{\xi} \\ &= \frac{1}{\epsilon(r)} \left\{ \hat{e}_r \left(k_z^2 \Psi(r) e^{ik_z z} \right) + \hat{e}_z \left(\frac{1}{r} \frac{d}{dr} (r \Psi(r)) e^{ik_z z} \right) \right\} \\ &= \hat{e}_r E_r(r) e^{ik_z z} + \hat{e}_z E_z(r) e^{ik_z z} \end{aligned} \quad (3-12)$$

and the wave Eq. (3-10) becomes

$$\frac{d^2\Psi}{dr^2} + \left(\frac{1}{r} - \frac{1}{\epsilon(r)} \frac{d\epsilon(r)}{dr} \right) \frac{d\Psi}{dr} + \left(\epsilon(r) \frac{\omega^2}{c^2} - k_z^2 - \frac{1}{r^2} - \frac{1}{\epsilon(r)} \frac{d\epsilon(r)}{dr} \frac{1}{r} \right) \Psi = 0.$$

This can be further manipulated into the type of Sturm-Liouville equation

$$\frac{d}{dr} \left(\frac{r}{\epsilon(r)} \frac{d\Psi}{dr} \right) + \left(g_k K^2 \frac{r}{\epsilon(r)} - \frac{1}{\epsilon(r)} \left(\frac{1}{r} + \frac{1}{\epsilon(r)} \frac{d\epsilon(r)}{dr} \right) \right) \Psi = 0 \quad (3-13)$$

where

$$g_k K^2 = \epsilon(r) \frac{\omega^2}{c^2} - k_z^2, \quad (3-14)$$

with

$$g_k = \begin{cases} +1 \\ -1 \end{cases} \quad \text{if } \epsilon(r) \frac{\omega^2}{c^2} - k_z^2 \begin{cases} \geq 0 \\ < 0 \end{cases}$$

Only a discrete set modes will match boundary conditions (corresponding to a discrete parameters K_n). These satisfy the following general Sturm-Liouville type of orthogonal relation

$$\int_0^{r_w} \Psi_m(r) \Psi_n(r) \frac{r}{\epsilon(r)} dr = C_n \delta_{m,n}.$$

To avoid ambiguity, we rewrite the wave Eq. (3-13) in the following form:

$$\frac{d}{dr} \left(\frac{r}{\epsilon(r)} \frac{d\Psi_n(r)}{dr} \right) + \left(g_k K_n^2 \frac{r}{\epsilon(r)} - \frac{1}{\epsilon(r)} \left(\frac{1}{r} + \frac{1}{\epsilon(r)} \frac{d\epsilon(r)}{dr} \right) \right) \Psi_n(r) = 0 \quad (3-15)$$

where

$$g_k K_n^2 = \epsilon(r) \frac{\omega_n^2}{c^2} - k_z^2$$

with n being the discrete mode number, which correspond to a TM_{0n} mode.

Solution in Region 1

Let us denote the vacuum region ($0 \leq r \leq r_d$) as region 1, and dielectric liner region ($r_d < r \leq r_w$) as region 2. In region 1, $\epsilon(r)=1$, so the wave Eq. (3-15) becomes

$$\frac{d}{dr} \left(r \frac{d\psi_{n1}(r)}{dr} \right) + \left(g_{k1} K_{n1}^2 r - \frac{1}{r} \right) \psi_{n1}(r) = 0 \quad (3-16)$$

with

$$g_{k1} K_{n1}^2 = \frac{\omega_n^2}{c^2} - k_z^2 \quad (3-17)$$

where g_{k1} can be +1 or -1, which is implicitly decided by the dispersion relation we are going to derive or more specifically, $g_{k1} = +1$ corresponds to a fast wave (wave with phase velocity faster than the speed of light in vacuum), $g_{k1} = -1$ correspond to a slow wave (wave with phase velocity slower than the speed of light in vacuum). Only this latter mode can couple to the negative energy slow space charge wave of the beam. The general solutions can be written as

$$\psi_{n_1}(r) = \frac{W_1(K_{n_1}r)}{ik_z K_{n_1}} \quad (3-18)$$

where

$$W_\ell(K_{n_1}r) = \begin{cases} J_\ell(K_{n_1}r) & \text{if } g_{k_1} = +1 \\ I_\ell(K_{n_1}r) & \text{if } g_{k_1} = -1 \end{cases} \quad (3-19)$$

and J_ℓ , I_ℓ are respectively ℓ^{th} order Bessel and modified Bessel functions of the first kind. From Eqs. (3-11), (3-12) we get

$$E_z(r) = W_0(K_{n_1}r)$$

$$E_r(r) = \frac{-ik}{K_{n_1}} W_1(K_{n_1}r) \quad (3-20)$$

$$B_\theta(r) = \frac{-i\omega}{K_{n_1}c} W_1(K_{n_1}r)$$

Solutions in region 2

In region 2 ($r_d < r \leq r_w$) $\epsilon(r) = \epsilon = \text{const}$, so the wave Eq. (3-15) becomes

$$\frac{d}{dr} \left(r \frac{d\psi_{n_2}(r)}{dr} \right) + \left(K_{n_2}^2 r - \frac{1}{r} \right) \psi_{n_2}(r) = 0$$

where

$$K_{n_2}^2 = \epsilon \frac{\omega_n^2}{c^2} - k_z^2, \quad (3-21)$$

Note that we have neglected g_{k_2} since $\epsilon \frac{\omega^2}{c^2} - k_z^2$ will be always positive. The general solutions for Ψ_{n_2} can be written as

$$\Psi_{n_2}(r) = \frac{\epsilon}{ik_z K_{n_2}} Z_1(K_{n_2} r) \quad (3-22)$$

with

$$Z_\ell(K_{n_2} r) = a_n J_\ell(K_{n_2} r) + b_n Y_\ell(K_{n_2} r) \quad (3-23)$$

where Y_ℓ is the ℓ^{th} order of the Bessel function of second kind and a_n, b_n are constants which are dependent on the mode and are decided by the boundary conditions. From Eqs. (3-11), (3-12) we get

$$E_z(r) = Z_0(K_{n_2} r)$$

$$E_r(r) = \frac{-ik_z}{K_{n_2}} Z_1(K_{n_2} r) \quad (3-24)$$

$$B_\theta(r) = \frac{-i\epsilon\omega_n}{K_{n_2} c} Z_1(K_{n_2} r)$$

The Dispersion Relation

Now, let us apply the boundary conditions at the conducting wall $r = r_w$, and at the interface $r = r_d$. At the conducting wall the parallel component of electric field has to be zero, that is, $E_z(r_w) = 0$, which yields

$$z_0(K_{n2}r_w) = 0$$

or

$$a_n J_0(K_{n2}r_w) + b_n Y_0(K_{n2}r_w) = 0 \quad (3-25)$$

At the interface, the radial component of the electric displacement \underline{D}_r and the parallel components of electric and magnetic fields have to be continuous, which yields

$$\frac{W_1(K_{n1}r_d)}{K_{n1}} = \frac{\epsilon}{K_{n2}} Z_1(K_{n2}r_d),$$

and

(3-26)

$$W_0(K_{n1}r_d) = Z_0(K_{n2}r_d).$$

From Eqs. (3-25), (3-26) we can solve the dispersion relation of the empty dielectric coated waveguide to be

$$\begin{aligned} & \frac{K_{n2}}{K_{n1}} W_1(K_{n1}r_d) \left(J_0(K_{n2}r_d) Y_0(K_{n2}r_w) - J_0(K_{n2}r_w) Y_0(K_{n2}r_d) \right) - \\ & \epsilon W_0(K_{n1}r_d) \left(J_1(K_{n2}r_d) Y_0(K_{n2}r_w) - J_0(K_{n2}r_w) Y_1(K_{n2}r_d) \right) = 0, \quad (3-27) \end{aligned}$$

and the two constants a_n , b_n to be

$$\begin{aligned} a_n &= \frac{\pi}{2} K_{n2} r_d \left(\frac{K_{n2}}{K_{n1} \epsilon} W_1(K_{n1}r_d) Y_0(K_{n2}r_d) - W_0(K_{n1}r_d) Y_1(K_{n2}r_d) \right) \\ b_n &= \frac{\pi}{2} K_{n2} r_d \left(W_0(K_{n1}r_d) J_1(K_{n2}r_d) - \frac{K_{n2}}{K_{n1} \epsilon} J_0(K_{n2}r_d) W_0(K_{n1}r_d) \right) \end{aligned} \quad (3-28)$$

Algorithm

From Eqs. (3-17) and (3-21), for a given k_z there are an infinite number of solutions for ω_n , K_{n1} , and K_{n2} . These eigenmodes, determined from dispersion relation, are orthogonal among each other as has been mentioned before. A general proof that is valid for all cylindrical symmetric systems in which the modes do not change (except for phase) along the axis has been given by Marcuse [19]. We want the algorithm adapted in our computer model to include transient phenomena, therefore, the frequency ω_n cannot appear explicitly in any of the equations used in the simulations. To satisfy this requirement, Eqs. (3-17) and (3-21) can be combined and replaced by:

$$K_{n1} = \left(\frac{1}{\epsilon} \left| K_{n2}^2 - (\epsilon-1)k_z^2 \right| \right)^{1/2}. \quad (3-29)$$

Therefore for each fourier mode specified by k_z , we can have Bessel basis specified by K_{n2} 's since K_{n1} can then be calculated from Eq. (3-29). Indeed, the expressions for the field components given by Eq. (3-20) for region 1 and given by Eq. (3-24) for region 2 are single-Fourier-Bessel modes. Similarly, the source term, i.e. the current density, which will appear for a Cherenkov maser, can also be expanded in this specified Fourier-Bessel space. The procedure is in essence to decompose the field into harmonic oscillators (the above modes) and then find their self consistent

response to the charge and current of the beam. The guided modes are waveforms that can actually be excited by electrons if they are in Cherenkov resonance with the wave (phase velocity matching). The electron density is assumed to be tenuous so that the waveform is unaffected by the presence of the electrons. The resulting time evolution equations to be solved for the electromagnetic field for each (k_z, K_{n2}) mode are

$$\left. \begin{aligned} \frac{\partial E_z}{\partial t}(k_z, K_{n2}, t) &= cK_{n1}(k_z, K_{n2}) B_\theta(k_z, K_{n2}, t) - 4\pi j_z(k_z, K_{n2}, t) \\ \frac{\partial E_r}{\partial t}(k_z, K_{n2}, t) &= -ick_z B_\theta(k_z, K_{n2}, t) - 4\pi j_r(k_z, K_{n2}, t) \end{aligned} \right\} (3-30)$$

$$\frac{\partial B_\theta}{\partial t}(k_z, K_{n2}, t) = -ick_z E_r(k_z, K_{n2}, t) - cK_{n1}(k_z, K_{n2}) E_z(k_z, K_{n2}, t)$$

where j_z and j_r are, respectively, the electron current in the axial and radial direction and are determined by summing electron axial and radial velocities. Every time step, the electromagnetic fields are transformed from the Fourier-Bessel space into the real space and the resulting electromagnetic forces are used in the relativistic equation of motion to push the electron momentum:

$$\frac{d\vec{P}}{dt} = q \left(\vec{E} + \frac{\vec{P} \times \vec{B}}{mc(1+P^2/m^2c^2)^{1/2}} \right) \quad (3-31)$$

where \vec{E} and \vec{B} consist of the self-consistent fields from Eq. (3-30), the imposed guiding DC magnetic field, as well as the externally

applied electromagnetic fields (if there are). The electron location can then be advanced by knowing its velocity. The code developed here is called a stretched one-and-two-halved dimensional code; z , v_z is one dimension, v_r , v_θ are each a half dimension. The code is stretched in the sense that some transverse dependence of the electromagnetic fields is kept through the assumption that the fields are superpositions of the modes of the empty dielectric-coated waveguide. The transverse positions of the electrons are kept fixed at their initial location.

In order to insure that each eigenmode in the simulation code has the correct propagation characteristic of the dielectric-coated waveguide described in (3-27), a small number of electrons is introduced into the waveguide to excite the guided mode fluctuations. The time evolutions of the first fifteen lowest k_z modes are followed and a frequency spectrum analysis was carried out. The dispersion relation calculated from the periodic code is shown in Fig. 3-1b as solid dots along with the theoretical calculation (solid line) for the following parameters: $r_d = 0.425\text{cm}$, $r_w = 0.625\text{cm}$, and $\epsilon = 3.78$. They agree quite well. The computer model includes multi-axial modes and can be easily modified to take into account many transverse modes (many n 's). However, only the results from a single transverse-mode calculation will be presented since this is the simplest meaningful case and the physics is not essentially changed by the inclusion of more modes.

§3. Thermal Effects on Saturated Output Power

The Cherenkov maser, which is investigated here, makes use of the interaction between a confined mildly relativistic electron beam (~ 200 Kev) and an electromagnetic wave guided by a dielectric-coated waveguide. The maser amplifying action of the device takes place by the continuous interaction between the axial component of the wave electric field and the electron beam. As shown in Fig. 3-1b, an electron beam with a specified energy will interact strongly with the wave which is in phase velocity synchronism with the beam. The initial electromagnetic field can come from thermal fluctuations on the electron-beam or it can be externally injected. The electrons initially tend to bunch in regions where the electric force ahead is decelerating and the electric force behind is accelerating. If the electron bunches move slightly faster than the wave, the wave on the average gains energy at the expense of the electron kinetic energy. The wave grows continually to reach an amplitude such that its quiver velocity $v_{os} = (2eE_z/mk_z)^{1/2}$ becomes larger than the velocity difference Δv between the initial electron drifting velocity v_b and the wave phase velocity v_p . At this instant, the electron orbits change from freely passing over the wave into trapped motion. The electron bunches that start on top of the potential well of the E_z field will reach the bottom through trapping oscillations. The maximum amount of kinetic energy an electron is able to transfer to the wave is given by $\Delta\gamma mc^2$, where $\Delta\gamma$

can be expressed as [20]:

$$\Delta\gamma = \gamma_0 - \frac{1}{\left(1 - \frac{(v_b - 2\Delta v)^2}{c^2}\right)^{1/2}}, \quad (3-32)$$

with γ_0 being the initial relativistic factor of the electron beam, i.e. $\gamma_0 = (1 - v_b^2/c^2)^{-1/2}$. The phase velocity of the wave can be determined from the linear dispersion relation of a beam-loaded dielectric waveguide and the efficiency of the device can be evaluated by the expression $\eta = \Delta\gamma/(\gamma_0-1)$.

In order to study the effects of an electron momentum spread and variation of the beam current on the output power, a series of computer simulations has been carried out. A mildly relativistic electron beam with energy of 217 keV ($\gamma_0=1.42$) and current of 12 A, which is relevant to the parameters of a recent experiment [1], has been chosen for simulations. Using a beam with a 1-percent momentum spread, the time evolutions of the wave energy of the most unstable mode, the averaged electron kinetic energy, and phase space plots of z , p_z are displayed in Figs. 3-2 and 3-3. The wave energy initially exhibits exponential growth (Fig. 3-2b) with a growth rate of $\omega_i = 0.058 \omega_c$ ($\omega_c=c/r_w$), which is in good agreement with the linear dispersion relation given in [14], and saturates at $\omega_c t \approx 145$. The slow oscillations after saturation are the signature of electron trapping. The oscillations in electron kinetic energy are out of

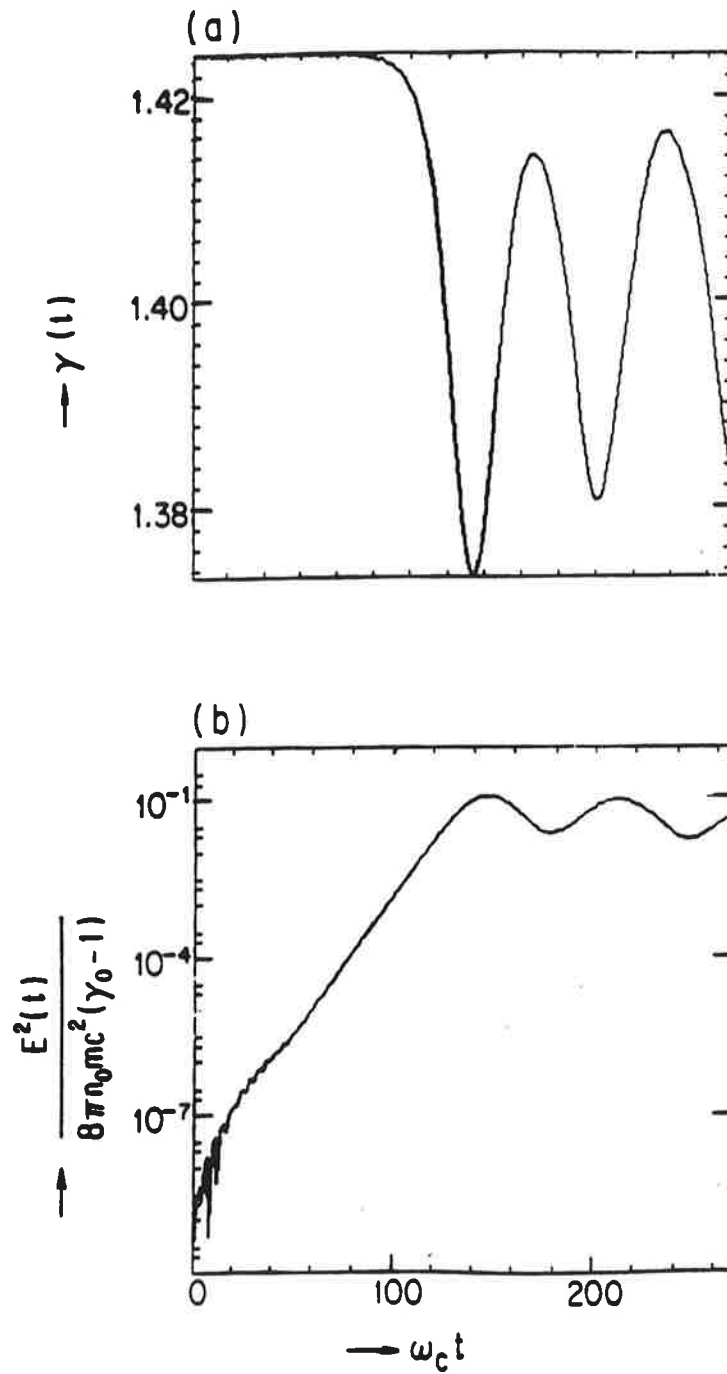


Fig. 3-2 The time evolution of (a) the averaged beam kinetic energy, (b) the wave energy using an electron beam with 1% momentum spread.

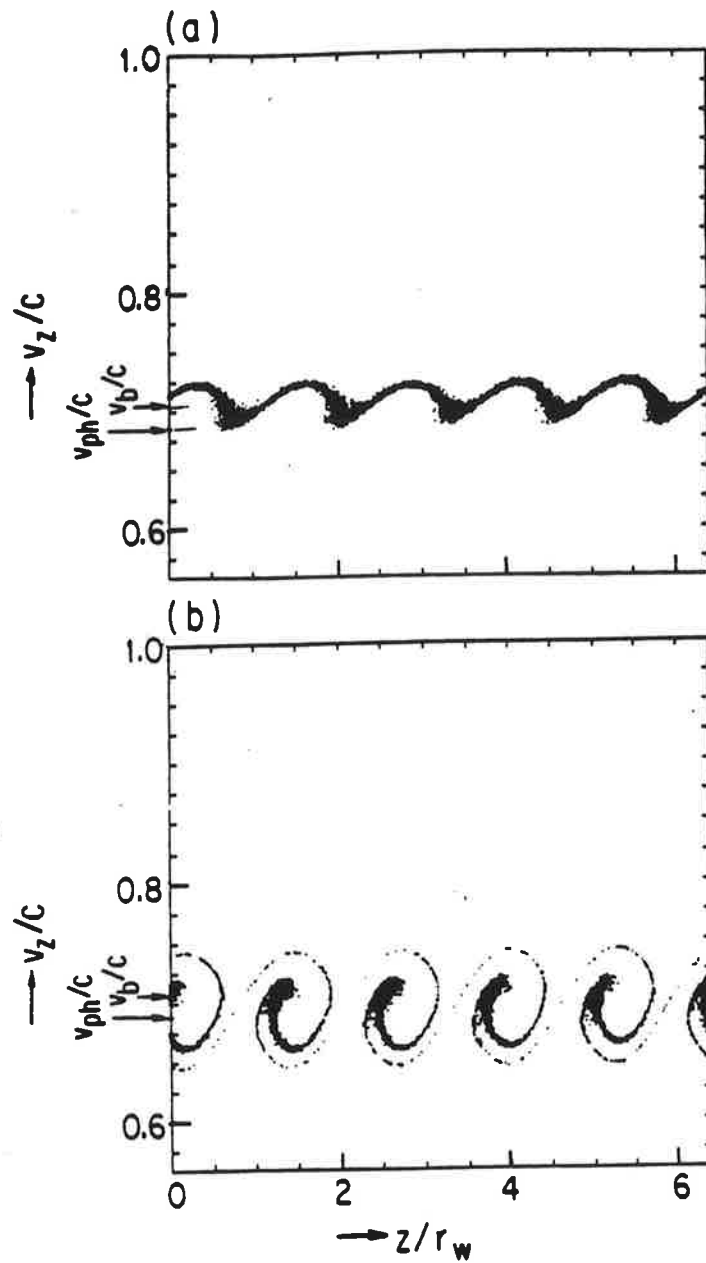


Fig. 3-3 The time history of the axial electron phase space at (a) $\omega_c t = 120$ and (b) $\omega_c t = 160$.

phase with the oscillation in wave energy because for half of the oscillation period the electron bunches give up kinetic energy to the wave and in the other half period the wave gives back part of its energy to the electrons. From Fig. 3-2, the saturation efficiency is about 12 percent, which gives a wave output power of 312 KW. The electron phase-space plot at $\omega_c t = 120$ (Fig. 3-3a) clearly demonstrates the early stage of electron-bunch formation by the electromagnetic wave, and Fig. 3-3b shows the electron bunches executing trapping oscillation in the potential well. The modulation period estimated from Fig. 3-2b is $\omega_c t_m \approx 60$ which is very close to the oscillation period for a resonant electron in the trough of a wave of amplitude $\omega_c t_p = 2\pi(m/keE_s)^{1/2}$, where E_s is the saturated electric-field amplitude. The velocity difference $\Delta v/c$ estimated from Fig. 3-3b is about 0.25, which should result in an efficiency of 15 percent. This is larger than the result from Fig. 3-2b and is due to the fact that (3-32) is an upper-bound estimation which assumes that all the electrons give up the same maximum amount of kinetic energy to the wave. As is evident from Fig. 3-3b, the electrons trapped in the potential well possess a broad distribution in energy. (The average $\Delta\gamma$ and wave energy are in good agreement).

The momentum spread of the experimental electron beam source is usually larger than 1 percent. It is important to investigate how much momentum spread a Cherenkov maser is able to tolerate before its gain or efficiency are seriously reduced. The ratio between the

axial length L of the system and the most unstable wavelength λ determines how many axial modes are within the gain curve. This ratio is about five in the simulations and only one axial mode is observed to reach large amplitude. The increase in momentum spread will broaden the gain curve to encompass more axial modes and reduce the obtainable gain because the finite electron momentum distribution moves the phase velocity of the unstable wave downward relative to the position where the maximum of the momentum distribution slope occurs [14]. If the ratio L/λ is small enough that only one axial mode is excited even with finite momentum spread, the downward shift in wave phase velocity tends to increase Δv , which should result in higher efficiency. To elucidate the consequences of a finite momentum spread, a series of computer simulations were carried out in which the momentum spread varied from 1 to 7.5 percent. The simulation result with 3.5 percent momentum spread reveal that the dominant mode in the system has the same axial wavenumber as that of the cold-beam case. The time evolution of the wave energy is plotted in Fig. 3-4a, which indicates that both the gain ($\omega_i = 0.033 \omega_c$) and efficiency ($\eta = 5$ percent) are reduced substantially from the cold-beam results. The gain is close to the value predicted from a warm-beam dispersion relation derived in [14]. These can be explained by observing the axial phase-space plot at the time of saturation (Fig. 3-4b), which shows that due to the initial axial velocity spread, the electron bunches are not as tight as for the cold-beam case and the electron

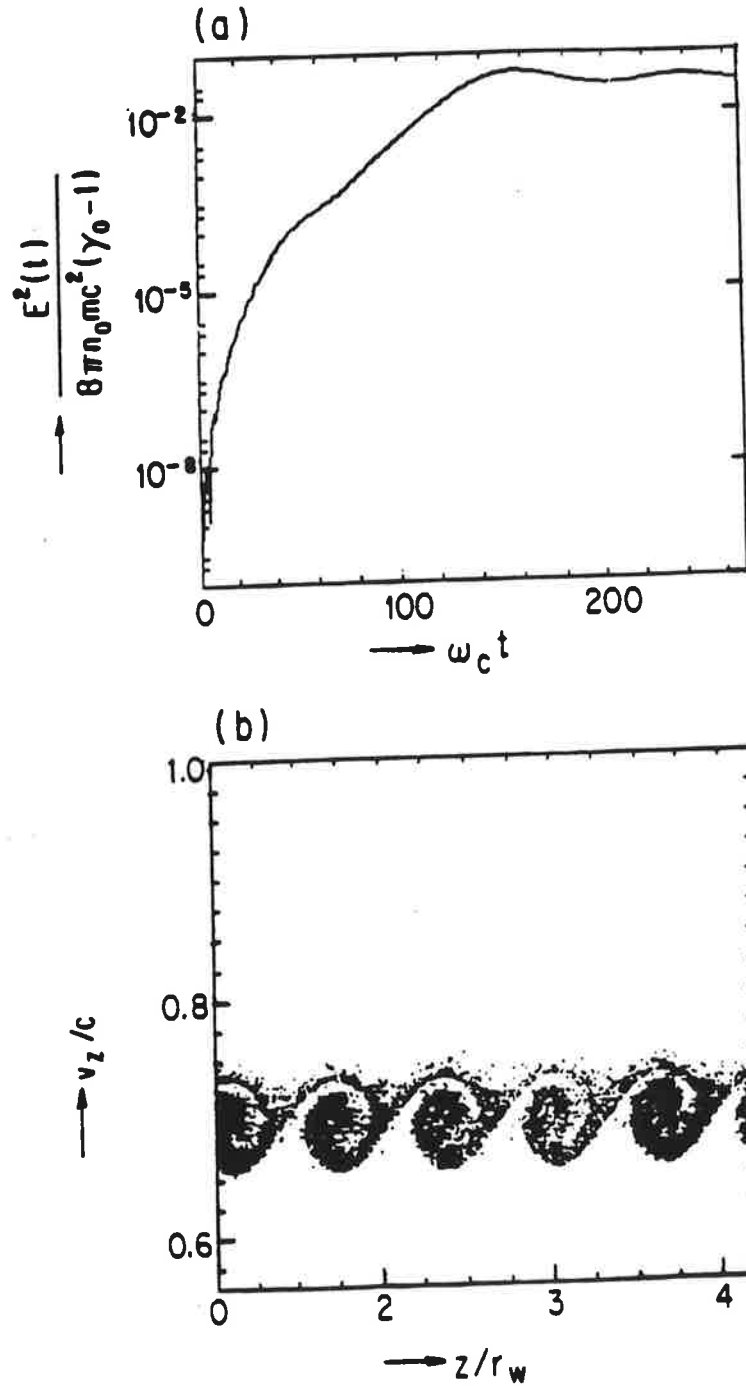


Fig. 3-4 The simulation results using an electron beam with 3.5% momentum spread. (a) the time evolution of the wave energy, (b) the axial electron phase space at $\omega_c t = 160$.

velocity distribution in the potential well is very broad. Overall, there are still more electrons losing energy than gaining energy and a finite but reduced amount of electron kinetic energy can still be transferred to the wave. It is important to know how the efficiency depends on the momentum spread. Fig. 3-5a shows the results obtained from simulation; the efficiency goes to zero at around 7.5-percent momentum spread.

For microwave devices it is important to know the non-linear output power scaling with the electron beam current. The scaling can be derived by arguing [14] that the saturated electron axial velocity perturbation induced by the axial component E_z of the wave electric field is $(v_p - v_b) \approx \omega_1/k$, and from the axial component of the equation of motion E_z is proportional to (ω_1^2/k) . Since the output wave power is proportional to $|E_z|^2$ and the growth rate ω_1 increases with the one-third power of the beam density, the scaling of the output power with the beam current can be expressed as

$$P_o \propto I^{1/3} P_b \quad (3-33)$$

Eq. (3-33) states that the nonlinear efficiency and wave output power of a Cherenkov maser increases, respectively, with the one-third and four-third power of the beam current. In order to verify these scaling laws, the current of for cold-beam case is varied from a few amperes to a few kiloamperes. The results from the simulation

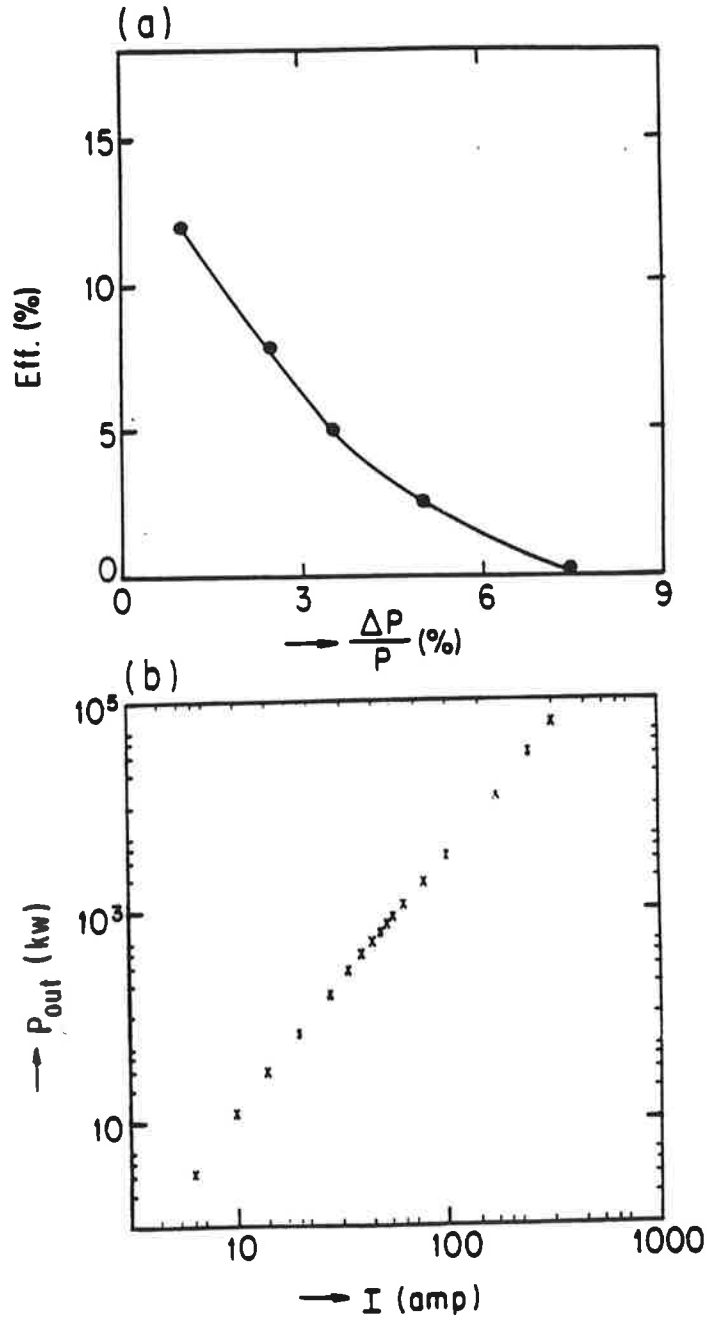


Fig. 3-5 The effects varying the momentum spread and the current on the performance of the Cherenkov maser (a) the nonlinear efficiency versus the momentum spread (b) the saturated power as a function of the electron beam current for cold beam.

are presented in Fig. 3-5b, which shows that the output power follows (3-33) very closely and there is no saturation in sight even with kiloamperes of beam current. However, as the beam current reaches kiloamperes, space-charge effects which are not treated correctly will become important. Since a Cherenkov maser is based on the coupling between the waveguide mode and the slow space-charge wave, the inclusion of the space-charge force, which has been discussed in [21], should reduce the growth rate but increase the efficiency. Enhancement in wave output power can be achieved by using various schemes which have been investigated in the area of wiggler free electron lasers. A dc electric-field-enhancement scheme will be explored through computer simulation in the following section.

§3-4. Output Power Enhancement

In a free electron laser the conversion of electron kinetic energy into wave energy can be enhanced by tapering either the wiggler strength or period [23] adiabatically to prolong the resonance interaction between the electrons and the wave. This conversion-enhancement concept was demonstrated in experiments with a few-percent taper [24]. For a Cherenkov maser the wavelength scaling is [25]

$$\lambda = 2\pi d \left(\frac{\epsilon-1}{\epsilon} \right)^2 \quad (3-34)$$

The same idea of conversion enhancement can be adopted in this case by tapering the thickness of the dielectric layer to compensate for the reduction in the electron energy. On the other hand, if the output power of the device is the only concern, a dc axial electric field can be imposed at the time or location of saturation. This dc electric field does work on trapped electrons without accelerating them and transforms the dc energy into wave energy. This output-power enhancement concept has been demonstrated by computer simulations for free electron lasers [21,22]. In this section, computer simulation will be carried out to show that the dc field-enhancement scheme will also work for Cherenkov masers because the saturation mechanism in this case is also due to electron trapping.

If only one axial mode is excited, a static potential well produced by the E_z field can be defined in the wave frame and the characteristics of electron-wave interactions, such as bunching and trapping, can be clearly displayed by following the time evolution of the electron axial phase space. In the trapping process, the electron bunches are in the decelerating phase until they reach the bottom of the potential well. It is plausible that electron bunches can be clamped to stay in the decelerating phase by imposing an axial force such as a dc axial electric field. In this way, the electron bunches behave like a transformer medium which convert dc

electric energy into wave energy. This enhancement scheme is most easily demonstrated by using a cold electron beam. At the time of saturation, virtually the entire electron population is observed to be trapped by the excited potential well in the conventional Cherenkov maser, which has been described in the previous section. However, it can be shown [23] that the imposition of an axial force will tilt the potential well and some of the originally trapped electrons will be spilled out of the well and become untrapped. This detrapping phenomenon is exhibited in Fig. 3-6, which shows the time history of the axial electron phase space. In generating the results for Fig. 3-6 the parameters of Fig. 3-3 are used and an axial dc electric field $E_{dc} = 0.16E_0$ ($eE_0/mc\omega_c = 0.05$) is imposed at $\omega_c t = 140$, which is slightly before the time of saturation, $\omega_c t = 145$, so that the electron bunches are still in the decelerating phase. As expected, the action of the axial electric field forces the main part of the trapped electrons to stay in the retarded phase of the wave (they are in force balance, i.e., $E_{DC} + \langle E_w \rangle = 0$) and the remaining part runs away from the potential well. The untrapped electrons are freely accelerated by the axial force and are lost to the interaction.

In order to obtain the optimal dc electric-field strength for the enhancement scheme, E_{dc} is varied from $0.06 E_0$ to $0.27 E_0$ and the resulting time evolution of the wave energy is shown in Fig. 3-7. The wave energy appears to increase linearly with time after the dc

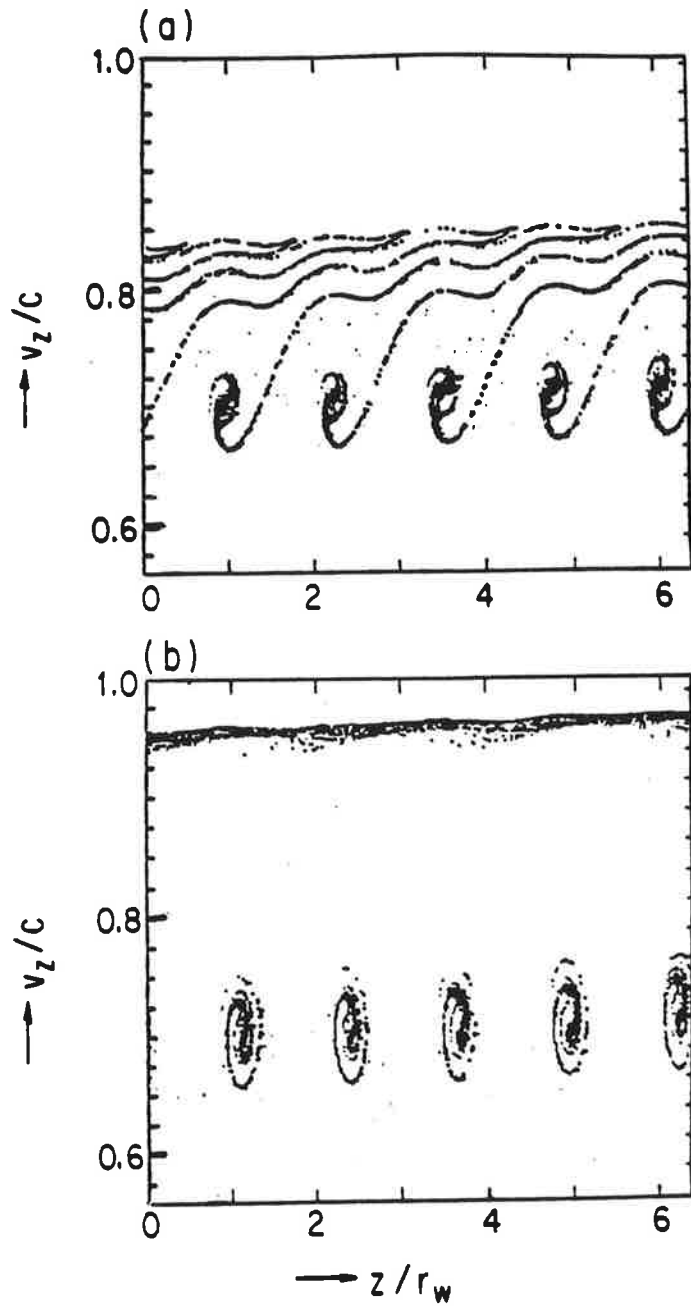


Fig. 3-6 The time history of the axial electron phase space with $E_{dc} = 0.18 E_0$ at (a) $\omega_c t = 192$, (b) $\omega_c t = 384$.

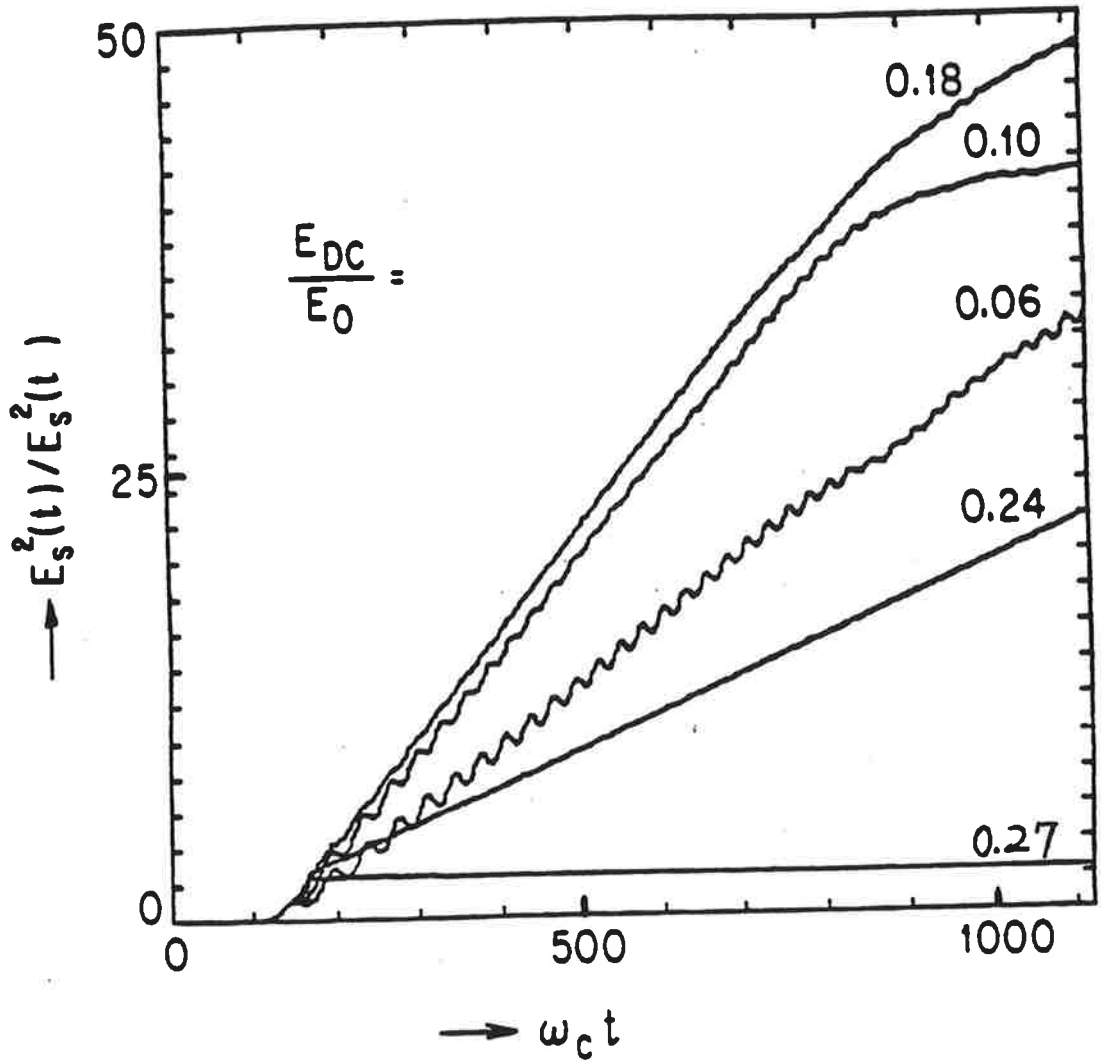


Fig. 3-7 The time evolution of the signal wave energy with different DC electric field strength imposed at $\omega_c t = 140$.

electric field is turned on and can be expressed by the relation

$$E_g^2(t) = E_g^2(\tau_0) \left(1 + \Gamma(t - \tau_0) \right) \quad (3-35)$$

where τ_0 is the dc electric field turn-on time, $E_g^2(\tau_0)$ is the wave energy at $t = \tau_0$, which is very close to the saturation energy of a conventional Cherenkov maser, and Γ is the rate of wave energy enhancement. The enhancement rate Γ is observed to be proportional to the product of the imposed dc electric-field strength and the number of the trapped electrons. This dependence can be understood by noting that the total rate of the radiation generation depends on the number of electrons in the radiating bunches and the radiating rate of a given electron depends on its phase and the force exerted on it. One may be tempted to use a strong dc electric field to achieve a large enhancement rate. However, if the imposed-field strength is too strong, the potential well is tilted and the particles will spill out over the lower peak; no electron will be left in the well to transfer the dc electric energy into wave energy. To find the optimal E_{dc} , the enhancement rate and the fraction of the electrons which remains trapped as a function of E_{dc} are given in Fig. 3-8. The curve for the enhancement rate peaks at $E_{dc} \approx 0.18E_0$. With this dc electric-field strength, a factor of 10 enhancement can be easily accomplished by just doubling the length of a conventional system. During the enhancement process, the dc electric-field energy required for the interaction is also increased

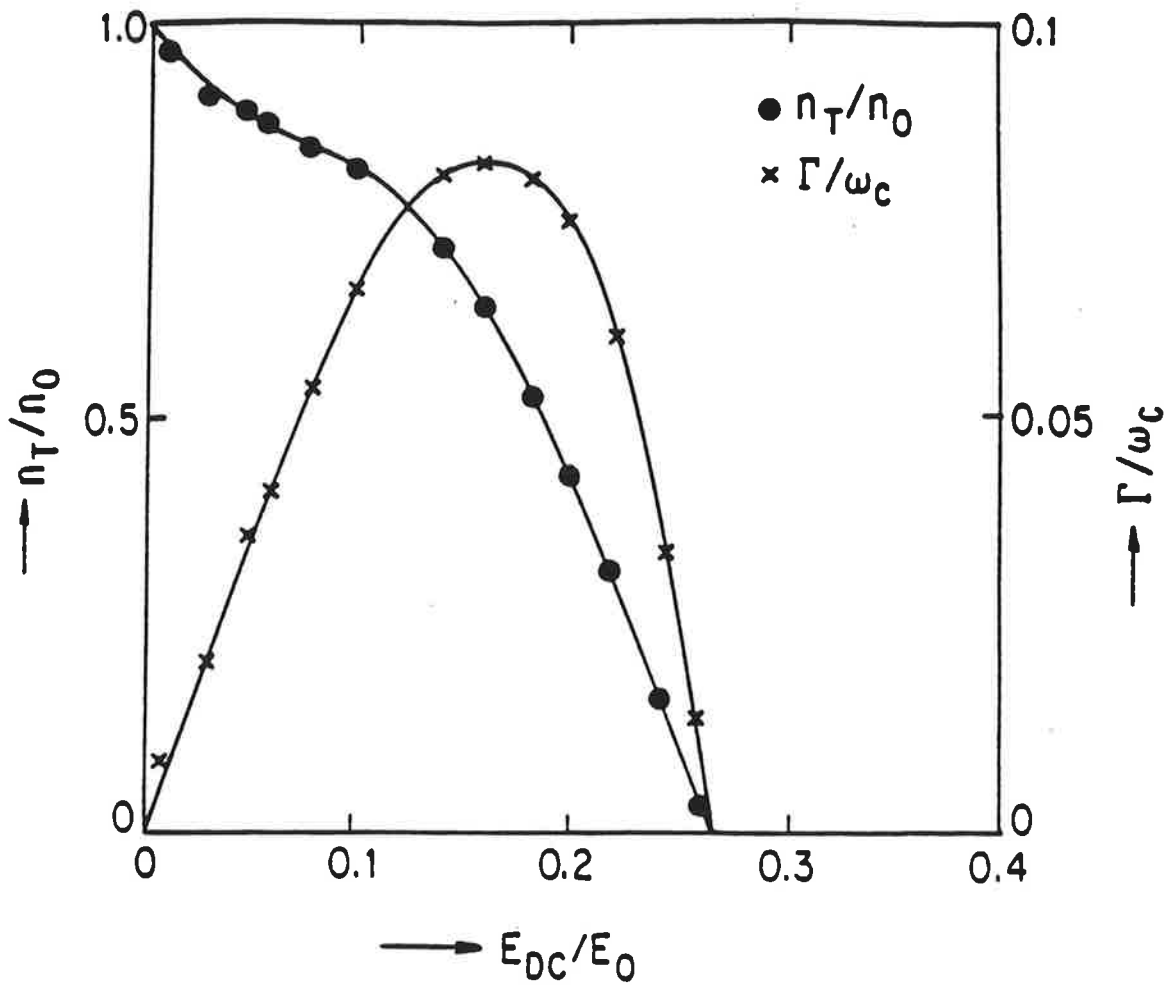


Fig. 3-8 The fraction of electrons that remains trapped and the enhancement rate of the signal wave energy as a function of the DC electric field strength.

with time and part of the externally supplied energy goes into accelerating the runaway electrons. Unless the untrapped electrons can be taken out of the system, the enhancement process can only improve the output power but not the overall efficiency.

§3-5. Summary

In this chapter we have successfully developed a particle simulation model to study the performance of a Cherenkov maser using a dielectric coated wave-guide. With a 12 Amp and 220 KV electron beam, the simulation results show that for a device where only single axial mode is excited, the frequency and the saturation output power of the excited wave are respectively about 26 GHz and 310 KW. The simulation results also show that the electron momentum spread tends to reduce the gain and the nonlinear efficiency. It has also been demonstrated by our simulations that the output power of a conventional Cherenkov maser can be improved by an order of magnitude if an appropriate axial DC electric field is imposed immediately prior to the saturation. However, the output power enhancement will ultimately be limited by the excitation of the side band modes through the coulomb interaction among the electrons in different bunches [26]. The effects of multi-mode excitation on the enhancement process remain to be investigated.

§3-6. Reference

- [1] S. Von Laven, J. Branscum, J. Golub, R. Layman, and J. Walsh, Appl. Phys. Lett. 41, 408 (1982).
- [2] K. L. Felch, K. O. Busby, R. W. Layman, D. Kapilow, And J. E. Walsh, Appl. Phys. Lett. 38, 601 (1981).
- [3] O. Heaviside, Philos. Mag. Feb., p. 130; Mar. p.202; May, p. 379; Oct., p. 360; Nov., p434; Dec., p. 488 (1888).
- [4] A. Sommerfeld, Göttinger, Nachrichten 99, 363 (1904).
- [5] P. A. Cherenkov, Dokl. Akad. Nauk SSSR 2, 451 (1934).
- [6] E. Curie, "Madame Curie." Heinemann, London, 1941.
- [7] L. Mallet, C.R. Acad. Sci. 183, 274; 187, 222; 188, 445 (1926).
- [8] I. M. Frank and I. Tamm, Dokl. Akad. Nauk SSSR 14 ,109 (1937).
- [9] V. L. Ginzburg, Dokl. Akad. Nauk SSSR 3, 253 (1947).
- [10] J. V. Jelley, Cherenkov Radiation and Its Applications, Pergamon, London (1958).
- [11] P. Coleman and C. Enderby, J. Appl. Phys. 31, 1695 (1960).
- [12] M. Danos, J. Appl. Phys. 26, 2 (1953).
- [13] H. Lashinsky, J. Appl. Phys. 27, 631 (1956).
- [14] J. E. Walsh, Advances in Electronics and Electron Physics, vol. 58, p. 271 (1982).
- [15] M. A. Piestrup, R. A. Powell, G. B. Rothbart, C. K. Chen, and R. H. Pantell, Appl. Phys. Lett. 28, 92 (1976).
- [16] A. N. Chu, M. A. Piestrup, T. W. Barbee, and R. H. Pantell, Proc. Int. Conf. Lasers, P.744-749 (1978).

- [17] J. M. Dawson, Rev. Mod. Phys. 55, 403 (1983).
- [18] J. M. Dawson and A. T. Lin, Handbook of Plasma Physics, Vol. II, edited by A. A. Galeev and R. N. Sudan, 555 (1984).
- [19] D. Marcuse, Light Transmission Optics (Bell Lab Series). New York, Van Nostrand Reinhold, 1972.
- [20] A. T. Lin, W. W. Chang, and Y. T. Yan, IEEE Trans. Plasma Sci. Vol. PS-13, No. 6, 531 (1985).
- [21] A. T. Lin, Phys. Rev. Lett., 46, 1515 (1981).
- [22] A. T. Lin, Phys. Fluids, 24, 316 (1981).
- [23] N. M. Kroll, P. L. Morton, and M. N. Rosenbluth, Phys. Quant. Elec., 7, 113 (1980).
- [24] J. A. Edighoffer, G. R. Neil, C. E. Hess, T. I. Smith, S. W. Fornaca, and H. A. Schwettman, Phys. Rev. Lett. 52, 344 (1984).
- [25] J. Walsh, B. Johnson, G. Dattoli, and A. Renieri, Phys. Rev. Lett., 53, 779 (1984).
- [26] A. T. Lin, Phys. Rev. Lett., 46, 1515 (1981); A. T. Lin, Quantum Electronics, Vol. 9, 867, (1982).

Chapter 4

Laser-Plasma Accelerators

In this chapter, we investigate electron acceleration by laser-plasma interaction. This is of special interest because the phase velocity of the generated plasma wave which is used to accelerate the electrons can be made to be close to the speed of light c , i.e., $v_p \lesssim c$, and the electric field supported by such a plasma wave can be as high as 10^9 volts/cm for a plasma with density of 10^{18}cm^{-3} . Particular attention is given to generating the wave by injecting a monochromatic laser from the side into the plasma column (A Side-Injected-Laser-Plasma Accelerator).

§4-1 Introduction

For the last two chapters we have been concentrating on the generation of radiation by relativistic electrons and their concomitant loss of energy. This process can be inverted so that the electrons can be accelerated by their interaction with radiation. While some physicists are interested in the acceleration of charged particles by their direct interaction with radiation such as in the inverse free electron laser scheme [1], and in the Cherenkov

accelerator scheme [2], we are particularly interested in the acceleration of electrons by their indirect interaction with radiation (lasers) through the plasma medium (Laser-Plasma Accelerators). There are special advantages of using plasmas as a medium to accelerate electrons; they are capable of supporting large longitudinal electrostatic waves (i.e. space charge waves for which the wave vector \underline{k} is parallel to the electric field \underline{E}) with phase velocity $v_p \lesssim c$. Furthermore, while the usual slow wave structures eventually break down as the accelerating gradient is increased, plasmas do not suffer from this limitation since they are already ionized.

§4-2 Plasma Wave Breaking

For the time being, let us not discuss how the plasma waves are set up but accept that there exist some schemes which can excite large amplitude plasma waves. In this section, we will discuss how large the acceleration gradients that the plasmas can potentially support can be.

The maximum amplitude that a plasma wave can reach is determined by the wave breaking condition [3] which occurs when the electrons at the crest of the wave (and moving with it) overtake the electrons in the trough of the wave (moving opposite to the wave). For such a

condition the electron density perturbation, δn , is roughly n_0 , the equilibrium density (Through this chapter we will assume that the neutralizing background ions are immobile since the ions are much heavier than the electrons. We also assume cold plasma systems). This is reasonable since the largest density rarefaction that can occur is when all of the plasma electrons are removed, as schematically shown in Figure 4-1. Then, assuming a sinusoidal wave, from poisson's equation $\nabla \cdot \vec{E} = 4\pi e(\delta n)$, we get

$$E_{\max} = \frac{4\pi n_0 e}{k},$$

where k is the plasma wave number. Since the natural frequency of the plasma wave for a cold plasma is $\omega_p^2 = 4\pi e^2 n_0 / m$ regardless of the plasma wave number, the phase velocity for a plasma electrostatic wave with wave number k is $v_p = \omega_p / k$ which is the maximum electron velocity at wavebreaking. For a good accelerator we require that the phase velocity of the plasma wave be close to the speed of light, i.e. $v_p \lesssim c$, so that the injected pre-accelerated electrons can be driven by and stay in phase with the electric field of the plasma wave for a sufficient distance to gain high energies. Indeed, there exist some mechanisms, as we shall discuss later, that can excite such a plasma wave (space charge wave with $v_p \lesssim c$). If we assume the approximation $v_p = \omega_p / k \approx c$, then we get

$$E_{\max} \sim \frac{mc\omega_p}{e} = E_m \sim \sqrt{n_0 \cdot [\text{cm}^{-3}]} \quad \text{V/cm}$$

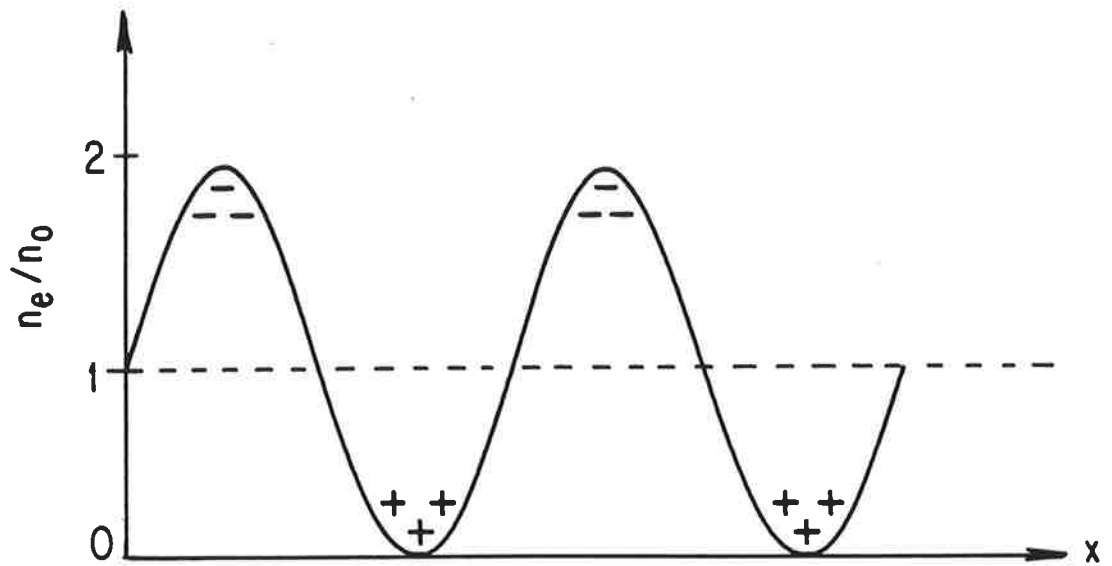


Fig. 4-1 Schematical illustration of the maximum electron density perturbation for a cold plasma with average density n_0 .

This is the maximum acceleration gradient that a plasma with density n_0 can support. Although this is a rough calculation, a more rigorous analysis shows it to be correct [3]. In practice, such a highly nonlinear wave will not be easily achieved. However, plasma electrostatic waves with saturated electrostatic field amplitude $E_g = \epsilon_g E_m$, where ϵ_g ranging from 0.2 to 0.5, are found to be possible in computer simulations. Let us take an example to see how large this acceleration gradient can be. For a plasma with density of 10^{16}cm^{-3} (a value which has been obtained over meter lengths), the acceleration gradient can be $E_g = 2-5 \text{ GV/m}$. Comparing it with 20-100 MV/m, typical acceleration gradients of the conventional accelerators, we see how effective it can be.

§4-3 Acceleration Mechanisms

Let us assume that we have a plasma electrostatic wave with amplitude $E_g = \epsilon_g E_m$ and relativistic phase velocity v_p . Then there are some questions which automatically come to our minds: "How does this wave accelerate electrons?", "Is there any initial required condition for those electrons to be accelerated?", "Is there a limit on the energy gain of the accelerated electrons?", "What about the luminosity and emittance of the driven electron beam after it has been

accelerated?". Although some questions will be answered toward the end of this chapter, most of the questions will be answered here.

Trapping Threshold

For an electron to be accelerated by the plasma wave, it has to be trapped by the wave and be positioned in the wave so as to feel a force in the same direction as the wave phase velocity v_p , as schematically shown in Figure 4-2. Although the wave amplitude is considered to be large with $\epsilon_g = 0.2 \sim 0.5$, due to the large phase velocity of the wave ($v_p \sim c$), there usually exists a trapping threshold, that is, an electron must have a minimum initial velocity along the direction of the wave phase velocity, v_p , in order for it to be trapped by the wave. We now calculate the trapping threshold.

From the relativistic velocity addition formula

$$v = \frac{v_p + v'}{1 + \frac{v_p v'}{c^2}}, \quad \text{or} \quad \beta = \frac{\beta_p + \beta'}{1 + \beta_p \beta'}$$

where v' is assumed to be the electron velocity in the wave frame (it could be positive or negative, with "positive" representing the direction along v_p), v is the electron velocity in the laboratory frame, $\beta' = v'/c$, $\beta_p = v_p/c$, and $\beta = v/c$, we get

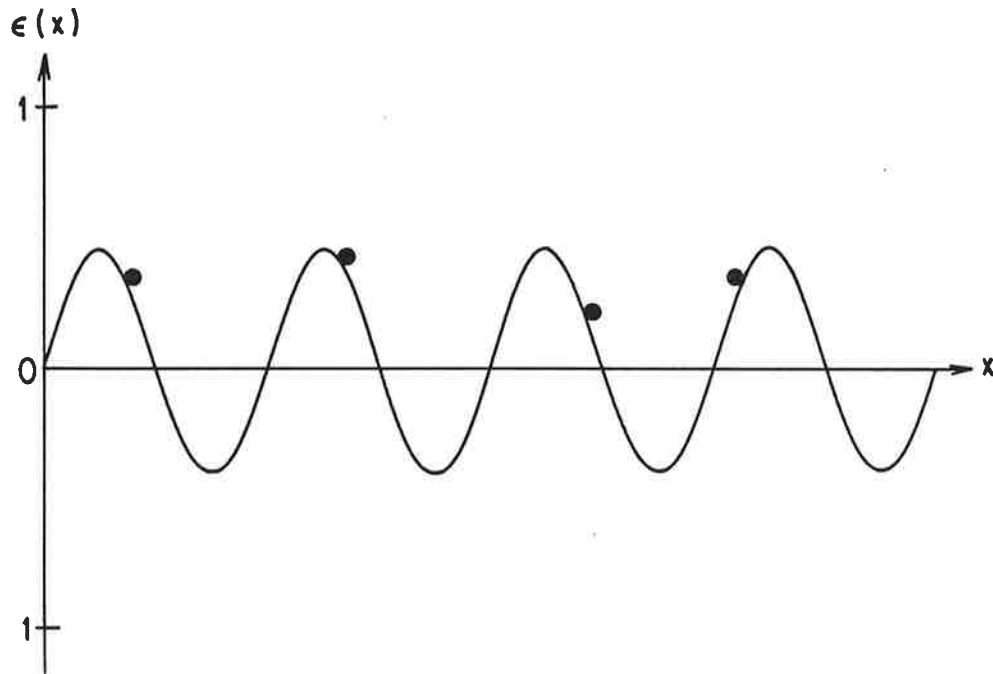


Fig. 4-2 Schematical illustration of the electron acceleration by a electrostatic plasma wave.

$$\begin{aligned}
\gamma &= (1-\beta^2)^{-1/2} = ((1+\beta)(1-\beta))^{-1/2} \\
&= \left(\left(\frac{1+\beta_p+\beta'+\beta_p\beta'}{1+\beta_p\beta'} \right) \left(\frac{1-\beta_p-\beta'+\beta_p\beta'}{1+\beta_p\beta'} \right) \right)^{-1/2} \\
&= \left(\frac{(1-\beta_p^2)(1-\beta'^2)}{(1+\beta_p\beta')^2} \right)^{-1/2}
\end{aligned}$$

or

$$\gamma = \gamma_p \gamma' (1 + \beta_p \beta'), \quad (4-1)$$

where

$$\gamma_p = (1 - \beta_p^2)^{-1/2}, \quad \gamma' = (1 - \beta'^2)^{-1/2}$$

In the wave frame, an electron can be trapped within the potential trough only if its kinetic energy, $(\gamma'-1)mc^2$, is less than the potential energy difference between the peak potential point and its position, that is,

$$(\gamma'-1)mc^2 < e(\phi'_{\text{peak}} - \phi'_{\text{electron}}) \equiv \Gamma\phi'_A, \quad (4-2)$$

where ϕ'_A is the plasma wave potential amplitude in the wave frame and $0 \leq \Gamma \leq 2$, depends on the electron position. As an example, for an electron that happens to be at the bottom of the potential trough, we have $\Gamma = 2$. Assuming a sinusoidal wave form, ϕ'_A can be calculated to be

$$\phi'_A = \frac{E'_A}{k'}$$

where E'_A and k' are the wave electric amplitude and wave number respectively in the wave frame. Since the longitudinal electric field is invariant under Lorentz transformation, we readily get

$$E'_A = E_s = \epsilon_s E_m = \epsilon_s \frac{mc\omega_p}{e}.$$

On the other hand, using the relativistic transformation formula

$$\begin{bmatrix} k'c \\ i\omega' \end{bmatrix} = \begin{bmatrix} \gamma_p & i\beta_p\gamma_p \\ -i\beta_p\gamma_p & \gamma_p \end{bmatrix} \begin{bmatrix} kc \\ i\omega_p \end{bmatrix}$$

for the wave number and frequency, and remembering that $v_p = \beta_p c = \omega_p / k$, we get $k' = k / \gamma_p$. This is reasonable since the wave length, $\lambda' = 1 / k'$, in the wave frame will be Lorentz contracted into the wave length, $\lambda = 1 / k$, in the laboratory frame such that $\lambda = \lambda' / \gamma_p$. We therefore get:

$$\phi'_A = \gamma_p \beta_p \epsilon_s mc^2 / e. \quad (4-3)$$

Substituting Equation (4-3) into Equation (4-2), we get

$$\gamma' < 1 + \Gamma \gamma_p \beta_p \epsilon_s, \quad (4-4)$$

and thus

$$-\left(1 - (1 + \Gamma \gamma_p \beta_p \epsilon_s)^{-2}\right)^{1/2} < \beta' < \left(1 - (1 + \Gamma \gamma_p \beta_p \epsilon_s)^{-2}\right)^{1/2}. \quad (4-5)$$

Substituting Equations (4-4), (4-5) into Equation (4-1), we get

$$\gamma > \gamma_p (1 + \Gamma \gamma_p \beta_p \epsilon_s) \left\{ 1 - \beta_p \left(1 - (1 + \Gamma \gamma_p \beta_p \epsilon_s)^{-2} \right)^{1/2} \right\} \equiv \gamma_{\text{th}}(\Gamma), \quad (4-6a)$$

or

$$\gamma < \gamma_p (1 + \Gamma \gamma_p \beta_p \epsilon_s) \left\{ 1 - \beta_p \left(1 - (1 + \Gamma \gamma_p \beta_p \epsilon_s)^{-2} \right)^{1/2} \right\} \equiv \gamma_{\ell}(\Gamma). \quad (4-6b)$$

Equation (4-6a) tells us the minimum energy an electron must possess in order to be trapped by the wave. It is this required minimum energy that prevents the background electrons from being trapped. Therefore we must inject a bunch of pre-accelerated electrons for it to be accelerated (driven bunch). The general criterion for the minimum energy the injected electrons must possess is obtained by taking $\Gamma=1$ (since the injected electrons will in general start at zero potential) in Equation (4-6a) so as to get

$$\gamma_{\text{th}}^{\text{av}} = \gamma_p (1 + \gamma_p \beta_p \epsilon_s) \left\{ 1 - \beta_p \left(1 - (1 + \gamma_p \beta_p \epsilon_s)^{-2} \right)^{1/2} \right\}. \quad (4-7)$$

Numerical examples with ϵ_s ranging from 0.1 to 0.6 and β_p ranging from 0.96 to 0.9999 are given in Table 4-1.

We wish to point out that an excellent approximate solution

$$\gamma_{\text{th}}^{\text{av}} \approx \gamma_p^2 \left(\epsilon_s + 1/\gamma_p - \beta_p \left((\epsilon_s + 2/\gamma_p) \epsilon_s \right) \right) \quad (4-8)$$

for the average trapping threshold can be found in Ref. [4]. If both Equation (4-7) and (4-8) do not look obvious, an even simpler solution

TABLE 4-1

Minimum energies the injected electrons should possess						
$\beta_p \backslash \epsilon_s$	0.10	0.20	0.30	0.40	0.50	0.60
0.9600	3.7e-1	1.9e-1	9.9e-2	5.0e-2	2.2e-2	6.8e-3
0.9700	4.3e-1	2.2e-1	1.2e-1	6.1e-2	2.8e-2	1.0e-2
0.9800	5.3e-1	2.7e-1	1.5e-1	7.8e-2	3.8e-2	1.6e-2
0.9900	7.2e-1	3.6e-1	1.9e-1	1.1e-1	5.5e-2	2.5e-2
0.9950	9.1e-1	4.4e-1	2.4e-1	1.3e-1	7.1e-2	3.4e-2
0.9980	1.2e+0	5.4e-1	2.9e-1	1.6e-1	8.8e-2	4.4e-2
0.9990	1.3e+0	6.0e-1	3.2e-1	1.8e-1	9.8e-2	5.0e-2
0.9995	1.5e+0	6.6e-1	3.5e-1	1.9e-1	1.1e-1	5.5e-2
0.9998	1.7e+0	7.1e-1	3.7e-1	2.0e-1	1.1e-1	6.0e-2
0.9999	1.8e+0	7.4e-1	3.8e-1	2.1e-1	1.2e-1	6.2e-2

TABLE 4-2

Maximum energies for an optimally trapped electron						
$\beta p \lambda \epsilon_g$	0.10	0.20	0.30	0.40	0.50	0.60
0.9600	4.9e+0	7.6e+0	1.0e+1	1.3e+1	1.5e+1	1.8e+1
0.9700	6.3e+0	9.8e+0	1.3e+1	1.7e+1	2.0e+1	2.3e+1
0.9800	8.9e+0	1.4e+1	1.9e+1	2.4e+1	2.9e+1	3.4e+1
0.9900	1.6e+1	2.6e+1	3.7e+1	4.7e+1	5.7e+1	6.7e+1
0.9950	2.9e+1	5.0e+1	7.0e+1	9.1e+1	1.1e+2	1.3e+2
0.9980	6.6e+1	1.2e+2	1.7e+2	2.2e+2	2.7e+2	3.2e+2
0.9990	1.2e+2	2.3e+2	3.3e+2	4.3e+2	5.3e+2	6.3e+2
0.9995	2.3e+2	4.4e+2	6.4e+2	8.5e+2	1.1e+3	1.3e+3
0.9998	5.6e+2	1.1e+3	1.6e+3	2.1e+3	2.6e+3	3.1e+3
0.9999	1.1e+3	2.1e+3	3.1e+3	4.2e+3	5.2e+3	6.2e+3

$$v_{th}^{av} \approx \frac{1 - \alpha^2}{1 + \alpha^2} c \quad \text{for } \alpha < 1,$$

with $\alpha = \epsilon_s + 1/\gamma_p$, can be found in Ref. [5].

Maximum Energy Gain

While Equation (4-6a) tells us the lower bound energy, $\gamma_{th}(\Gamma)$, an electron must possess in order to be trapped by the wave, Equation (4-6b) tells us the upper bound energy, $\gamma_\ell(\Gamma)$, a trapped electron can reach. Taking $\Gamma=2$, that is, considering that the electron position happens to be at the bottom of the wave potential trough, we get

$$\gamma_{th}^{max} = \gamma_p (1 + 2\gamma_p \beta_p \epsilon_s) \left\{ 1 + \beta_p \left[1 - (1 + 2\gamma_p \beta_p \epsilon_s)^{-2} \right]^{1/2} \right\}. \quad (4-9)$$

This is the maximum energy an optimally trapped electron can reach. Numerical examples for Equation (4-9) are given in Table 4-2. Initially, For an optimally trapped electron to be at the the bottom of the potential trough, its required energy is (taking $\Gamma=2$ in Equation (4-6a))

$$\gamma_{th}^{min} = \gamma_p (1 + 2\gamma_p \beta_p \epsilon_s) \left\{ 1 - \beta_p \left[1 - (1 + 2\gamma_p \beta_p \epsilon_s)^{-2} \right]^{1/2} \right\}. \quad (4-10)$$

Therefore its possible maximum energy gain after being accelerated

is

$$\gamma_{\text{Gain}}^{\text{max}} = \gamma_{\ell}^{\text{max}} - \gamma_{\text{th}}^{\text{min}} = 2 \gamma_p (1 + 2\gamma_p \beta_p \epsilon_s). \quad (4-11)$$

With a typical ϵ_s ($\epsilon_s = 0.2 \sim 0.5$), for $\gamma_p \gg 1$, the maximum energy gain can be expressed as

$$\gamma_{\text{Gain}}^{\text{max}} \approx 4 \epsilon_s \gamma_p^2,$$

or

$$\gamma_{\text{Gain}}^{\text{max}} \approx \gamma_p^2, \quad (4-12)$$

if we take $\epsilon_s \approx 0.25$.

Surfatron

From Equation (4-11) or (4-12), we find out that the energy gain for a driven particle is essentially proportional to γ_p^2 . Therefore, as long as we can excite a plasma wave with an extremely high γ_p , we would be able to achieve ultra-high energy gain for the driven particles. For example, if $\gamma_p = 1000$, we would be able to get $\gamma_{\text{Gain}}^{\text{max}} \approx 10^6$, i.e. 0.5 TeV energy gain for an driven electron. However, high γ_p means high trapping thresholds. Furthermore, there may be a problem in exciting very high γ_p waves and obtain high gradients

simultaneously, particularly with the laser beat wave excitation scheme. Remember that $\gamma_p \cong \omega/\omega_p$ (where ω is the laser frequency) and plasma wave electrostatic field, E , is proportional to ω_p . Since the maximum energy gain of the driven particle is limited by dephasing to $4\gamma_p^2 mc^2$, this severely restricts the energy output of such an accelerator if a very high gradient is desired. We therefore ask the question, whether there is any way to increase the energy gain beyond the dephasing limit without increasing γ_p ?

Before we answer this question, let us briefly review the reason for the limited energy gain. The energy gain limitation is basically due to the dephasing of trapped electrons with the wave, that is, a trapped electron which is at an accelerating phase will eventually reach a velocity that is larger than the plasma wave phase velocity, v_p , and then begin to outrun the plasma wave so as to slide down the potential well until it reaches the bottom of the potential trough where it attains its maximum energy. After that, it begins to lose energy by climbing the potential hill. In view of this, the only way to improve the energy gain without increasing γ_p is to prevent the driven electrons from outrunning the plasma wave, that is, to keep the driven electron longitudinal velocity, $v_{||}$, at v_p (or around v_p) so that the electrons can be kept in an accelerating part of the bucket. To achieve this, we need to allow each of the driven electrons to be accelerated transverse to \underline{k} in such a way that

$$v_{||} = p_{||}/m\gamma \cong v_p \quad (4-13)$$

where

$$\gamma = \left(1 - \frac{v_{||}^2}{c^2} - \frac{v_{\perp}^2}{c^2} \right)^{-1/2} = \left(1 + \frac{p_{||}^2 + p_{\perp}^2}{m^2 c^2} \right)^{1/2}$$

Is this possible? Let us assume there exists an appropriate constant (or near constant) transverse force acting on each of the driven electrons. Then, while $p_{||}$ is increasing due to the longitudinal force $eE_g \sin k(x-v_p t)$, γ is also increasing, not only due to the increase of $p_{||}$, but also due to the increase of p_{\perp} so that Equation (4-13) could be satisfied. If $v_{||} > v_p$ (or $v_{||} < v_p$), then the driven electron will outrun (or be outrun by) the plasma wave and reach a position with a smaller (or larger) longitudinal electric field such that the increasing rate of $p_{||}$ is smaller (or larger) than that of γ , and thus $v_{||}$ will eventually reach a value $\leq v_p$ (or $\geq v_p$), and the process starts over again; $v_{||}$ will asymptotically reach v_p at some point in the wave. While $v_{||}$ is oscillating around v_p , both $p_{||}$ and p_{\perp} keep increasing such that the velocity of the driven electron, $v = (v_{||}^2 + v_{\perp}^2)^{1/2} = (p_{||}^2 + p_{\perp}^2)^{1/2}/m\gamma$, asymptotically reach c , the speed of light.

There are two possible ways to achieve this constant (or near constant) transverse force on the driven electrons; One is to apply

a transverse DC electric field \underline{E}_t , and the other is to apply a transverse DC magnetic field \underline{B}_t . However, the imposition of a transverse DC electric field will also accelerate the background plasma so as to destroy the plasma wave. On the other hand, the DC magnetic field, \underline{B}_t , will not; although it exerts a large transverse force, $e v_{||} B_t / c \sim e v_p B_t / c$, on the driven electrons, the background electrons are essentially not affected except doing harmless cyclotron motion since their velocities are small. Indeed, this (imposition of a transverse DC magnetic field of magnitude $B_t \lesssim E_s / \gamma_p$ on the system) is found to be a successful scheme in 1D computer simulations [6]. It is the so-called "surfatron" mechanism and was originally suggested by Katsouleas and Dawson [7] in trying to improve the performance of the Plasma-Beat-Wave Accelerator (PBWA).

Special care has to be taken with the magnitude of the imposed transverse DC magnetic field. If the transverse force is too large, the increase in $p_{||}$ will not be able to compete with the increase in γ even at the position of the peak plasma wave electric field E_s . In such a case, $v_{||}$ keeps reducing and thus the driven electrons will be eventually outrun by the plasma wave so as to become detrapped. To decide the maximum allowable B_t , the best way is to work in the wave frame instead of the laboratory frame. In this frame, the longitudinal equation of motion can be written as:

$$F_{||}' = \frac{dp_{||}'}{dt} = -e(E_s \sin k'x' - \beta_{||}' B_{\perp}')$$

where $B_{\perp}' = \gamma_p B_{\perp}$, $\beta_{||}' = v_{||}'/c$. In order that the driven electrons will not become detrapped, $v_{||}' = p_{||}'/\gamma'$ has to be kept around 0. This requires that $F_{||}'$ be around 0, which is possible only if $\beta_{||}' B_{\perp}'$ can always be less than E_s , i.e. $B_{\perp}' < E_s/\beta_{||}'$. Since $\beta_{||}'$ can be as large as 1, the maximum allowable B_{\perp} would be

$$B_{\perp}^{\max} = E_s/\gamma_p.$$

Similarly, if a transverse DC electric field E_{\perp} is applied (only for theoretical reference), the maximum allowable E_{\perp} would be $E_{\perp}^{\max} = E_s/\gamma_p \beta_p$, since, in this case, we would have $B_{\perp}' = \gamma_p \beta_p E_{\perp}$.

§4-4 Laser-Driven Plasma Waves

So far we have always assumed the existence of a relativistic plasma wave. In this section, we begin to discuss some of the possible ways to set them up by using one or more laser beams.

Beat-Wave Accelerator

One way to excite the plasma wave is to send an intense pulse of light through the plasma consisting of two colinear beating laser beams with beat frequency near the plasma frequency ω_p . If the laser frequencies are much larger than the plasma frequency, the phase velocity of the generated plasma wave will be near c , the speed of light. This is the so-called beat-wave accelerator and has received a great deal of attention since first proposed for accelerating electrons by Tajima and Dawson [8] in 1979. There have been some experimental works [9] in addition to a large number of theoretical publications on it. We now give a brief review.

Assume that the frequencies of the two colinear beating lasers are respectively ω_1 , ω_2 with $\omega_1 \approx \omega_2 \approx \omega \equiv (\omega_1 + \omega_2)/2 \gg \omega_p$ and the beating frequency $\Delta\omega = \omega_1 - \omega_2 = \omega_p$. Then, from the dispersion relation $\omega^2 = \omega_p^2 + k^2c^2$ for a light wave with frequency ω in the plasma, the phase velocity and group velocity of the light can be

readily calculated respectively to be

$$v_p^{\text{light}} = c \left(1 - \frac{\omega_p^2}{\omega^2}\right)^{-1/2} \gtrsim c$$

$$v_g^{\text{light}} = c \left(1 - \frac{\omega_p^2}{\omega^2}\right)^{1/2} \lesssim c$$

and the corresponding wavenumbers for the two lasers in the plasma are $k_1 = (\omega_1^2 - \omega_p^2)^{1/2}/c$, $k_2 = (\omega_2^2 - \omega_p^2)^{1/2}/c$. The beating wave length is $\lambda_{\text{beat}} = 2\pi/\Delta k$ where $\Delta k = k_1 - k_2$. It is the beating field envelope which exerts a pondermotive force to the plasma electrons in the longitudinal direction due to the gradient of the stress tensor [10] ($\propto \nabla E_{\text{beat}}^2$) that bunches and debunches the plasma electrons so as to generate the electrostatic plasma wave, as schematically shown in Figure 4-3. Since the driving frequency and wave length are respectively $\Delta\omega$ and λ_{beat} , the phase velocity of the electrostatic plasma wave is $v_p = \frac{\Delta\omega}{\Delta k} \cong \frac{\partial\omega}{\partial k} = v_g^{\text{light}} \lesssim c$, which fulfils the basic requirement for a good accelerator. The Eulerian [11] equation of motion for the plasma-wave electric field can be approximately expressed as (neglecting relativistic effects for the plasma electron motion):

$$\frac{\partial^2 \epsilon}{\partial t^2} + \omega_p^2 \epsilon = \frac{1}{2} \omega_p^2 \alpha_1 \alpha_2 \sin(\Delta k x - \Delta\omega t)$$

where ϵ is the wave electric field normalized to the cold-plasma wave-braking amplitude, $E_m = mc\omega_p/e$; $\alpha_1 = eE_1/mc\omega_1$ is a measure of

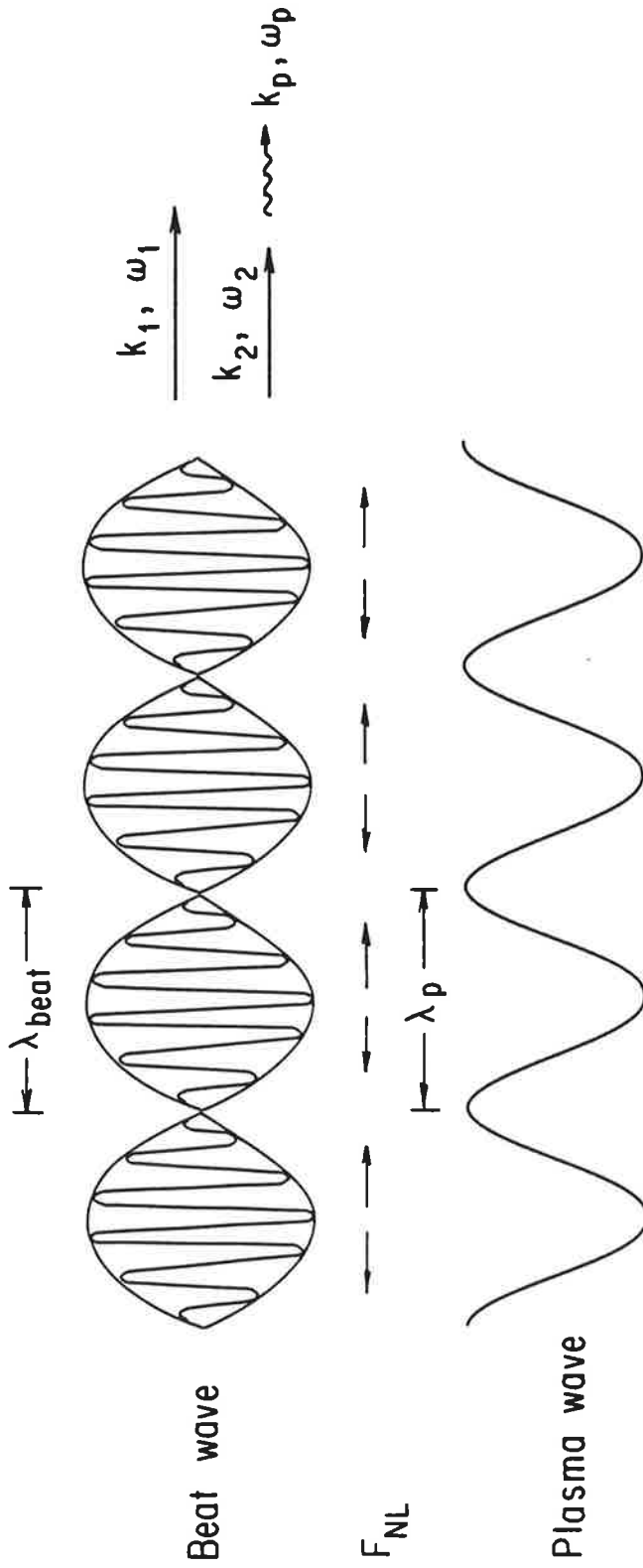


Fig. 4-3 Schematical illustration of the plasma wave excitation by a beat-wave.

the i^{th} laser pump intensity. The left hand side, $\partial^2 \epsilon / \partial t^2 + \omega_p^2 \epsilon = 0$ is the equation for the natural oscillation of the plasma and the right hand side, $\frac{1}{2} \omega_p^2 \alpha_1 \alpha_2 \sin(\Delta k x - \Delta \omega t)$ represents the driver which comes from the pondermotive force $(\underline{j}_1 \times \underline{B}_2 / c + \underline{j}_2 \times \underline{B}_1 / c)$ due to the two beating lasers. Since $\Delta \omega = \omega_p$, that is the plasma oscillation is in resonance with the driver, the plasma wave amplitude exhibits secular growth

$$\epsilon_A(t) = \frac{\alpha_1 \alpha_2}{4} \omega_p t \quad (4-15)$$

As ϵ_A grows, the electron oscillating velocity amplitude increase, and eventually relativistic effects sets in so that the effective electron plasma frequency is reduced due to the relativistic increase of the electron mass. This can be expressed as [12]

$$\omega_{\text{eff}} \approx \omega_p (1 - 3\epsilon_A^2 / 16).$$

This relativistic detuning effect is one of the important factor which causes the saturation of the driven plasma wave. Rosenbluth and Liu [12] derived the saturation amplitude due to this effect:

$$\epsilon_s = \left(\frac{16}{3} \alpha_1 \alpha_2 \right)^{1/3}, \quad (4-16)$$

which is valid for $\alpha_1, \alpha_2 \ll 1$.

In view of the relativistic mass change detuning effect, in order to get an optimal saturation electric amplitude, C.M. Tang, et al. [13] suggest that the beating frequency $\Delta\omega$ be slightly lower than ω_p . They gave the following formula for choosing the optimized beating frequency

$$\Delta\omega = \omega_p \left(1 - \frac{1}{2} (9\alpha_1\alpha_2/8)^{2/3} \right), \quad (4-17)$$

with corresponding saturation amplitude

$$\epsilon_s \approx 4(\alpha_1\alpha_2/3)^{1/3} \quad (4-18)$$

For example, if $\alpha_1=\alpha_2=0.1$, equation(4-17) would give $\Delta\omega = 0.975\omega_p$ and Equation (4-16), (4-18) would respectively give $\epsilon_s \approx 0.38, 0.6$. We find that a 2.5% down-shift in the laser beat frequency can cause about 50% increase in the saturation amplitude. We wish to point out that a controversy has arisen over the magnitude and sign of the nonlinear frequency shift recently. On the one hand, the work of Rosenbluth and Liu [12], Tang, Sprangle, and Sudan [13], and Noble [18] conclude that only relativistic effects contribute to the nonlinear frequency shift, while on the other hand Bingham, Cairns, and Evans [19], and Mendonca [20] claim that harmonics contribute an additional frequency shift larger in magnitude and opposite in sign to the relativistic one. With the exception of Noble the former group used Lagrangian coordinates. The later group used Eulerian

coordinates and also used the continuity equation rather than Ampere' law. More recently Warren Mori [14] has made a detailed investigation of this problem including effects not included in the earlier treatments. He finds that the conclusions of the former group, that only a relativistic amplitude dependent frequency shift exists, are correct. Since the later group used the continuity equation rather than Ampere' law which is a stronger condition in one dimension. Therefore, their set of equations possessed an ambiguity which they eliminated by requiring that the second order fluid velocity vanish, i.e. $\langle v_2 \rangle = 0$. This leads to a plasma drift and a doppler shifted frequency. This doppler shift is the additional frequency shift. By using Ampere's law, this drift is eliminated due to the induced electric field. If the later group had imposed the condition $\langle j_2 \rangle = 0$ instead of $\langle v_2 \rangle = 0$ in their derivation using the continuity equation, they would have obtained the correct result. Consequently, no plasma drift ensues and no doppler frequency shift exists.

A Side-Injected-Laser Plasma Accelerator

Although both theoretical and experimental studies have shown that the beat-wave accelerators can, achieve ultra-high acceleration gradients, as the light pulse propagates along exciting the plasma wave it suffers from pump depletion; that is, energy is transferred

from the lasers to the plasma waves causing their intensities to decrease. The laser frequencies cascade to lower values and the laser group velocities decrease. Since the dephasing length is comparable to the pump depletion length, It is reasonable therefore to consider multiple stages to achieve high energy. On the other hand, to circumvent the staging problem, due to dephasing the surfatron idea was invented, but the problem of pump depletion still remains. In view of this, if somehow we can inject the laser(s) into the plasma perpendicularly to the direction of acceleration and can still excite the desired plasma wave, then pump depletion could be overcome since fresh laser energy could be supplied to the acceleration region along its entire length. Let us introduce an initial density ripple in the plasma parallel to the plasma axis and assume that using a special arrangement, we can inject pulses of a linear polarized monochromatic laser, perpendicularly side by side, into the plasma column as shown in Figure 4-4. Let us further make the following assumptions:

1.) The laser frequency, ω_o , is only a little bit higher than ω_p , i.e. $\omega_o = (1 + \delta) \omega_p$, with $\delta \ll 1$.

2.) The laser electric field is linearly polarized along the axial (longitudinal) direction (here labeled as the x-direction) of the plasma column, or more specifically let the laser electric field in the plasma to be

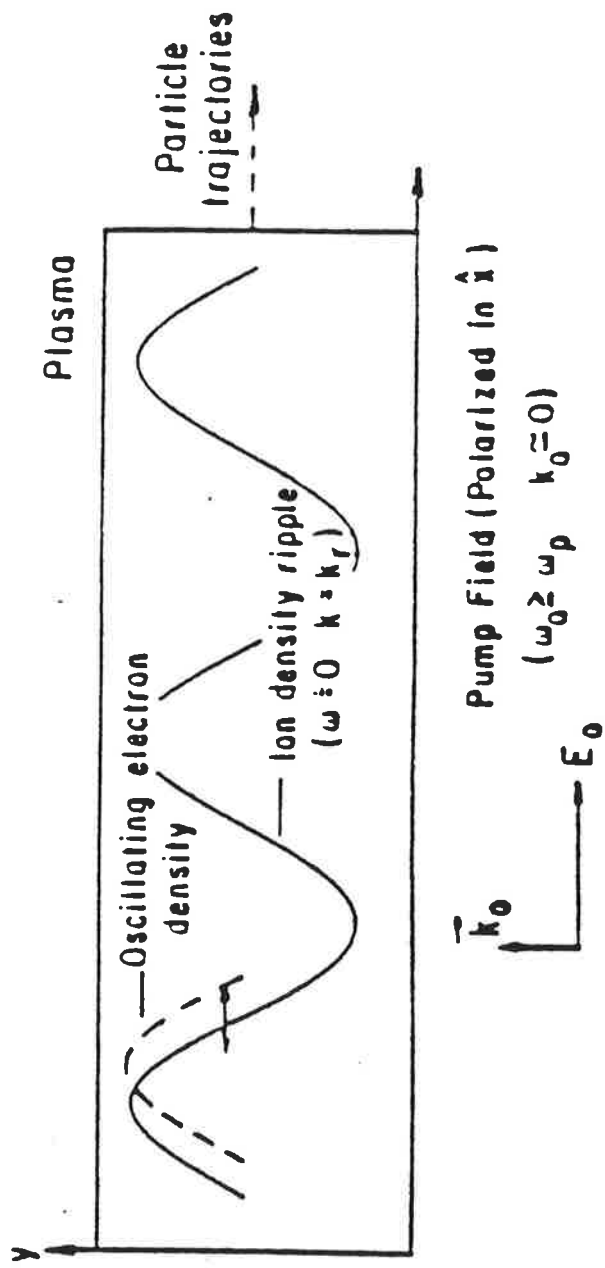


Fig. 4-4 A laser polarized along a preformed plasma density ripple wiggles electrons to produce a relativistic space charge wave.

$$\underline{E}_{\text{pump}} = E_0 \underline{e}_x \cos(k_0 y - \omega_0 t + \phi(x)), \quad (4-19)$$

where $k_0 \underline{e}_y$ is the wave vector of the laser in the plasma; $\phi(x)$ is the phase, which is dependent on x .

3.) The phase difference, $\Delta\phi$, between any two pulses of the laser is 0.

4.) The width of each laser pulse, w , equals to the distance between two consecutive pulses of the laser.

5.) The initial density ripple can be expressed as the following:

$$n_1(x) = n_0 + \delta n_0 \sin(k_1 x), \quad \text{with } \delta n_0 \ll n_0, \quad \omega_0/k_1 \lesssim c,$$

$$n_e(x, t=0) = n_1(x),$$

where n_1 and n_e are respectively the ion and electron density.

Assumption 1 gives ω_0 to be as close as possible to ω_p so that the plasma oscillation will be nearly resonant with the laser and thus respond strongly, but still high enough to allow the laser to penetrate the plasma. From the transmission coefficient for a plasma with a sharp boundary, which is given by $\tau = 4N(\omega_0)/(N(\omega_0) + 1)^2$,

where $N(\omega_0) = \left(1 - \frac{\omega_p^2}{\omega_0^2}\right)^{1/2}$, we get $\tau \approx 40\%$ to 80% for values of δ between 0.01 and 0.1; by using more gentle gradients, even better penetration can be obtained. Assumptions 3 & 4 imply that we can replace the phase, $\phi(x)$, in Equation (4-19) by a constant or 0. Furthermore, from the dispersion relation $\omega_0^2 = \omega_p^2 + k_0^2 c^2$ for the laser in the plasma, Assumption 5 gives $k_0 \approx \sqrt{2\delta} \omega_0/c \ll k_1$. Thus we can neglect the effects of the magnetic field of the laser since the magnitude of the magnetic field of the laser in the plasma is given by $B_{\text{pump}} = E_{\text{pump}} c k_0 / \omega_0 \lesssim \sqrt{2\delta} E_{\text{pump}} \ll E_{\text{pump}}$, and conclude that there is only one pump given by

$$\underline{E}_{\text{pump}} = E_0 \underline{e}_x \cos(k_0 y - \omega_0 t). \quad (4-20a)$$

This pump will couple to the plasma-density ripple so as to parametrically excite an electrostatic plasma wave. The resultant plasma wave has a wave vector $\underline{k}_p = k_0 \underline{e}_y \pm k_1 \underline{e}_x \cong k_1 \underline{e}_x$ ($k_0 \cong \sqrt{2\delta} \omega_p/c \ll k_1$) and frequency $\omega = \omega_0 \pm \omega_i \cong \omega_0$ (ω_i being the frequency of the ion acoustic wave, which is much smaller than ω_p) so that its phase velocity will be $v_p = \omega/k_p \cong \omega_0/k_1$. By a proper choice of k_1 , any phase velocity desired can be achieved; in particular, a phase velocity close to c can be obtained. Since k_0 is very small for $\omega_0 \gtrsim \omega_p$ and we are only interested in a limited range, Δy , from the plasma column edge in the y -direction such that $k_0 \Delta y \cong \sqrt{2\delta} \omega_0/c \Delta y \ll 2\pi$, we can neglect $k_0 y$ in Equation (4-20a). We then rewrite Equation (4-20a) as

$$\underline{E}_{\text{pump}} = E_0 \underline{e}_x \cos(\omega_0 t). \quad (4-20b)$$

We now give a linear derivation for the initial growth of the plasma wave. The electron density can be assumed to be

$$n_e(x,t) = n_1 + n_1(x,t).$$

Then, from poisson's equation, we get:

$$\frac{\partial E_p(x,t)}{\partial x} = -4\pi e n_1(x,t), \quad (4-21)$$

where E_p is the self-consistent plasma electrostatic field. The equation of motion can be expressed as:

$$\frac{dv(x,t)}{dt} = -\frac{e}{m} (E_p(x,t) + E_0 \cos(\omega_0 t)).$$

Taking $v(x,t) = 0 + v_{os}(t) + v_1(x,t)$, where $v_{os}(t) = -eE_0/m\omega_0$ is the response term to the laser field $\underline{E}_{\text{pump}}$, we get:

$$\frac{\partial v_1}{\partial t} = \frac{e}{m} E_p - v_{os} \frac{\partial v_1}{\partial x} \quad (4-22)$$

From the continuity equation

$$\frac{\partial n_e}{\partial t} + \frac{\partial}{\partial x} (n_e v) = 0,$$

we get

$$\frac{\partial n_1}{\partial t} + v_{os} \frac{\partial n_1}{\partial x} + n_1 \frac{\partial v_1}{\partial x} = 0. \quad (4-23)$$

Treating δn_0 and v_{os} as quasilinear terms, which is realistic for most of the cases, and substituting the partial derivative $\frac{\partial}{\partial x}$ of Equation (4-22) into the partial derivative $\frac{\partial}{\partial t}$ of Equation (4-27), we get

$$\frac{\partial^2 n_1}{\partial t^2} + \omega_p^2 n_1 = \delta n_0 \frac{eE_0}{m} k_i \cos k_i x \cos \omega_0 t, \quad (4-24)$$

where Equation (4-21) has been used. By using $\frac{\omega_p}{k_i} \sim c$, which is required for a good accelerator, Equation (4-24) can be further simplified as:

$$\frac{\partial^2 \epsilon}{\partial t^2} + \omega_p^2 \epsilon = \frac{\delta n_0}{n_0} \epsilon_0 \omega_p^2 \cos(k_i x) \cos(\omega_0 t), \quad (4-25)$$

where

$$\epsilon = \frac{n_1}{n_0} = \frac{E_p}{E_m}.$$

The right hand side of Equation (4-25) represents a driver for the plasma wave which is bilinear in the pre-density ripple, $\delta n_0/n_0$, and the laser intensity ϵ_0 . Since $\omega_0 \sim \omega_p$, It can be solved for the initial plasma wave growth:

$$\epsilon_A(t) = \frac{1}{2} \frac{\delta n_0}{n_0} \epsilon_0 \omega_p t, \quad (4-26)$$

where $\epsilon_A(t)E_m$ represents the superposed electric amplitude of two

waves, traveling in opposite directions, each with amplitude $\frac{1}{2} \epsilon_A E_m$ and phase velocity $\sim \omega_0/k_1$. The saturation amplitude can be roughly solved:

$$\epsilon_s = \epsilon_0(\delta n_0/n_0)/(1 - \omega_p^2/\omega_0^2) \sim \epsilon_0(\delta n_0/n_0)/2\delta. \quad (4-27)$$

This can compete with the beat wave accelerators as long as a small δ (say $\delta=0.01$ [$\tau \sim 40\%$]) is chosen.

Discussion

In order to match the available high power CO₂ lasers, the plasma density in the Side-Injected-Laser-Plasma Accelerator scheme (SIPLA) needs $n_0 \sim 10^{19} \text{ cm}^{-3}$, i.e., $\omega_p \sim 1.8 \times 10^{14} \text{ sec}^{-1}$. To excite a plasma wave with phase velocity near c in such a plasma, the wavelength of the pre-formed density ripple needs to be about $10 \mu\text{m}$. This can be done in a number of ways. One method uses a CO₂ laser pre-pulse to ionize a solid target upon which has been etched a grating of ten micron periodicity [15]. Since the etched grating can be controlled, we should be able to achieve a pre-formed density ripple with the desired wave number k_1 ; k_1 could in fact be a function of x so that the excited plasma wave phase velocity $v_p = \omega_0/k_1(x)$ matches that of the accelerated electrons and asymptotically reach c . For this to be successful, the maintenance of the accuracy of the

density ripple spacing and the plasma density over the length of the plasma column is severe. A second method that could be employed would be to set up a sound wave of the desired wave length in an unioized gas; the gas is then ionized by a flash of ultra-violet light and the resulting plasma irradiated with the laser.

§4-5 Computer Simulations

The processes for generating the plasma waves described in the last section are stongly nonlinear. A mixture of other nonlinear processes and instabilities may also appear. Therefore computer simulations which are capable of duplicating much of the nonlinear behavior of real plasmas are generally very helpful in investigating such problems. In this section, we use the side-injected-laser with rippled-plasma as an example for performing computer simulations to illustrate the validity of the approximations of our derivations and to identify the important self-consistant effects.

A one and two-halves dimensional (x, v_x, v_y, v_z) , relativistic, electromagnetic particle code has been used to simulate the process of the plasma wave generation and electron acceleration. this computational plasma model can follow the motion of more than 10^4 charged particles in their self-consitent electric and magnetic fields so as to duplicate much of the behavior of a real plasmas.

Immobile ions are distributed with a density profile of the form $n_i(x) = n_o + \delta n_o \sin k_i x$, and the electrons have the same distribution at the initial time. The laser field is modeled by simply applying to each electron at each time step a force of specified amplitude and frequency, $E_o \cos \omega_o t$, in the longitudinal direction (\underline{e}_x) in addition to the self-consistent field. In order to overcome the trapping threshold, a pre-accelerated monoenergetic electron beam with mean density of 10^{-N} of the background electron mean density and initial momentum $(\beta_x \gamma)_o$ serves as the driven beam. The normalized, dimensionless speed of light c' and plasma frequency ω_p' are adjusted to fit the condition $\beta_{p\omega} < 1$. We first show results for a case without an imposed transverse DC magnetic field; we chose the following parameters: $\delta n_o / n_o = 0.1$, $N=3$, $(\beta_x \gamma)_o = 2$, $\epsilon_o = 0.095$, $\delta = 0.01$, $\omega_o / k_i = 0.98$.

Figure 4-5 shows the longitudinal electric field time history at a peak point. We see that initially the plasma wave amplitude grows linearly with linear growth rate $\epsilon_A / \omega_p t \approx 0.004$ which is about 15% smaller than that of the theoretical prediction of Eq. (4-26) ($\epsilon_A / \omega_p t = \frac{1}{2} \delta n_o / n_o \epsilon_o = 0.5 \times 0.1 \times 0.095 = 0.00475$). This is reasonable because, in our derivation for Eq. (4-26), we have treated the terms δn_o and v_{os} as linear terms, and we have also neglected the small difference between the driving frequency ω_o and the plasma frequency ω_p and thermal effects. Plasma damping (wave-wave interaction or Landau damping) may also play a role in this reduced growth rate. We also see that the amplitude of the

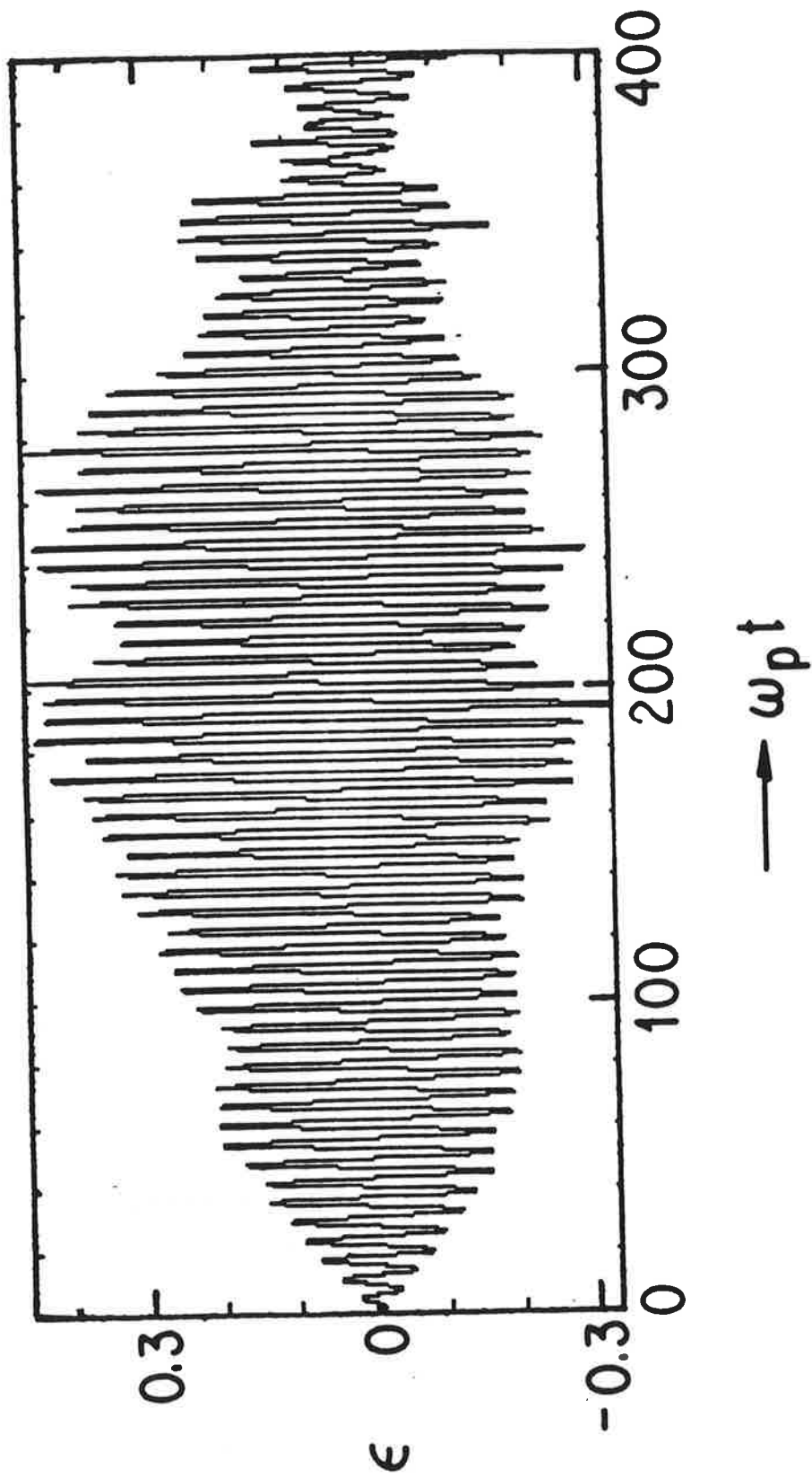


Fig. 4-5 Plasma wave electric field, ϵ vs. $\omega_p t$ at fixed X in 1-D simulation.

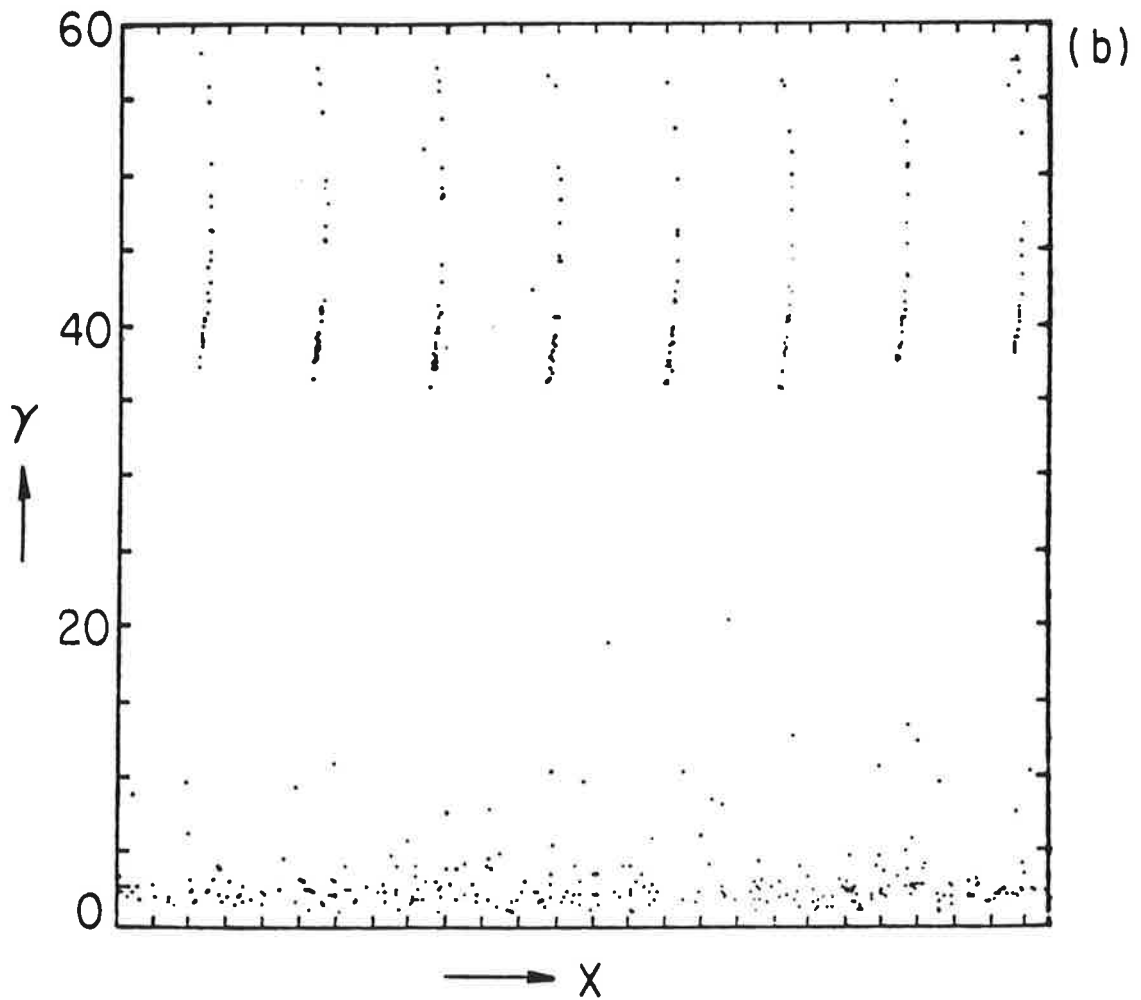
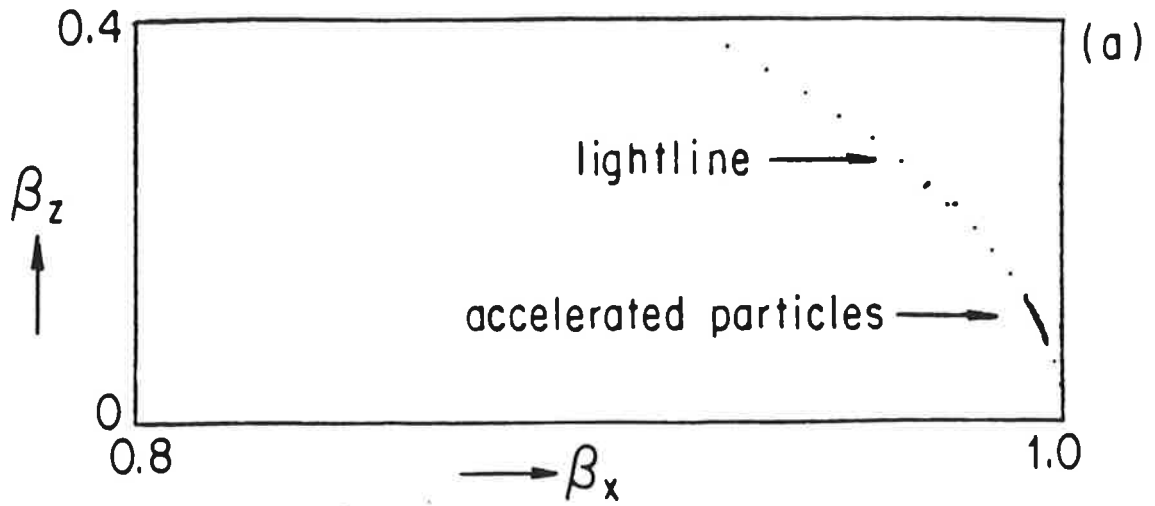


Fig. 4-7 (a) Accelerated electron's velocity space β_z vs. β_x at $\omega_c t = 480$.

(b) Accelerated electron's energy γ vs. x at $\omega_p t = 480$.

discussed in §4-3. Figure 4-7b shows the driven beam particle energies at time $\omega_p t = 480$. We see that the accelerated beam quality is better than that without surfing as can be judged by $|\Delta\gamma|/\gamma$ (compare Figure 4-6c to Figure 4-7b). In these simulations, we do not accelerate the particles indefinitely; we only reach $\gamma_{\max} \approx 60$, which is only about 50% larger than that without surfing. The reason for this is that plasma turbulence arises after a long period of pumping. This is the same reason why we did not impose a larger B_c (say $b_c = 90\% b_c^{\max}$) at a time when the plasma wave has almost saturated and most of the driven electrons have velocities much closer to v_p instead of imposing a smaller B_c at time $\omega_p t = 0$. Had we not done this, particle detrapping would have occurred long before the plasma turbulence arose to destroy the plasma wave. This obstacle can be easily overcome. Since the group velocity of the plasma wave is essentially 0 ($d\omega/dt \ll c$), instead of pumping everywhere, we can scan the laser along the accelerator to excite a local plasma wave that just keeps phase with the bunch of driven particles; the bunch will leave the turbulence behind as it moves into fresh undisturbed plasma.

§4-6 Discussion and Future Work

The high accelerating fields possible in the laser-plasma accelerators make these schemes among the most promising candidates for consideration for future generations of particle accelerators. However, the realization of these schemes for full scale high energy accelerators faces several technological hurdles as discussed in the following:

The pump depletion problem in the PBWA must be completely understood and practical methods to overcome it must be found before this scheme can be employed to achieve the energies of interest to high energy physicists. This will involve studying the long distance propagation of a beat wave in a plasma. An ideal way to study this problem is to employ a large scale computer simulation which allows the temporal simulation box to be advanced to keep up with the laser pulse. This technique has recently been employed in 1D electrostatic plasma-wake-field accelerator studies [16]. However, the fully electromagnetic case (e.g. PBWA), presents technical computational problems not encountered in the earlier work.

The plasma density must be maintained uniform over long distance; this presents a strong challenge to plasma experimentalists. We showed, For example, in §4 that a 2.5% plasma frequency shift in the

PBWA can result in a 50% change of the excited plasma wave saturation amplitude. Also, a 2% plasma frequency increase in the SILPA scheme can, in some cases (if $\delta < 0.02$), causes the incident monochromatic laser to be cut off. Technological progress in generating and maintaining plasmas probably is a key to practical realization of these schemes as high energy particle accelerators.

In the SILPA scheme [17], practical way of sweeping the laser energy along the system must be developed. As we showed in §5 by computer simulations, without scanning the laser along the plasma column to excite local plasma waves, plasma turbulence arises which will severely limit the length of each accelerator stage. The effects of the pondermotive force caused by a finite width to the lasers as well as ion ripple decay times and finite k_0 effects require further investigation.

§4-7. References

- [1] C. Pellegrini, AIP Conf. Proc., 91, 138 (1982).
W. Colson and S. Ride, Appl. Phys., 20, 61 (1979).
- [2] J. Fontana, Laser Acceleration of Particles (Malibu, 1985),
C. Joshi and T. Katsouleas, eds., AIP Conf. Proc., 130, 357
(AIP, NY, 1985).
- [3] J. M. Dawson, Phys. Rev. 113, 383 (1959).
- [4] T. Katsouleas, et al., Laser Acceleration of Particles
(Malibu, 1985), C. Joshi and T. Katsouleas, eds., AIP Conf.
Proc., 130, 63 (AIP, NY, 1985)
- [5] Y. T. Yan, D. Sultana, T. Katsouleas, J. M. Dawson, UCLA
Report PPG-870 (1985).
- [6] C. Joshi, et al., Nature 311, 525 (1984).
- [7] T. Katsouleas and J.M. Dawson, Phys. Rev. Lett. 51, 392 (1983)
- [8] T. Tajima and J. M. Dawson, Phys. Rev. Lett. 43, 267 (1979)
- [9] C. E. Clayton, C. Joshi, C. Darrow, and D. Umstadter, Phys.
Rev. Lett., 54, 2343 (1985).
C. Darrow, et al., Phys. Rev. Lett., 56, 2629 (1986).
- [10] Landau and Lifshitz, Electrodynamics of Continuous Media,
Section 15, (Pergamon Press, Oxford, 1960).
- [11] Norman N. Kroll et al., Phys. Rev. Lett. 13, 83 (1964);
D. Montgomery, Physica (Utrecht) 31, 693 (1965);
R. A. Stern and N. Tzoar, Phys. Rev. Lett. 16, 785 (1966).
- [12] M. N. Rosenbluth and C. S. Liu, Phys. Rev. Lett., 29, 701

- (1972).
- [13] C. M. Tang, P. Sprangle, R. Sudan, Appl. Phys. Lett., 45,
(1984).
- [14] W. Mori, UCLA Report, PPG-959 (1986).
- [15] C. Joshi, private communication.
- [16] P. Chen, et al., Phys. Rev. Lett., 56, 1253 (1986).
- [17] T. Katsouleas, J. M. Dawson, D. Sultana, Y. T. Yan, IEEE
Trans. Nucl. Sci., NS-32, 3554 (1985).
- [18] R. J. Noble, Phys. Rev. A32, 460 (1985).
- [19] R. Bingham, R. A. Cairns, And R. G. Evans, Report RAL-84-122,
Rutherford Appleton Laboratory, 1984.
- [20] J. T. Mendonca, J. Plasma Physics, 34, 115 (1985).

Chapter 5

Conclusions

In this dissertation, we have discussed several topics related to the interaction of relativistic electrons and radiation. These topics have been investigated using fully electromagnetic, fully relativistic particle simulation codes and analytic theory. These topics can be summarized into two categories: Tunable coherent radiation generation, and its inverse process, particle acceleration.

In the first category, we first investigated the AC free-electron laser. This type of free-electron laser replaces the magnetic wigglers of the conventional magnet free-electron laser by an AC (temporally oscillating but spatially uniform) transverse electric or magnetic fields. The simulation results showed that this type of free-electron laser is comparable to the conventional magnet free-electron laser. Furthermore, there are some advantages over the conventional magnet free-electron laser as presented in Table 2-2. We therefore encourage experimental exploration of the AC free-electron laser. We secondly investigated the Cherenkov maser using a dielectric-lined wave-guide. Simulation results were in good

agreement with the experimental results performed at Dartmouth College. In particular we investigated the nonlinear effects which are not amenable to analytical technique. We also suggested one way to enhance the output power by appropriately imposing an axial DC electric field; an order of magnitude enhancement in power is achievable. Although the overall efficiency may not be improved, this enhanced output power is quite useful. To improve the efficiency, means must be found to eliminate parasitic losses such as the acceleration of electrons not trapped in the so-called buckets (pondermotive wells formed by the radiation and the wigglers)

In the second category, we first discussed the acceleration mechanisms for plasma accelerators in general. The energy gain limitation were calculated with the assumption of a pure sinusoidal electrostatic plasma wave. We secondly discussed the excitation of plasma waves. In particular, we suggested that the plasma wave could be excited by injecting a monochromatic laser perpendicularly to the acceleration axis. We carried out simple model calculations to illustrate the concept. The pump depletion problem which is inherent in colinear schemes can then be avoided. Our simulation results showed that the saturation amplitude of the excited plasma wave can be high; 40% of the cold wave breaking field was obtained with the incident monochromatic laser frequency being 1% larger than the plasma frequency. Although there remain several technological

hurdles as discussed in §4-6 before such a scheme can be realized, the high acceleration gradients (1Gev/cm) that the plasmas can support makes this a topic worth further investigation.

